Elucidating the Modes of Action of the Antitumour New Zealand Marine Natural Product Pterocellin A

A thesis

submitted in partial fulfilment

of the requirements for the degree

of

Master of Science (Research) in Chemistry

at

The University of Waikato

by

Alice Tansi Wang

THE UNIVERSITY OF
WAIKATO
Te Whare Wānanga o Waikato

2015

Abstract

Pterocellin A is a novel bioactive alkaloid isolated from the New Zealand marine bryozoan *Pterocella vesiculosa*. It exhibits potent antitumour activity towards the P388 (murine leukaemia) cell line *in vitro* with an IC_{50} value of 477 ng/mL. Further screening at the NCI indicated that it was selectively sensitive towards certain non-small cell lung, melanoma, and breast cancer cell lines, however, the biological mode of action of pterocellin A is unknown.

This project investigated and elucidated the cytotoxicity of pterocellin A using the human cervical cancer cell line HeLa. Cellular toxicity can be manifested as either necrotic or apoptotic cell death. Cancer cells are prone to resisting apoptosis, and one of the key mechanisms recognised in anticancer agents is the induction of apoptosis. Pterocellin A exhibited similar cytotoxicity against the HeLa cell line compared to P388 cells with an IC_{50} value of 886 ng/mL. In this study, HeLa cells were incubated with various concentrations (up to 2000 ng/mL) of pure pterocellin A, and characteristic markers of apoptotic and necrotic cell death were investigated using several *in vitro* biochemistry techniques. Assessments were made on the morphological and biochemical changes in HeLa cells after treatment with pterocellin A.

Time-course MTT and LDH assays were carried out and the results showed that only a low level of cytosolic LDH was detected in the supernatant after all the cells had died from pterocellin A treatment at 2000 ng/mL. This indicated the cells maintained membrane integrity upon death which suggested apoptosis. Additionally, morphological changes were observed under the microscope after six hours of treatment. Cell shrinkage and nucleus condensation were observed, as

well as apparent membrane blebbing, a key feature of apoptosis. The MTT data were also indicative of mitochondria impairment which could suggest that pterocellin A targets the mitochondria. This idea was supported by the observed changes in the morphology and location of the mitochondria after exposure to pterocellin A. Furthermore, the level of activated caspase-3 in HeLa cells increased after treatment with pterocellin A; activated caspase-3 can only be detected after a series of signalling events following the induction of apoptosis. These data support the notion that pterocellin A is an inducer of apoptosis in HeLa cells.

This project also utilised the biochemical assays to develop a systematic bioassay screening system at the University of Waikato, and further investigated the bioactive metabolites of *P. vesiculosa.* The same approach taken to study pure pterocellin A in HeLa cells was successfully applied to the bioassay development. The bioactive fractions separated from the crude extract were analysed by LC-MS and several unknown metabolites were observed, however due to time constraints associated with the project, no further investigation was carried out.

Acknowledgements

I would like to express my upmost gratitude to my supervisors Dr. Michèle Prinsep and Dr. Ryan Martinus at the University of Waikato. Thank you for your assistance, guidance and advice throughout the year. I sincerely appreciate your teaching efforts and you have always been prompt with answering my questions. I have learned so much from this project and I am truly thankful for having you both as my supervisors.

I would like to thank the staff at the School of Science, University of Waikato. In particular, thanks to Dr. Linda Peters and Dr. Ray Cursons for your helpful suggestions and recommendations for my project when I was stuck. A big thank you to Kerry Allen who made sure I was well equipped with everything in the lab. Also, I'd like to thank Dr. Barry O'Brien for taking the time to teach me a crash course in laser scanning confocal microscopy. To my scholarship providers, University of Waikato, Brian Perry Charitable Trust, and The Todd Foundation: thank you for alleviating the financial pressure so I could solely focus on my project, I'm grateful for the monetary support.

I'm very thankful for the support from my family. Mum and Dad, thanks for believing in me, I really enjoyed your wise words and encouragements. A special thanks to my partner Andrew Stewart, thank you for being my emotional support and my rock, I'm sorry for all those things I said when I was ~~hungry~~ stressed. Lastly, cheers to all my friends for being there for me and keeping me sane; especially to Kirsty Mayall for being my lab buddy; and to Nikki Webb for being my best friend. Thank you all for being a part of this journey with me.

Table of Contents

List of Tables

List of Figures

List of Abbreviations

AIF	Apoptosis Inducing Factor
Apaf-1	Apoptotic Protease Activating Factor 1
BAK	Bcl-2 Antagonist Killer 1
BAX	Bcl-2 Associated X Protein
Bcl-2	B-Cell Lymphoma Protein 2
Bcl-X_L	Bcl-2 Related Protein-Long Isoform
BID	BH3 interacting domain death agonist
CAD	Endonuclease Caspase-Activated DNAse
Cyt *c*	Cytochrome C
DIC	Differential Interference Contrast
DISC	Death-Inducing Signalling Complex
ED_{50}	Effective Dose For 50 % Of Tested Subjects
FABMS	Fast Atom Bombardment Mass Spectrometry
FACS	Flow Fluorocytometry
FADD	Fas-Associated Death Domain Protein
HPLC	High Performance Liquid Chromatography
IC_{50}	Concentration At 50 % Of Growth Inhibition
ICAD	Inhibitor Of Endonuclease Caspase-Activated DNAse
LDH	Lactate Dehydrogenase
LC-MS	Liquid Chromatography-Mass Spectrometry
MIC	Minimum Inhibitory Concentration
MID	Minimum Inhibitory Dose
NCI	National Cancer Institute
NMR	Nuclear Magnetic Resonance

PKC	Protein Kinase C
PI	Propium Iodide
PUMA	Upregulated Modulator Of Apoptosis
R_f	Retention Factor
RIPK	Receptor-Interacting Protein Kinases
TLC	Thin-Layer Chromatography
TNF	Tumour Necrosis Factor
UV	Ultraviolet

List of Equations

1. Literature Review and Research Aims

1.1 Natural Products

Natural products, also known as secondary metabolites, are organic compounds produced by living organisms. Unlike primary metabolites such as carbohydrates and amino acids, secondary metabolites are considered non-essential to life and have no apparent function within the organism.[1] These compounds attract research interest because they can exert physiological effects on other organisms, often playing an ecological role in regulating a wide range of chemical interactions. These include pheromone chemical communication, chemical defence mechanisms, and mutualistic interactions between plants, microorganisms, insects and animals.[2] Natural products are known for their characteristic chemical diversity, novelty and structural complexity, often containing unusual combinations of functional groups which attribute to biochemical specificity and other molecular properties.[3] Many bioactive compounds have been found to have therapeutic effects in humans. These properties thus make natural products ideal candidates for lead compounds in drug discovery in the pharmaceutical industry.

Historic uses of terrestrial organisms for medicinal purposes prompted early work in natural product studies.[4] Traditionally, the extensive screening of natural products has been largely focused on terrestrial environments, with many of the known natural products isolated from higher plants and microorganisms.[5] Some of the most well-known drugs are derived from terrestrial sources such as morphine and aspirin (Figure 1.1). Morphine was isolated from the opium poppy in 1806

and this small molecule led to the development of pain medicine and an understanding of the pain receptor pathways.[6] Aspirin, discovered in 1897, is a synthetic derivative of salicin, a natural product found in the bark of the willow tree.[6]

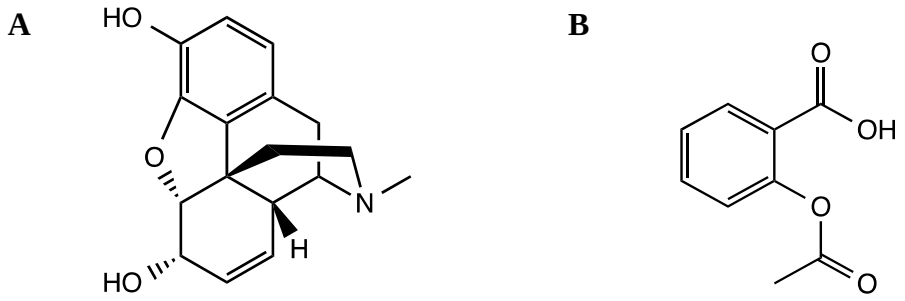

Figure 1.1 (A). Structure of morphine. **(B).** Structure of aspirin.

However, the rate of discovery of novel bioactive compounds from terrestrial organisms has decreased in recent years, due to an increased frequency of rediscovery.[5] This led to the search being extended to unexplored habitats in marine environments. The marine environment is a rich source of biological and chemical biodiversity. The ocean covers greater than 70% of the earth's surface but the chemical resources from this environment are largely untapped.[7] Thirty two of the thirty three animal phyla are represented in aquatic environments and fifteen phyla are exclusive to the marine environment.[8] Potential pharmaceutical leads from natural products are likely to be found in places with high biodiversity, such as the ocean fringe or coral reefs in marine environments.[9] Marine natural products are often produced in sessile, colonial marine species such as soft-bodied invertebrates including sponges, bryozoans, and tunicates. These organisms, living in such a highly competitive environment, have evolved to overcome the ecological pressure to compete for space with surrounding species and to evade

predators.[10] Due to their lack of movement and physical defence structures, it is thought that these organisms survive by utilising natural products as chemical defence mechanisms.[11] The compounds produced in the marine environment are unique from their terrestrial counterpart. Differences in the environments such as food chain and available nutrients meant that the classes of compounds produced are vastly different, with the presence of halogenated compounds being a frequent occurrence in the marine environment.[11] Therefore the marine environment represents a great place to explore natural products for pharmaceutical potential. With advanced diving technology and greater accessibility, marine biodiversity is attracting increasing attention for this type of research.

1.2 Biology of Bryozoans

Bryozoans, commonly known as sea moss or moss animals, are sedentary, filter-feeding invertebrates found in aquatic environments. There are over 8000 species of bryozoans described, many more were observed in fossil records.[12] Most species inhabit marine environments with very few in freshwater lakes and rivers.[13] The phylum Bryozoa, also known as Ectoprocta, is made up of three classes: Gymnolaemata, Phylactolaemata, and Stenolaemata; Phylactolaemata consists of species that are exclusively marine.[13] Currently there are just under 1000 species found in and around New Zealand, of which the vast majority are marine species.[14]

Bryozoans can be found in a variety of marine habitats due to their sessile nature. These include coral reefs and rocks, as well as man-made environments such as

on the bottom of ships. Bryozoans are colonial animals; forming colonies made up of large numbers of intercommunicating individuals termed zooids.[13] A zooid body plan consists of two parts, the polypide and the cystid (Figure 1.2). Although zooids vary in shape and the detail of their structures, the basic body plan has little variation between species.[13] Colonies of bryozoans grow typically by asexual reproduction; a single zooid can reproduce itself to form genetically identical textured formations with a variety of external morphology.[12] Being sessile filter feeders, bryozoans collect food from the surrounding water via a circle of ciliated post-oral tentacles (the lophophore) covered by the epistome. Due to their small size, bryozoans have no respiratory or circulatory system.[13]

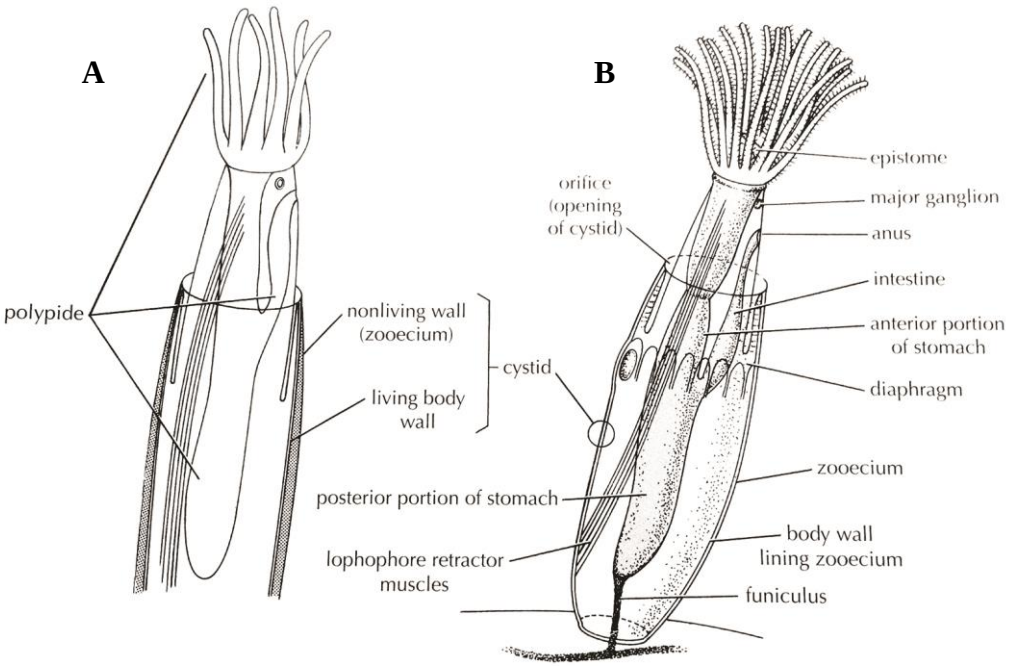

Figure 1.2 Zooid structure (adapted from Reference 12).[12] **(A).** Body plan of a zooid. **(B).** Internal anatomy of a freshwater bryozoan *Fredericella*. (Marine species share the same anatomy)

1.3 Bioactive Natural Products from Marine Bryozoans

Much of the research on marine natural products has been focused on the phyla Porifera and Cnidaria, with little investigation into Bryozoa. Bryozoans are of particular research interest due to the variety of secondary metabolites they contain. A number of novel natural products from bryozoans have been isolated to date. These have been extensively reviewed including in the annual reviews in *Natural Products Reports* detailing marine natural products classified by phylum.[5, 15-43] A discussion of selected literature focusing on bioactive natural products from bryozoans is presented here.

The best-known examples of bioactive bryozoan metabolites are the bryostatins, a class of structurally related compounds originally isolated from the marine bryozoan *Bulgula neritina*.[44] To date, 20 bryostatins have been identified and one more noted bryostatin is yet to be identified.[44-56] The bryostatins share a common, complex macrolide ring structure with various substituents. This ring structure has been given the name bryopyran (Figure 1.3).[45]

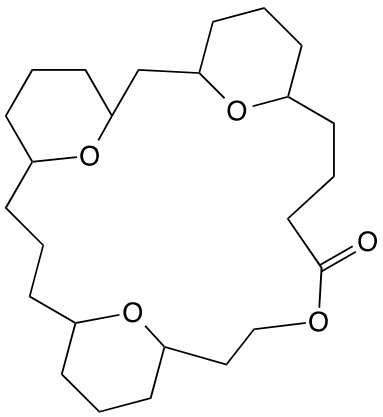

Figure 1.3 Bryopyran ring system.[45]

The first compound of the family, bryostatin 1 **(1)**, was isolated from an extract of *B. neritina* obtained from the Gulf of Mexico in 1968. The structure was elucidated and published in 1982 by Pettit *et al.* It was found to have notable antineoplastic activity with an ED_{50} of 0.89 μg/mL against the P388 murine leukaemia cell line.[44] The structures of bryostatin 2 **(2)** and bryostatin 3 **(3)** were obtained from *B. neritina* collected from the eastern Pacific Ocean and published in the following year.[45-46]

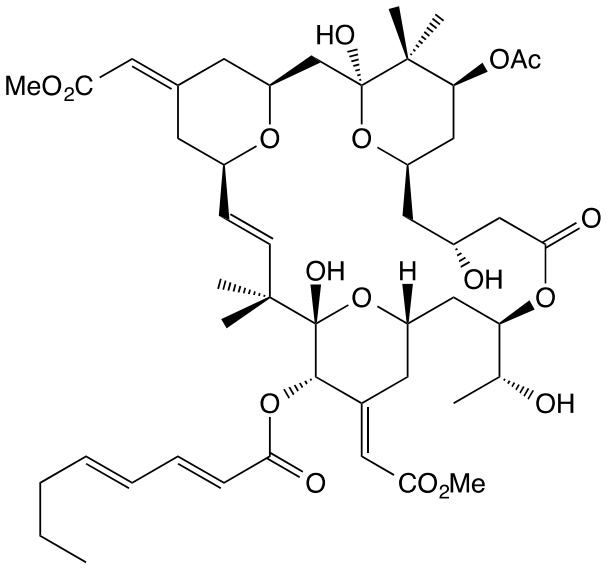

(1)

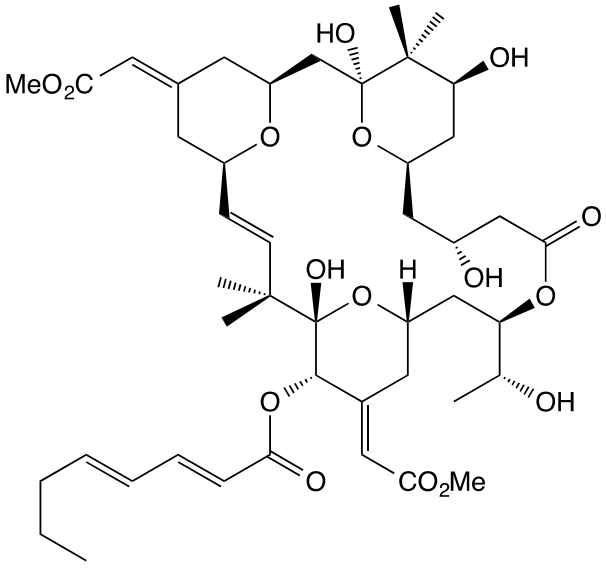

(2)

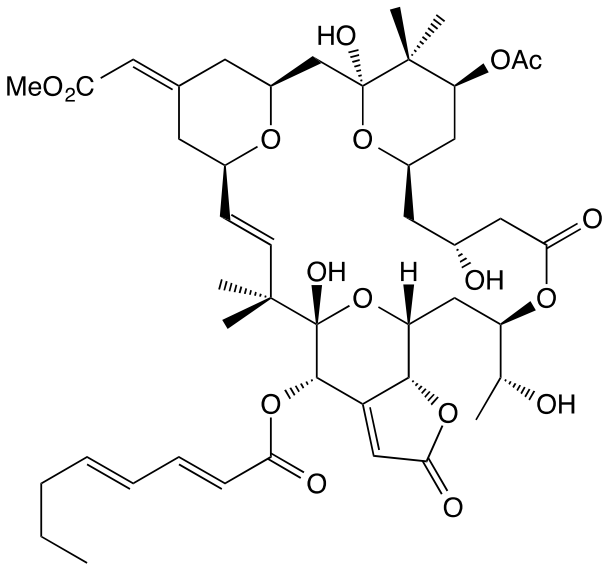

(3)

Over the next 20 years, further bryostatins were isolated from *B. neritina* sourced from various locations and possessed similar bioactivities comparable to bryostatin 1. The isolation process was directed by bioactivity screening of the fractions, and the structural elucidation was achieved by a number of methods including high performance liquid chromatography (HPLC), liquid chromatography-mass spectrometry (LC-MS), one and two-dimensional ^{1}H and ^{13}C nuclear magnetic resonance (NMR) spectroscopy, and X-ray diffraction techniques.

Bryostatins 4 **(4)** – 18 **(18)** were isolated from extracts collected from the Gulfs of Mexico, California, and Sagami; bryostatins 19 **(19)** and 20 **(20)** were from the South China Sea and the east coast of America respectively.[47-56]

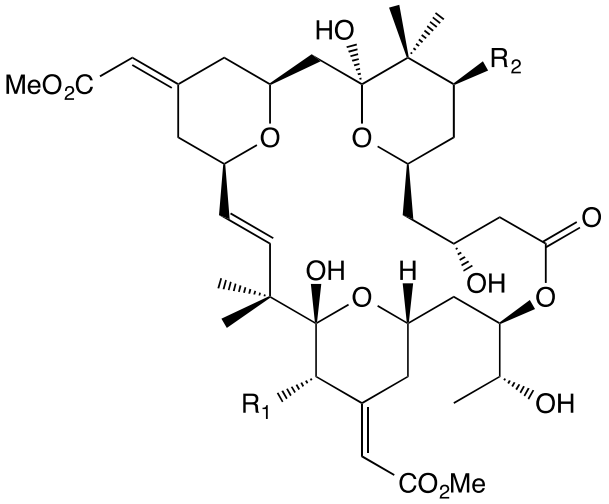

(4)	**R_1 = B; R_2 = C**	**(5)**	**R_1 = -H; R_2 = C**
(6)	**R_1 = A; R_2 = C**	**(7)**	**R_1 = -H; R_2 = A**
(8)	**R_1 = A; R_2 = B**	**(9)**	**R_1 = E; R_2 = B**
(10)	**R_1, R_2 =A**	**(11)**	**R_1 = -H; R_2 = B**
(12)	**R_1, R_2 = B**	**(13)**	**R_1= -OH; R_2 = D**
(14)	**R_1 = A; R_2 = B**	**(15)**	**R_1 = F; R_2 = A**

A = 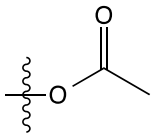

B = 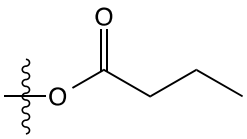

C= 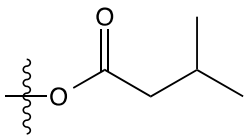

D = 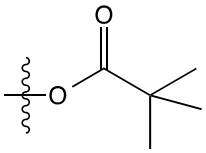

E = 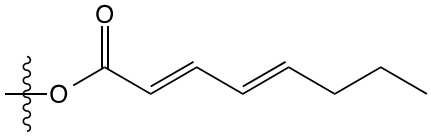

F = 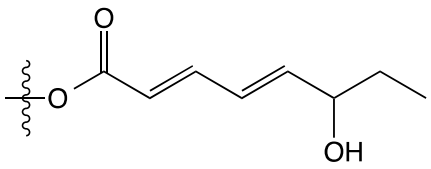

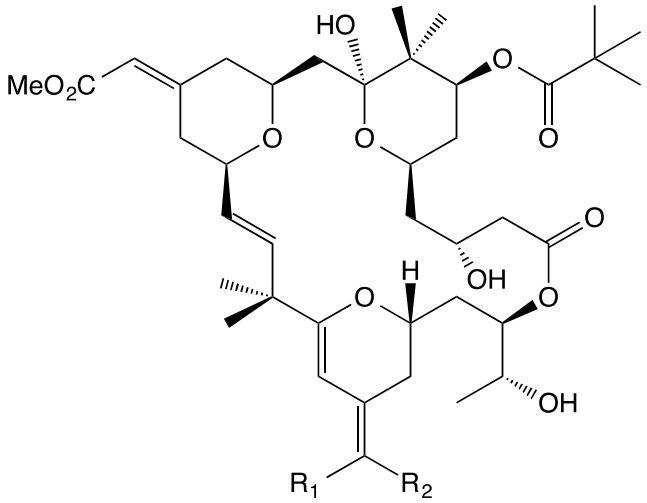

(16) R_1 = -H; R_2 = CO_2CH_3

(17) R_1 = CO_2CH_3; R_2 = -H

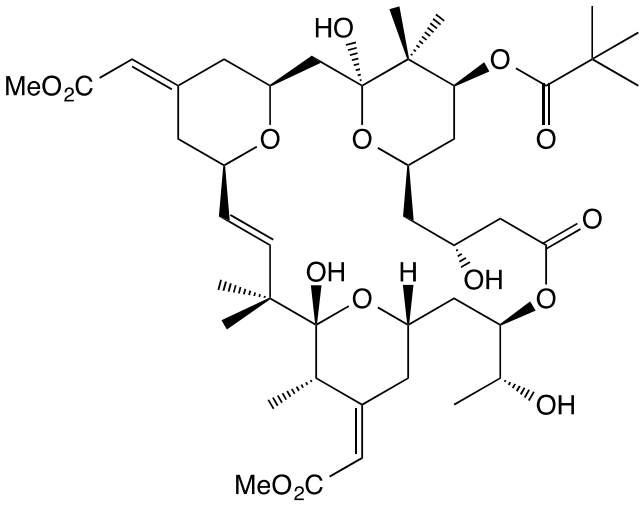

(18)

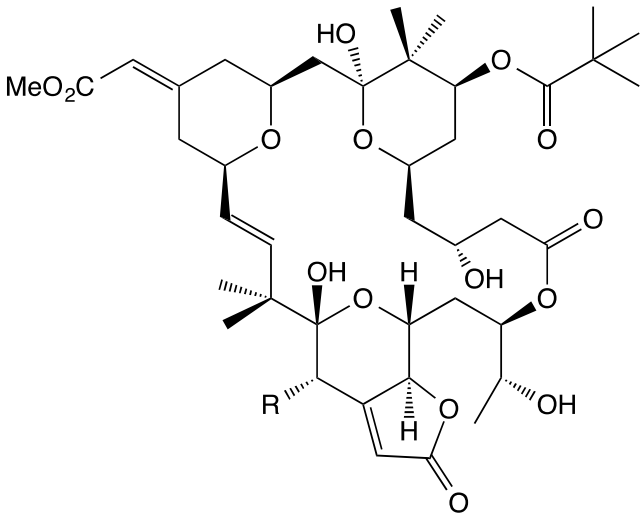

(19) R = $CO_2(CH_2)_2CH_3$

(20) R = -H

For many years, it was thought that the bryostatins were produced by *B. neritina* due to their isolation from a diverse distribution of bryostatins in different geographical locations. However, all but one bryostatin were isolated from *B. neritina*; bryostatin 8 was isolated from the species *Amanthia convoluta.*[48] Questions were raised about the origin of the bryostatins as to whether they were produced endogenously, sequestered through diet, or perhaps the result of a bacterial symbiotic relationship. Studies have shown that antibiotic treated *B. neritina* had reduced levels of bryostatins, which supported the theory of a bacterial symbiotic relationship.[57] In 2004, Lopanik *et al.* demonstrated for the first time the symbiotic relationship between the bacterium *Endobugula sertula* and *B. neritina*.[58] Treatments of antibiotic gentamicin were applied to *B. neritina* larvae since the larvae possess much higher concentrations of bryostatins than the adults. The untreated larvae were highly unpalatable to pinfish, reducing their consumption of food pellets by 80%. In contrast, antibiotic treated larvae only decreased the feeding consumption of the pinfish by 20%. It was found that the larvae with antibiotic-knockout of *E. sertula* significantly lacked bryostatin production compared to the control. Also, the extract of larvae from Delaware *B. cf. neritina* contained no bryostatins. Interestingly Delaware *B. cf. neritina* larvae do not possess *E. sertula.* This further supported the notion that the production of bryostatins was due to bacterial symbionts.[56, 58]

There have been a number of studies on the bryostatins and their biological activity but bryostatin 1 is by far the most studied compound of its class. Bryostatin 1 has been shown to have antitumour and immune stimulation properties. It inhibits tumour growth *in vitro* and *in vivo* as well as the inhibition of tumour invasion and angiogenesis.[59] It has been found that bryostatin 1

interacts with the enzyme protein kinase C (PKC), a family of serine/threonine kinases that play important roles in cell signalling. Bryostatin 1 can bind to the regulatory domain of the PKC with a binding affinity of $1.35\pm0.17\text{x}10^{-9}$ M and competes with the natural PKC ligands such as phorbol esters.[60] Although binding of phorbol ester to PKC promotes tumour growth, bryostatin 1 produces an antineoplastic effect. Initial short-term incubation with bryostatin 1 induces activation of PKC by autophosphorylation and translocation to the cell membrane, whilst long-term exposure leads to ubiquitination of PKC and subsequent degradation and therefore significant down-regulation of the PKC pathway. Bryostatin 1 has been in over thirty phase I and II clinical trials for a variety of cancers such as myeloid leukaemia, melanoma, lymphocytic leukaemia, non-Hodgkin's lymphoma, metastatic myeloma, relapsed lymphoma, chronic lymphocytic leukaemia and non-small cell lung cancer.[11, 61] As a single agent, bryostatin 1 only had minimal effects in phase II trials and did not progress to phase III as a cancer treatment; it did however show improved results in combination with other chemotherapeutic agents in potentiating pro-apoptotic effects.[11, 61] More recently, the clinical applications of bryostatin 1 have been explored in areas other than cancer, current clinical trials are in progress for Alzheimer's disease and HIV.[61]

Another bryostatin was recently found to induce apoptosis in acute monocytic leukaemia cells both *in vitro* and *in vivo*, as well as in primary U937 cells.[62] Bryostatin 5 inhibited tumour growth (IC_{50} 10.71±72.11 nM) and induced apoptosis through upregulated modulator of apoptosis (PUMA), a decrease in the mitochondrial membrane potential, and the activation of p53, a tumour suppressor protein. The cells displayed distinct morphological characteristics of apoptosis

using transmission electron microscopy. Bryostatin 5 also significantly decreased the expression of anti-apoptotic protein Bcl-X_L and increased the expression of pro-apoptotic proteins such as the Bcl-2 associated X protein (BAX), Bcl-2 antagonist killer 1 (BAK), cleaved caspase-9 and cleaved caspase-3.[62] This finding might facilitate clinical development of bryostatin 5 for the treatment of acute monocytic leukaemia.

There have been other novel bioactive compounds isolated from bryozoans, although unlike the bryostatins, the biological mechanisms of action are often unknown. However, due to their excellent anticancer/antimicrobial activity, they have the potential to be used as lead compounds for pharmaceutical research.

Caulibugulones A – F **(21) – (24)** are a group of six novel alkaloids isolated from *Calibugula intermis* collected in the south Pacific near Palau.[63] The isolation process was guided by bioassay. Final isolation and structural elucidation of the metabolites was achieved by HPLC, positive-ion fast-atom bombardment mass spectrometry (FABMS), and NMR spectroscopy.

All caulibugulone alkaloids displayed cytotoxicity against the murine IC-2^{WT} tumour cell line *in vitro* (Table 1.1). The mode of action is not fully understood. One group proposed that the caulibugulones are selective inhibitors of the Cdc25 family of cell cycle-controlling protein phosphatases.[64] It was demonstrated *in vitro* that caulibugulone A could irreversibly bind to Cdc25B protein in HeLa cells. This binding interaction directly inhibited the Cdc25B activity, generated reactive oxygen species, and consequently led to cell arrest at both G_1 and G_2/M phases of the cell cycle.[64]

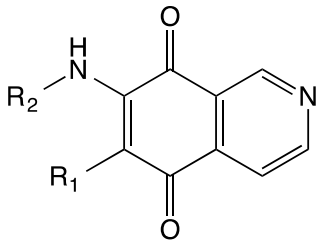

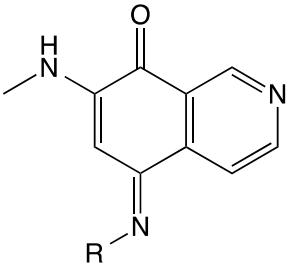

(21) **R_1 = -H; R_2 = -CH_3**

(22) **R = -H**

(23) **R_1 = -Br; R_2 = -CH_3**

(24) **R = -CH_2CH_2OH**

(25) **R_1 = -Cl; R_2 = -CH_3**

(26) **R_1 = -H; R_2 = -CH_2CH_2OH**

Table 1.1 IC_{50} values of caulibugulones A–F against the murine IC-2^{WT} cell line.[63]

Compound	IC_{50} (μg/mL)
Caulibugulone A	0.34
Caulibugulone B	0.22
Caulibugulone C	0.28
Caulibugulone D	1.67
Caulibugulone E	0.03
Caulibugulone F	0.10

Four novel bioactive polyketide-derived metabolites, myriaporones 1 – 4 **(27) – (30)** were isolated form *Myriapora truncata* collected from the Western Mediterranean Sea.[65] Myriaporones 1 and 2 were active against murine leukaemia L1210 cells (99% inhibition at 50 μg/mL, 87% inhibition at 25 μg/mL). The isolation of myriaporones 3 and 4 proved to be difficult due to being in inseparable equilibrium as interconverting isomers. The bioactivity of the mixture was analysed and displayed 88% growth inhibition at 0.20 μg/mL.[65]

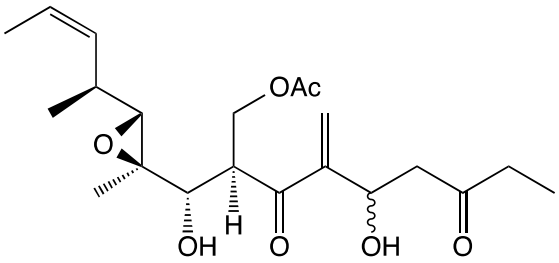

(27)

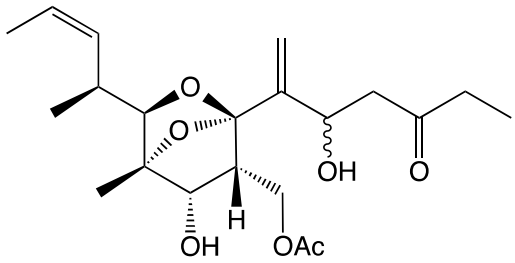

(28)

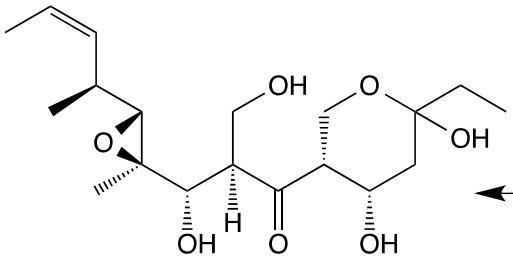

(29)

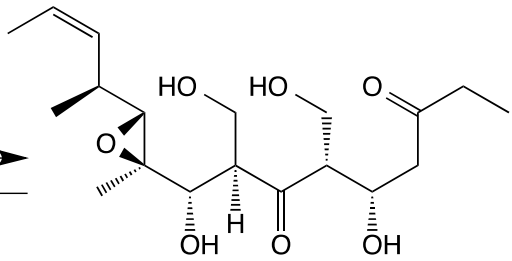

(30)

Eusynstyelamides are tryptophan-derived compounds originally isolated from the ascidian *Eusynstyela latericius*.[66] Four novel eusynstyelamides, *ent*-eusynstyelamide B **(31)**, and eusynstyelamides D – F **(32)** – **(34)** have also been isolated from the Arctic bryozoan *Tegella cf. spitzbergensis.*[67] *Ent*-eusynstyelamide B is an enantiomer of the previously published eusynstyelamide B. These four eusynstyelamides exhibited antimicrobial activities with minimum inhibitory concentration (MIC) values against various bacteria listed in Table 1.2. Eusynstyelamides D and E also displayed weak activity against the melanoma cell line A-2058 with IC_{50} values of 57 μM and 114.3 μM respectively.[67]

Table 1.2 Antibacterial activities of Eusynstyelamides isolated from the Arctic bryozoan *Tegella cf. spitzbergensis*.[67]

	MIC (μg/mL)			
	Ent-B	**D**	**E**	**F**
Staphylococcus aureus	6.25	12.5	12.5	6.25
Escherichia coli	12.5	12.5	12.5	12.5
Pseudomonas aeruginosa	25	25	25	12.5
Corynebacterium glutamicum	12.5	12.5	12.5	6.25
Methicillin-resistant *Staphylococcus aureus*	20	20	20	>50

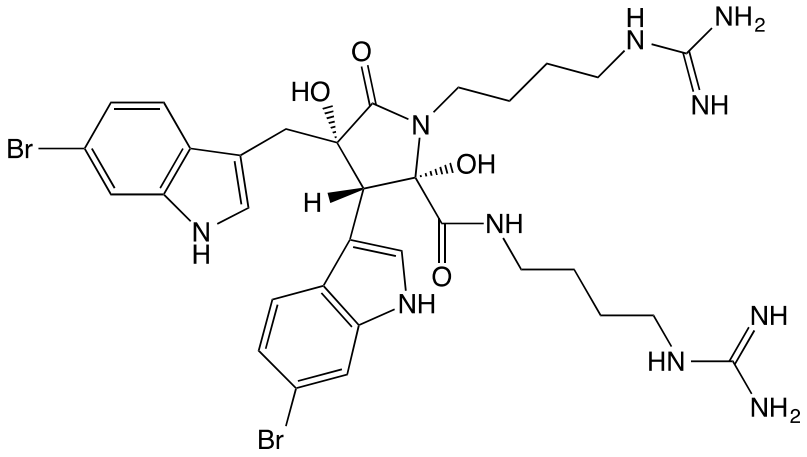

(31)

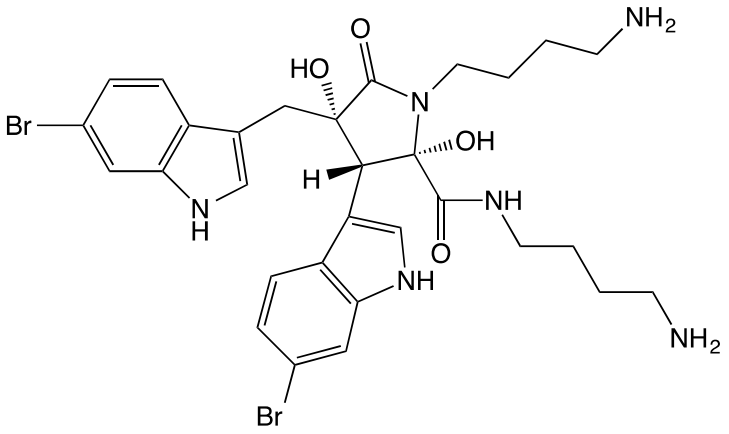

(32)

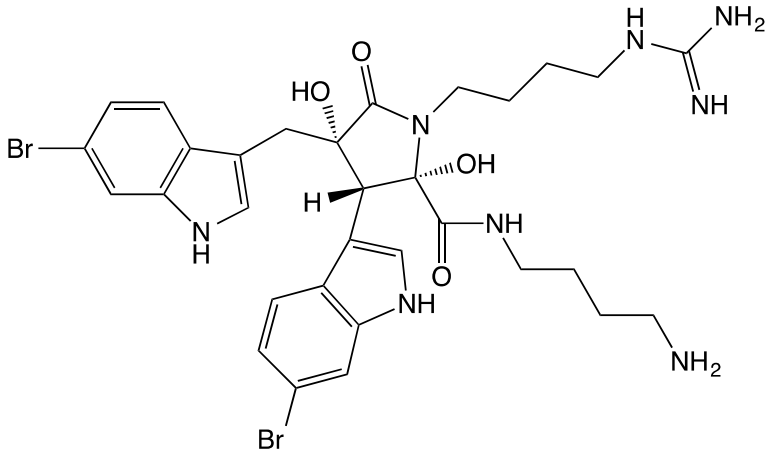

(33)

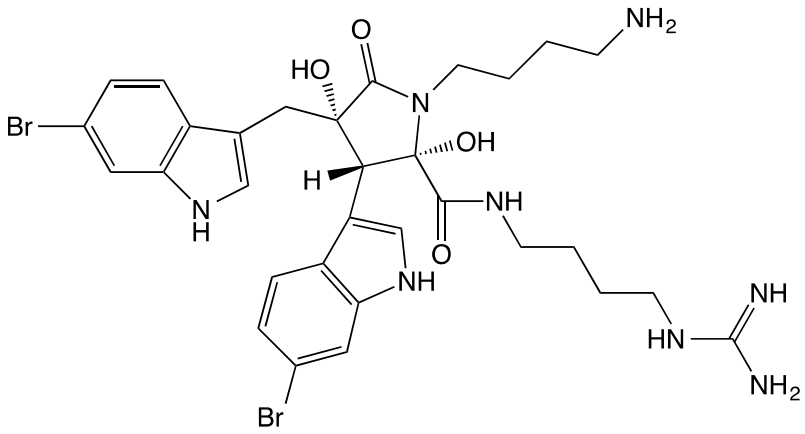

(34)

Pterocellins are a class of novel alkaloids isolated from the marine bryozoan *Pterocella vesiculosa* collected off the coast of the North Island, New Zealand. The isolation and structural elucidation of these compounds was achieved using various chromatographic and analytical techniques. The extracts were characterised using LC-MS and isolation and purification were also guided by bioactivity (cell viability) assays (carried out at the University of Canterbury). The structures of the compounds were elucidated using NMR spectroscopy and confirmed by single-crystal X-ray diffraction of pterocellin A.[68-69]

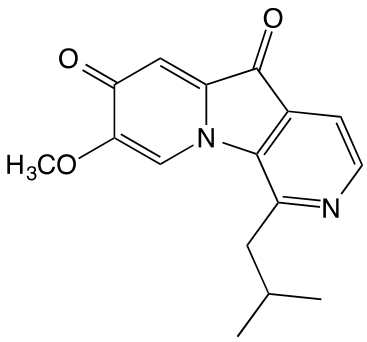

(35)

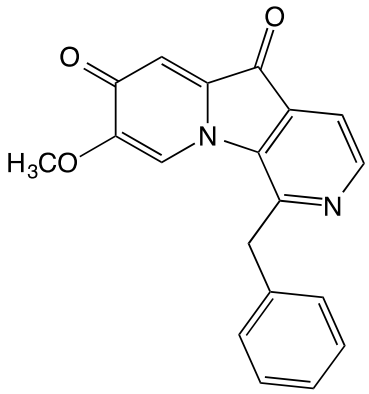

(36)

Bioactivity testing of two pterocellins A **(35)** and B **(36)** indicated promising antibacterial, antitumour, and antifungal activities.[68] It was found that pterocellins A and B were active against the P388 murine leukaemia cell line (IC_{50} values 477 and 323 ng/mL, respectively); the bacterium *Bacillus subtilis* (MIC = 0-0.3 μg/disc), and the fungus *Tricophyton mentagrophytes* (MIC = 3.9-7.5 μg/disc). Further *in vitro* screening at the NCI showed that these compounds were selectively cytotoxic towards certain cell lines (Table 1.3); namely non-small cell lung (NCI-H23), melanoma (MALME-3M, M14, SK-MEL-5), and breast (MDA-MB-435, MDA-N) (Table 1.4).[68] However, when pterocellin A was selected for *in vivo* hollow fibre assay, it was found to be ineffective. As *in vivo* systems are complex, it is possible that pterocellin A was deactivated through metabolic processes. Interestingly, there are recent debates on the origin of the breast cancer cell line MDA-MB-435 and MDA-N used in the 60-cell line panel at the NCI. Gene expression studies have suggested that the breast cancer cell lines MDA-MB-435 and its derivative MDA-N actually belong to the melanoma lineage and are related to the melanoma cell line M14.[70-71] If this was indeed the case, then it would appear that pterocellins A and B are selectively cytotoxic towards

melanoma cell lines, as five of the six cell lines would belong to the melanoma family.

Table 1.3 Panel average values for Pterocellins A and B from the 60-cell line panel screening at the NCI.[68]

	GI_{50}[a] (μM)	TGI[b] (μM)	LC_{50}[c] (μM)
Pterocellin A	1.4	4.8	17.0
Pterocellin B	0.7	2.1	6.9

[a] growth inhibition; [b] total growth inhibition; [c] lethal concentration

Table 1.4 Selective cell lines from the NCI 60-cell line panel, sensitive to the cytotoxicity of pterocellins A and B

	GI_{50} (μM)		TGI (μM)		LC_{50} (μM)	
	A	**B**	**A**	**B**	**A**	**B**
Non-small cell lung cancer						
NCI-H23	0.3	0.1	1.0	0.3	6.1	0.7
Melanoma						
MALME-3M	0.1	0.03	0.3	0.1	0.8	0.3
M14	0.2	0.1	0.8	0.2	4.6	0.5
SK-MEL-5	0.2	0.1	0.3	0.3	0.6	0.5
Breast Cancer						
MDA-MB-435	0.2	0.2	0.3	0.3	0.6	0.6
MDA-N	0.2	0.2	0.4	0.3	0.6	0.6

There have been six pterocellin compounds published to date (A **(35)** – F **(40)**), another six proposed structures (G **(41)** – L **(46)**) are yet to be fully characterised.[72] Unlike the potent pterocellins A and B, pterocellins C **(37)**, E **(39)**, F **(40)**, H **(42)**, I **(43)** possessed little or no activity against the P388 murine

leukaemia cell line. [69, 73] Pterocellin D (38) displayed moderate bioactivity activity against the same cell line with an IC_{50} value of 4773 ng/mL (Table 1.5).[69]

Table 1.5 Biological activity of Pterocellins A – I. [68-69, 74]

		P388 IC_{50} (ng/mL)	Bs[a] MIC (μg/disc)	Tm[b] MIC (μg/disc)
(35)	Pterocellin A	477	0-0.3	3.9-7.5
(36)	Pterocellin B	323	0-0.3	3.9-7.5
(37)	Pterocellin C[c]	>6250	0-0.5	ND[d]
(38)	Pterocellin D	4773	0.5-1	10-15
(39)	Pterocellin E	>6250	0-0.5	ND
(40)	Pterocellin F	>6250	0-0.5	ND
(41)	Pterocellin G	Not yet tested		
(42)	Pterocellin H	>6250	ND	ND
(43)	Pterocellin I	>6250	ND	ND

[a] *Bacillus subtilis;* [b] *Tricophyton mentagrophytes;* [c] MIC values to be confirmed; [d] No activity observed.

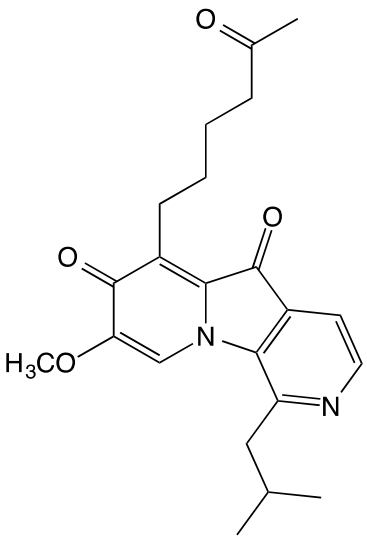

(37)

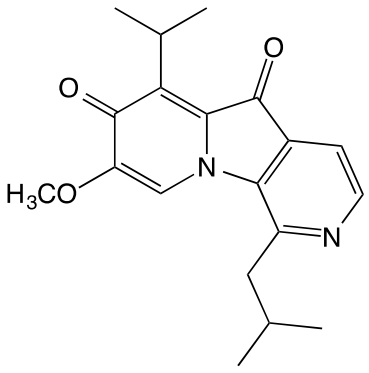

(38)

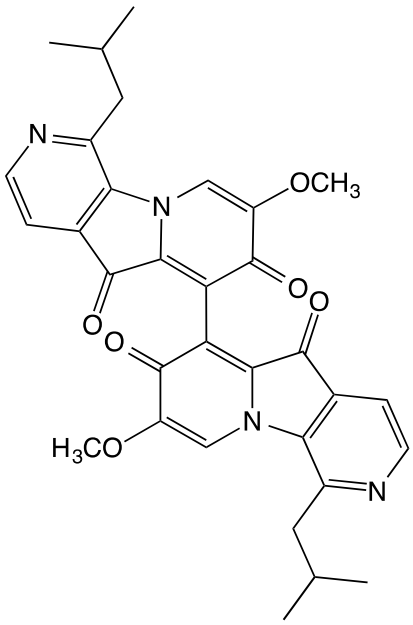

(39)

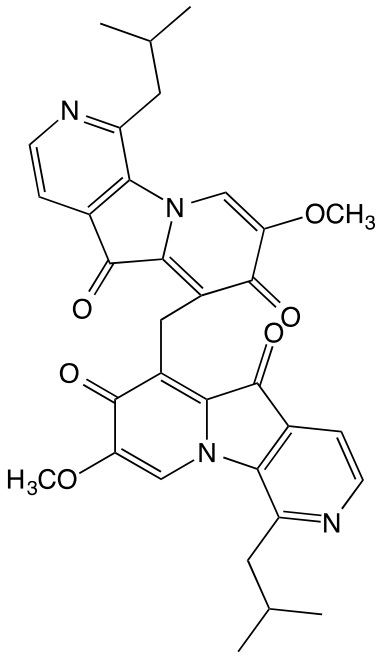

(40)

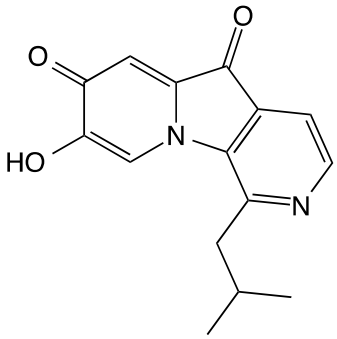

(41)

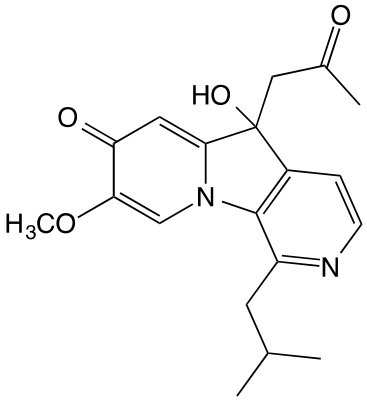

(42)

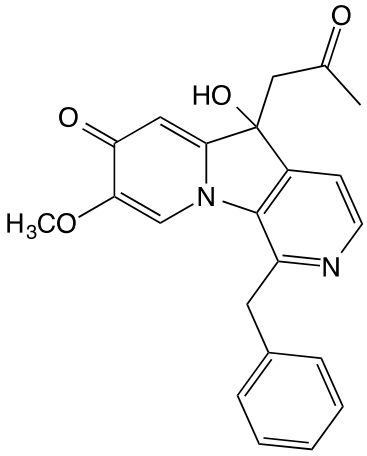

(43)

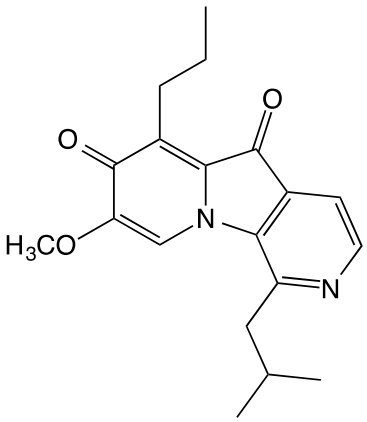

(44)

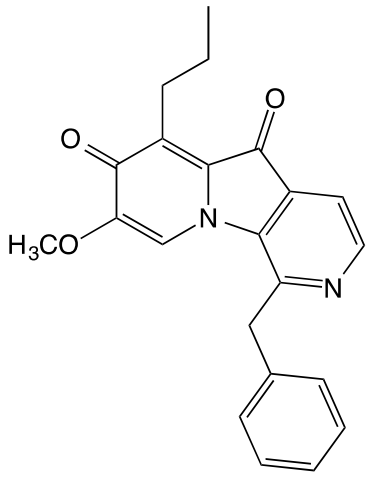

(45)

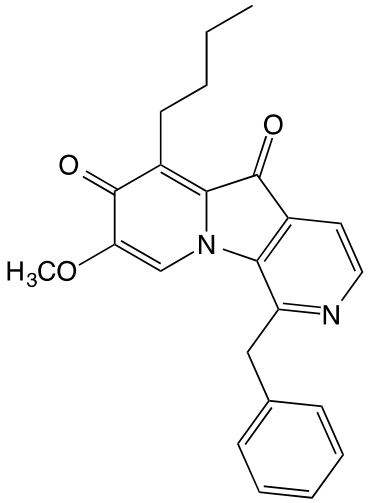

(46)

β-carboline alkaloids are commonly found in terrestrial plants, however their occurrence in the marine environment is uncommon.[75] As well as the bioactive pterocellin alkaloids, a number of β-carboline alkaloids were also found in *P. vesiculosa*. In particular, 5-bromo-8-methoxy-1-methyl-β-carboline **(47)** was isolated from an extract collected from the Alderman Islands, New Zealand. It exhibited moderate cytotoxicity against the P388 murine leukaemia cell line with an IC_{50} value of 5089 ng/mL and also displayed antimicrobial and antifungal activities against the Gram-positive bacterium *Bacillus subtilis* (minimum inhibitory dose (MID) = 2-4 μg/mL) and the fungi *Candida albicans* (MIC = 4-5 μg/mL) and *Trichlophyton mentagrophytes* (MIC = 4-5 μg/mL).[76] Although β-carboline alkaloids have been previously found in the same bryozoan family Catenicellidae, this was the first report of β-carboline alkaloids in the genus *Pterocella.*[76]

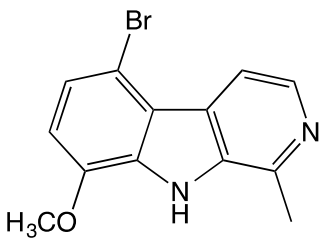

(47)

Three species within the same bryozoan family: *Costaticella hastata*, *Cribricellina cribraria*, and *Catenicella cribraria* have also all produced β-carboline alkaloids.

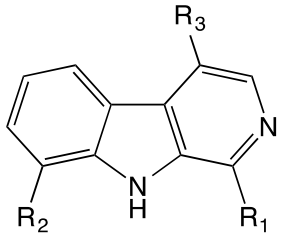

(48) **R_1 = CH(OH)CH_3; R_2, R_3 = H**
(49) **R_1 = CH_3; R_2, R_3 = H**
(50) **R_1 = CH_2CH_3; R_2, R_3 = H**
(51) **R_1 = $CHCH_3$; R_2, R_3 = H**
(52) **R_1 = $CHCH_3$; R_2 = OH; R_3 = H**

The first β-carboline alkaloids from a bryozoan were isolated from *Costaticella hastata.* One of the isolated compounds, *(S)*-1-(1'-hydroxyethy1)-β-carboline **(48)**, was a novel β-carboline metabolite. The other three were known β-carboline alkaloids previously isolated from terrestrial organisms.[77] These were 1-methyl-β-carboline **(49)** (also known as harman), 1-ethyl-β-carboline **(50)**, and 1-vinyl-β-carboline **(51)** (pavettine).[77] Another β-carboline with vinyl substitution at the C1 position was found in both *Cribricellina cribraria* and *Catenicella cribraria*.

1-Vinyl-8-hydroxy-β-carboline **(52)** exhibited strong bioactivity against the P388 murine leukaemia cell line. Both pavettine **(51)** and 1-vinyl-8-hydroxy-β-carboline **(52)** had an IC_{50} value of 100 ng/mL.[75] 1-Vinyl-8-hydroxy-β-carboline **(52)** was also screened against the 60-cell line panel at the NCI with panel average values of GI_{50} 1.8 μM, TGI 5.8 μM, and LC_{50} 19 μM.[78] It was suggested that the vinyl substitution at C-1 was important for cytotoxicity as the other β-carboline

alkaloids, harman **(49)** and 1-ethyl- β-carboline **(50)** did not exhibit a high level of bioactivity against the P388 cell line in comparison.[75]

1.4 Cell Death: Apoptosis and Necrosis

Cell death is divided into two main forms: apoptosis and necrosis. Cell death is an essential part of normal development and tissue homeostasis in multicellular organisms.[79] To maintain homeostasis and regeneration, there is a regulated balance between cell proliferation and cell death in all dividing cell populations. Cells that are lost during this normal turnover under physiological conditions are attributed to a process known as apoptosis. The term apoptosis originated in 1972 when Kerr *et al.* described the observation of distinct morphological changes in cell death.[80] Since this study, apoptosis remained one of the most investigated processes in biological research.

1.4.1 Overview of Apoptosis

Apoptosis is characterised by cell shrinkage, nuclear condensation, non-random DNA fragmentation, and membrane blebbing (protrusion of the plasma membrane) with no loss of membrane integrity. This targeted and regulated process retains the intracellular contents, therefore no inflammatory response is triggered.[81] Just as mitosis is a significant process in cell proliferation, the role of apoptosis in normal physiology is just as important in regulating cell populations. As well as being important in physiological development, apoptosis can also

occur under pathological conditions. Alterations to the natural mechanisms of apoptosis can lead to many diseases such as neurodegenerative, autoimmune and cardiovascular diseases, and cancer.[82-85]

Apoptosis is a critical defence mechanism against the formation and progression of cancer. Cancer cells are prone to resisting apoptosis, and one of the key mechanisms recognised in anticancer agents is the induction of apoptosis. Apoptosis can be initiated in response to a variety of stimuli via two distinct, but interconnected pathways: the extrinsic death receptor pathway and the intrinsic mitochondrial pathway (Figure 1.4).[86] Both pathways converge on the same execution pathway involving a group of cysteine proteases known as 'caspases'.[87] Caspases are responsible for the biochemical changes observed in apoptosis and are considered to be the executioner of apoptosis.[86] In normal cells, caspases are found in an inactive form, expressed as a pro-enzyme. The proteolytic activities possessed by caspases are able to cleave substrates at highly conserved aspartic acid residues. This specificity is determined by the four residues amino-terminal to the cleavage site.[86] The functions of caspases can be categorised into upstream initiator caspases (caspase-2, -8, -9, -10) and downstream effector caspases (caspase-3, -6, -7).[87, 88] Effector caspases are activated proteolytically by upstream caspases, whereas initiator caspases are activated by regulated protein-protein interactions. This in turn triggers a cascade of signalling events in the commitment of apoptosis.[89] It is still unclear what molecular mechanisms mediate the activation of initiator caspases; it is likely to be a more complex concept than understood currently.[89]

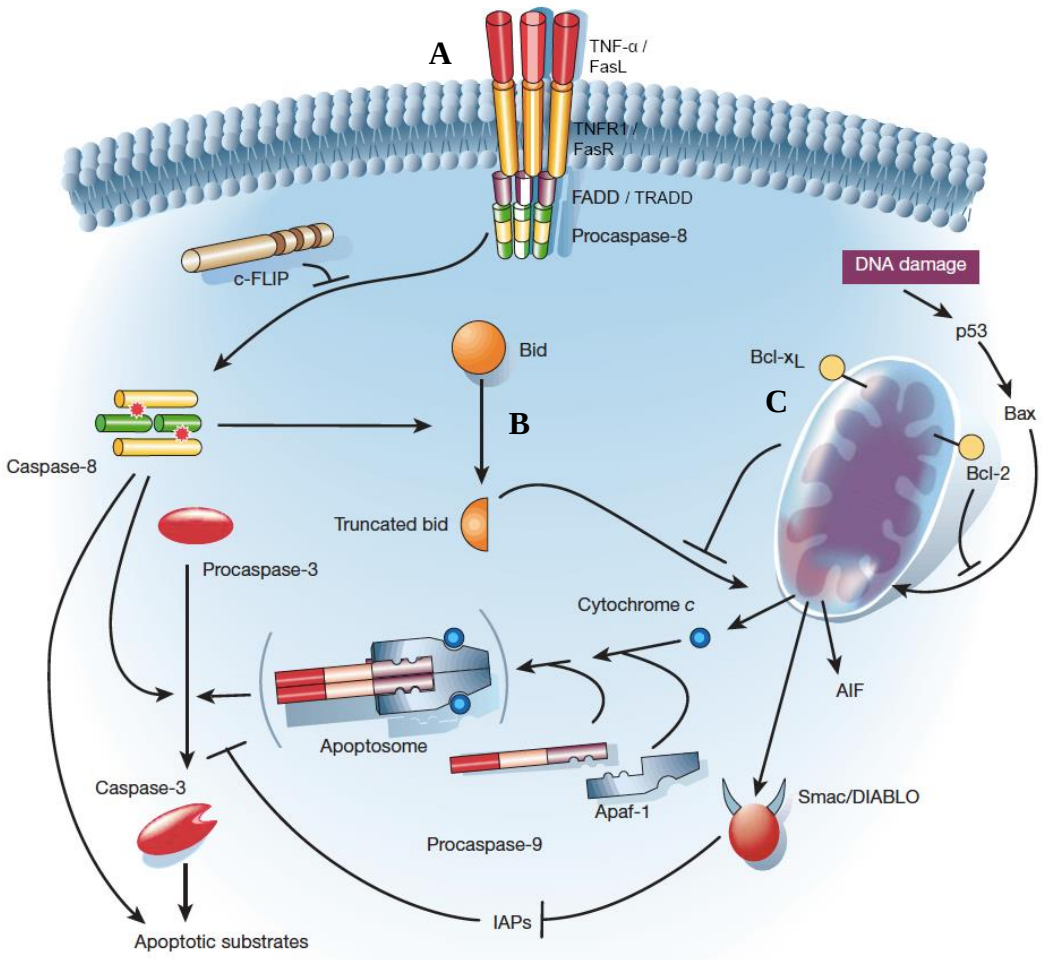

Figure 1.4 Apoptosis and caspase activation pathways (adapted from Reference 86).[86]

(A). The extrinsic pathway is activated when a specific ligand binds to the death receptor, inducing the formation of DISC and triggering the caspase signaling cascade. **(B).** BID protein provides 'cross-talk' between the death receptor and mitochondrial pathway, promoting the release of cytochrome *c* from the mitochondria. **(C).** The intrinsic pathway is initiated by the release of cytochrome *c* from the mitochondria in response to various stimuli. Cytochrome *c* binds to Apaf-1 and promotes the recruitment of procaspase-9, forming an 'apoptosome' and activates caspase-9, which proceeds to activate caspase-3.

Activation of initiator caspases by either extrinsic or intrinsic pathways will lead to biochemical modifications including DNA fragmentations, degradation and cross-linking of proteins, formation of apoptotic bodies, and expression of inward-facing phosphatidylserine groups on the cell surface for phagocytic recognition.[87,90] The extrinsic death receptor pathway involves trans-membrane

receptor-mediated interactions with members of the tumour necrosis factor (TNF) receptor gene superfamily such as TNFR1 and FasR receptors.[87] Apoptosis is triggered when a specific ligand binds to the corresponding death receptors on the cell surface. This results in the recruitment of the adapter molecule Fas-associated death domain protein (FADD) and the oligomerisation of procaspase-8 monomers to form the death-inducing signalling complex (DISC). The formation of the DISC induces autoproteolytic activation of the inactive procaspase to active caspase-8, triggering the execution phase of apoptosis.[87, 89] The intrinsic mitochondrial pathway can be initiated by a variety of receptor-independent stimuli such as free radicals, radiation, DNA damage, viral infections, and toxins.[87] These stimuli result in the loss of mitochondrial transmembrane potential and subsequently two main groups of intermembrane space proteins are released into the cytosol. The first group consists of pro-apoptotic proteins such as cytochrome *c* (cyt *c*) and Smac/DIABLO (second mitochondria-derived cyt *c*) that can activate the caspase-dependent mitochondrial pathway.[89] The binding of cytosolic cyt *c* to the apoptotic protease activating factor (Apaf-1) prompts the recruitment and oligomerisation of procaspases-9, leading to the activation of caspase-9. The formation of the complex cyt *c*/Apaf-1/caspase-9, also known as an "apoptosome", proceeds to activate caspase-3 and caspase-7 in the execution phase of apoptosis.[89] The second group of proteins released from the mitochondria at a later stage are the apoptosis inducing factor (AIF) and endonuclease G.[87] These proteins translocate to the nucleus after release and promote nuclear condensation and DNA fragmentation independent of the caspase activities.[89]

The intrinsic caspase activation by cyt *c* release from the mitochondria is a highly regulated process mediated by the Bcl-2 family of anti-apoptotic and pro-apoptotic proteins. The anti-apoptotic proteins include B-cell lymphoma protein 2 (Bcl-2) and Bcl-2 related protein-long isoform (Bcl-X_L), and the pro-apoptotic proteins include BAX, BAK, and BH3 interacting domain death agonist (BID) protein.[87] There is a degree of 'cross-talk' between the apoptotic pathways and BID is considered to play an important role in this. The DISC complex in the extrinsic pathway can proteolytically activate BID by truncating the C-terminal fragment of BID (tBID), which then promotes cyt *c* release after translocation to the mitochondria.[91]

Both extrinsic and intrinsic pathways end up at the final execution phase of apoptosis involving caspase -3, -6, -7 with caspase-3 being the most important.[87] Once activated, caspase-3 specifically activates the endonuclease caspase-activated DNAse (CAD) that is complexed with its inhibitor, ICAD, in its native state. Cleavage of ICAD releases CAD, which leads to the degradation of DNA and chromatin condensation.[87] Caspase-3 is also responsible for the dismantling of the cell into apoptotic bodies.[87]

In the absence of phagocytosis in *in vitro* systems, apoptotic cells proceed to secondary necrosis which shares many features of primary necrosis such as loss of membrane integrity and leakage of cell contents.[92] This becomes problematic when trying to distinguish the cell death mechanisms, however there are other biochemical parameters that can be explored to distinguish between apoptosis and primary necrosis.

One of the ways to discriminate between apoptosis and primary necrosis is to utilise the fluorescent stains annexin-v and propium iodide. Annexin-v is a Ca^{2+} dependent protein that can bind to the phosphatidylserine groups exposed on the cell surface in the early stages of apoptosis.[93] Propium iodide (PI) is a dye that is able to bind to DNA when the integrity of the nucleus is compromised. Apoptotic cells can be analysed using flow fluorocytometry (FACS) and distinguished from primary necrosis if they are positively stained with annexin-v with negative PI stain. Secondary necrosis can be identified if a shift from PI- to PI+ signal was observed, whereas primary necrosis would show PI+ staining straight away.[92]

Another method to distinguish between apoptotic cells in secondary necrosis and primary necrosis is the detection of activated caspase-3 and caspase-7 in the supernatant by Western blot. Since these proteins are activated at the onset of apoptosis, they become detectable upon disruption of the plasma membrane during secondary necrosis. Caspase activation is not characteristic of primary necrosis and therefore no activated caspases will be detected in the supernatant, instead procaspases-3 and -7 will be observed.[92]

1.4.2 Overview of Necrosis

In contrast to apoptosis, necrosis is a passive form of cell death often triggered by injury to the cell. For a long time, the term necrosis was used to describe non-apoptotic and accidental cell death as a consequence of injury caused by ischaemia and extreme trauma in pathological conditions.[94] Necrosis is characterised by cellular swelling (oncosis), vacuolisation of the cytoplasm, and

loss of membrane integrity. This results in the uncontrolled release of intracellular contents into the surrounding environment which subsequently provokes an inflammatory response.[95]

Due to its accidental nature, it was thought that necrosis was an unregulated and uncontrolled process that occurred after cell damage beyond repair, however emerging evidence have showed that this may not be the case.[96, 94] Necrotic cell death can be induced by ligand binding at specific receptors on the plasma membrane. It has been found that certain types of cell death that resemble the morphological changes of necrosis in fact have distinct signalling pathways. Cross-regulation can occur between the apoptotic and necrotic pathways and it has been suggested that necrosis is a default cell death pathway.[97] A shift from apoptosis to necrosis can be observed when cells are unable to propagate the signalling cascade of apoptosis due to the inhibition of its effectors. This type of regulated non-apoptotic cell death has been termed programmed necrosis, specifically, necroptosis.[98]

Necroptosis was first described in 2005 when a study by Degterev *et al.* demonstrated that TNF-α, an inducer of apoptosis, was capable of activating a non-apoptotic cell death in the presence of caspase inhibitors.[99] Although activated by the same stimulus, the morphological changes of the latter form of cell death were consistent with those of necrosis, not apoptosis.[99] Several mediators of the necroptotic pathway have since been identified involving the receptor-interacting protein kinases (RIPK) and the poly(ADP-ribose) polymerase. The complete processes are however not fully understood.[100]

Table 1.6 Differences between apoptosis and necrosis

Cell Death	Morphological Differences
Apoptosis	• Targets single cells • Membrane blebbing but maintains integrity of the membrane • Increased mitochondria membrane permeability, release of pro-apoptotic proteins, and formation of apoptotic bodies • Chromatin condensation and non-random DNA fragmentation • Apoptotic bodies ingested by neighbouring phagocytes • No inflammatory response
Necrosis	• Less regulated than apoptosis • Affects neighbouring cells • Cell and organelle swelling and lysosomal leakage • Loss of membrane integrity • Random degradation of DNA • Contents leak into the surrounding environment • Triggers inflammatory response

1.4.1 Apoptosis Studies of Marine Natural Products

Marine natural products have become important sources in the discovery of antitumour drugs. Cytotoxic natural products that selectively target the apoptotic pathways of cancer cells are particularly of interest in the development of chemotherapeutic agents. There are limited numbers of cytotoxicity studies on marine bryozoan natural products. Therefore a small selection of apoptosis studies on natural products from other marine organisms is described here to demonstrate some approaches taken to investigate the mechanism of cell death.

Mycalamide A **(53)** and pateamine **(54)** are natural products isolated from the marine sponges of the *Mycale* species collected from New Zealand.[101] In the

preliminary screening, both compounds showed potent antiviral, antifungal and cytotoxic activities. Mycalamide A **(53)** and pateamine **(54)** were found to be apoptotic inducers as determined by visualised DNA fragmentation, annexin-v staining, and characteristic morphology changes in H441, LLC-PK1 and SY5Y cells such as membrane blebbing and nuclear fragmentation.[101] The DNA fragmentation was more pronounced in LLC-PK1 and SY5Y cells than in H441 cells, which illustrate the difference in susceptibility in DNA laddering effects despite the similarity in the MTT responses. The IC_{50} values calculated from the MTT data were: 0.51 (H441), 0.64 (LLC-PK1) and 0.5 (SY5Y) nM for mycalamide A **(53)**; and 0.37 nM (H441), 0.76 nM (LLC-PK1), and 0.26 nM (SY5Y) for pateamine **(54)**.[101]

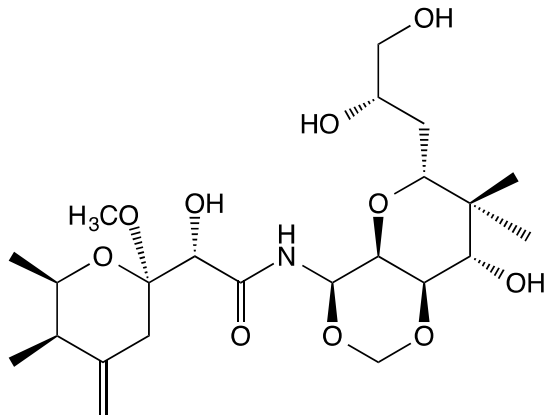

(53)

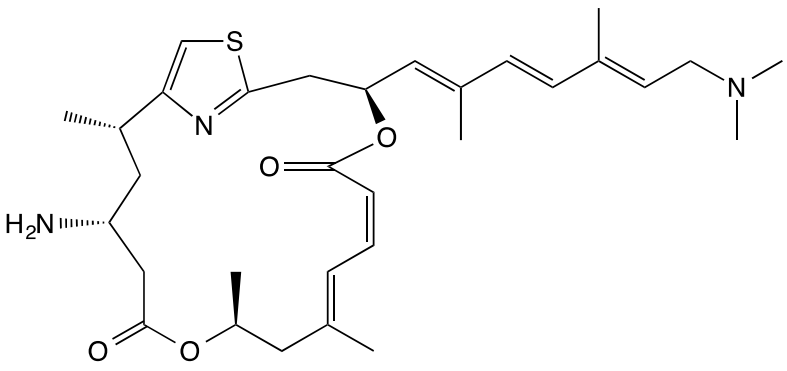

(54)

Gliotoxin **(55)** is a natural product produced by the marine fungus *Aspergillus* sp. [102] Cytotoxicity studies were carried out in HeLa and human chondrosarcoma (SW1353) cells and found that gliotoxin induced apoptosis in both cell lines. This was demonstrated by DAPI [4',6-diamidino-2-phenylindole] and annexin-v/PI double staining analysis, disruption of mitochondrial membrane potential, cyt *c* release, DNA fragmentation, nucleus fragmentation, and morphological changes. Apoptosis was further confirmed by the activation of the caspases-3, -8 and -9; as well as down-regulation of the anti-apoptotic protein Bcl-2 and up-regulation of the pro-apoptotic protein BAX. These results indicate that gliotoxin is an inducer of apoptosis via the intrinsic mitochondrial pathway.[102]

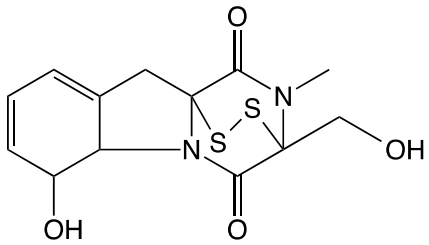

(55)

Physcion **(56)** is an anthraquinone derivative isolated from the marine-derived fungus *Microsporum* sp.[103]

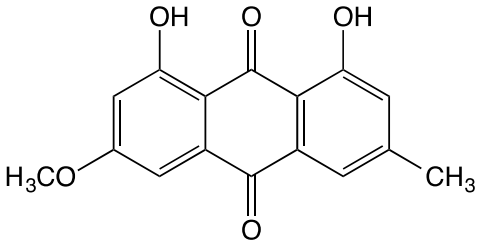

(56)

Physcion induced apoptosis in HeLa cells as demonstrated by the expression of apoptotic proteins p53, p21, BAX, Bcl-2, caspase-3 and -9. The expression of the pro-apoptotic protein BAX was up-regulated after treatment with physcion as

determined by Western blot analysis, subsequently activating the caspase-3 pathway; whilst the anti-apoptotic protein Bcl-2 was down-regulated.

These studies shared a common perspective in their approach to determining the mechanism of cell death by investigating typical apoptotic markers such as changes in cell morphology, DNA fragmentation, intracellular markers and the expression of specific apoptotic proteins.

1.5 Outline of This Study

Pterocellin A is a potent antitumour agent isolated from the marine bryozoan *P. vesiculosa. In vitro* bioactivity screening at the NCI showed promising results, however when pterocellin A was selected for *in vivo* hollow fibre assay, it was found to be ineffective.[68] To find out how pterocellin A is cytotoxic, the biochemical processes need to be understood so modification or derivatisation of the compound can be made to enhance its *in vivo* activity for clinical development.

The aim of this study is to elucidate the mechanism of cytotoxicity of pterocellin A; and to develop a systematic bioactivity screening process to be utilised for future natural product research at the University of Waikato. The objectives are: (i) identify the pathway of cell death induced by pterocellin A by assessing the characteristic markers of apoptosis and necrosis; (ii) investigate bioactive compounds from bryozoan crude extracts; and (iii) utilising the crude extracts for bioassay development.

2. Detection of Apoptosis in HeLa Cells

2.1 Introduction

Cellular toxicity can be manifested as either necrotic or apoptotic cell death. To study the cytotoxic effects of pterocellin A on HeLa cells, characteristic markers of apoptosis and necrosis were examined using various biochemical techniques. One of the characteristics of apoptosis is the ability for cells to maintain plasma membrane integrity after death. This was investigated using [3-(4,5-Dimethylthiazol-2-yl)-2,5-diphenyltetrazolium bromide] (MTT) and lactate dehydrogenase (LDH) biochemical assays, as well as using the trypan blue exclusion experiment. Distinct morphological changes characteristic of cells undergoing apoptosis were examined under the microscope and other markers such as caspase-3 activation and DNA fragmentation were also investigated.

2.2 Results

2.2.1 HeLa Cell Growth Curve

To find out the growth rate of HeLa cells under standard incubation conditions, a growth curve was plotted. The HeLa growth curve showed that the cells entered the exponential growth phase after two days, and the log phase is between day three to day six (Figure 2.1). From visual observations, cells reached 100% confluency at day six (Figure 2.2). This observation was consistent with the log phase plotted on the growth curve.

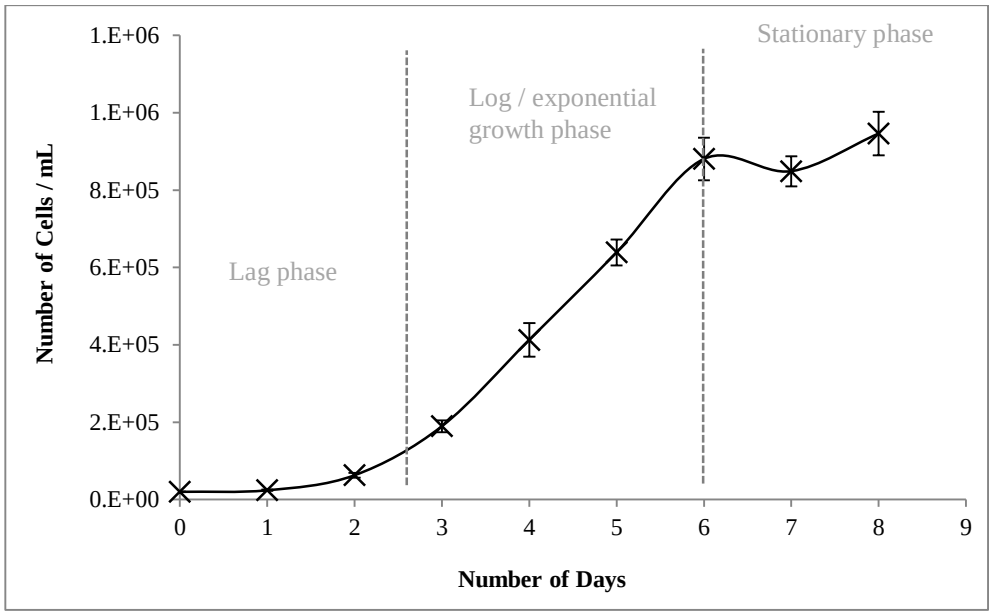

Figure 2.1 HeLa growth curve over 8 days.
Graph showing the mean cell count ± S.E.M. N = 3.

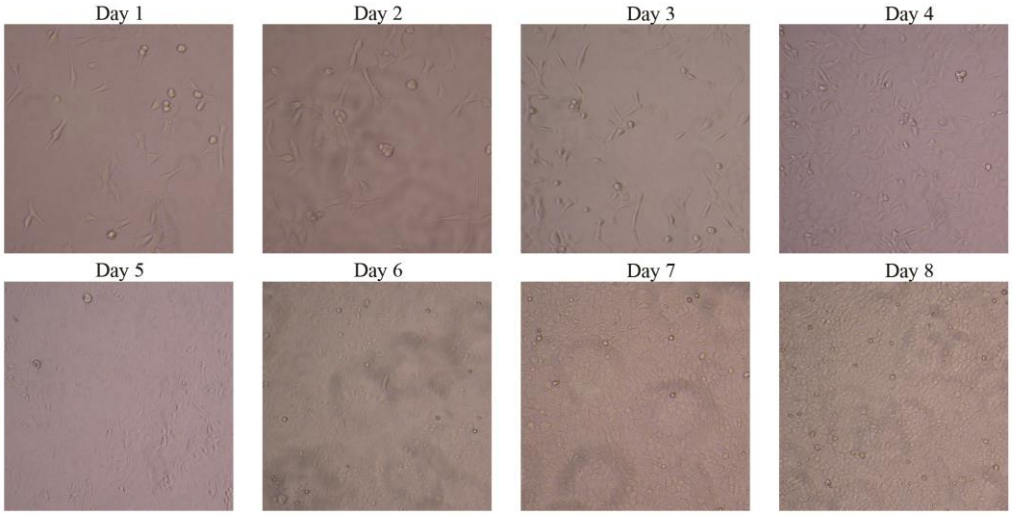

Figure 2.2 Corresponding images of HeLa cell growth curve over 8 days.
(Photos taken on an inverted Nikon eclipse TS100 microscope
at 100X magnification with a Nikon COOLPIX 4500 camera).

2.2.2 Determining Optimal Cell Counts

Preliminary MTT and LDH assays were carried out to determine the optimal number of cells to be used for each experiment. This ensured that each experiment

could be reproduced if performed under the same conditions. According to the Beer Lambert law, the absorbance of a solution is directly proportional to its concentration. Since the formazan product from the MTT assay was representative of cellular metabolic activities, the absorbance was plotted against cell densities to determine a linear working range for the MTT assay (Figure 2.3). From the graph, the linear working range for the MTT assay had a maximum cell count of $5x10^4$ cells before the relationship was no longer linear.

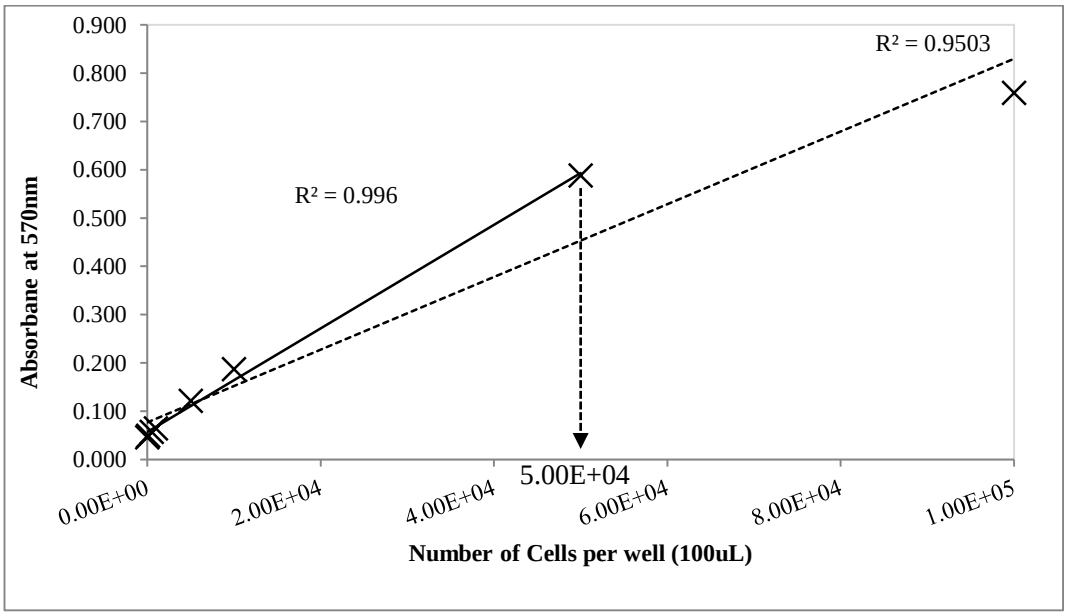

Figure 2.3 Optimal range of HeLa cell count for MTT assays.

A similar experiment was carried out for the LDH assay to determine its linear working range (Figure 2.4). It was found that the LDH assay had a much smaller linear range than the MTT assay and the maximum cell number was $1x10^4$ cells. This number was determined to be the optimal cell count as it lay within the linear range of the MTT assay also.

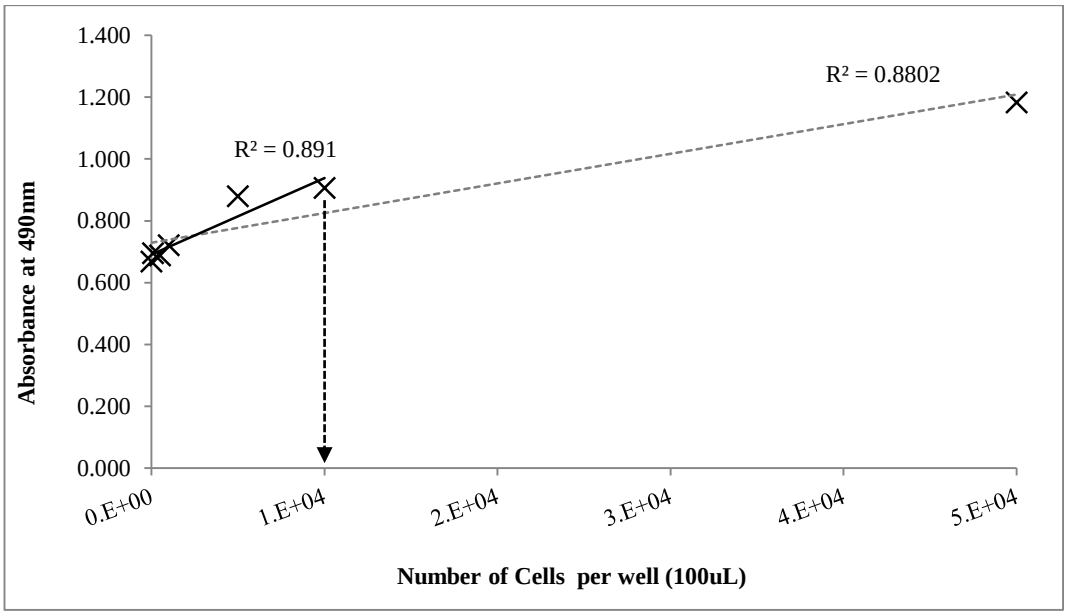

Figure 2.4 Optimum range of HeLa cell count for LDH assays.

2.2.3 Determining Experimental Conditions for Pterocellin A

Before studying the effects of pterocellin A on HeLa cells, basic experimental information was needed. This information included experimental parameters such as the incubation time, concentration range, and the experimental set up. There was no prior knowledge of such information on the HeLa cell line as previous work on pterocellin A was carried out on the P388 murine leukaemia cell line.[68] Therefore, in order to study the effects of pterocellin A on HeLa cells, an experimental protocol was developed. The first approach was to determine the concentration range and incubation period.

After 24 hours incubation, cells treated with pterocellin A at a concentration greater than 3125 ng/mL were all killed (Table 2.1). This was also the same for 48 and 72 hours incubation. The student t-test was used to determine any statistical

significance; statistically significant results were labelled with '*' ($p<0.05$) (Figure 2.5).

Table 2.1 Inhibition (%) at 24, 48 and 72 hours relative to solvent control

Concentration (ng/mL)	Mean % Relative Inhibition (to Solvent Control)		
	24 hrs	48 hrs	72 hrs
Growth Control	7.52	2.81	9.29
98	25.17	4.51	4.12
195	43.52	12.42	-3.22
391	47.09	15.92	-2.06
781	47.35	16.24	3.96
1563	78.52	60.50	83.44
3125	99.74	99.56	93.64
6250	99.96	99.84	99.50
12500	100.17	100.39	99.55

From this, it was decided that a 24-hour incubation period was sufficient for further work. The IC_{50} values for each 24, 48 and 72 hour incubation period were 886, 1175, and 1425 ng/mL respectively. Interestingly the relative inhibition of cells treated with the lower concentrations decreased over this time which attributed to the higher IC_{50} values (Figure 2.5). This suggests the cells were able to recover and overcome the cytotoxic effects of pterocellin A after a period of time. The IC_{50} value of pterocellin A on HeLa cells of 886 ng/mL was within the same order of magnitude as the IC_{50} of P388 cell line (477 ng/mL). This indicated that pterocellin A was cytotoxic against HeLa cells and that it was a good candidate cell line for this study.

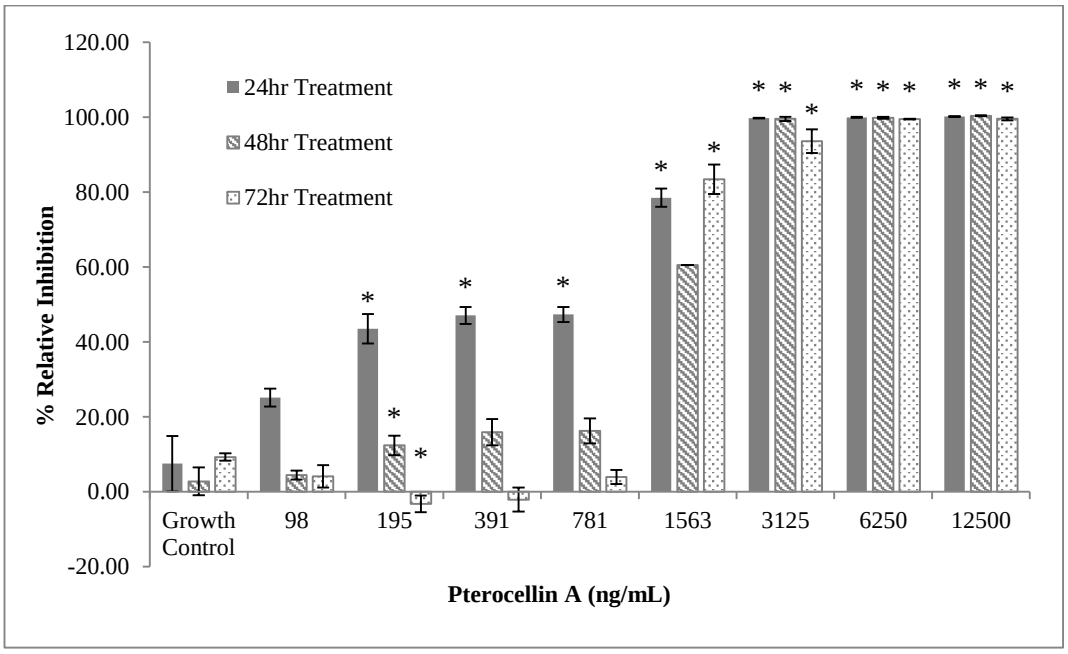

Figure 2.5 Pterocellin A toxicity against HeLa cells after 24, 48 and 72 hours treatment, MTT assay. Bar graph showing the mean ± S.E.M. * = $p < 0.05$. N = 3.

2.2.4 Membrane Integrity

Once the incubation time was chosen, an LDH assay was carried out to find out if the decrease in cell viability affected the plasma membrane integrity. A proportional increase in detected LDH to cell viability measured by MTT would suggest cell lysis upon death, and therefore a necrotic cell death.

It was found that although the level of LDH increased with higher concentration, there were variations in the calculated relative inhibition (%) between LDH and MTT assays (Figure 2.6). For example, at the lower concentration of 781 ng/mL, the calculated inhibition relative to the solvent control for the MTT assay was 30.10% (Table 2.2). However, the result for the LDH assay, calculated relative to the maximum release of LDH, was 2.41%.

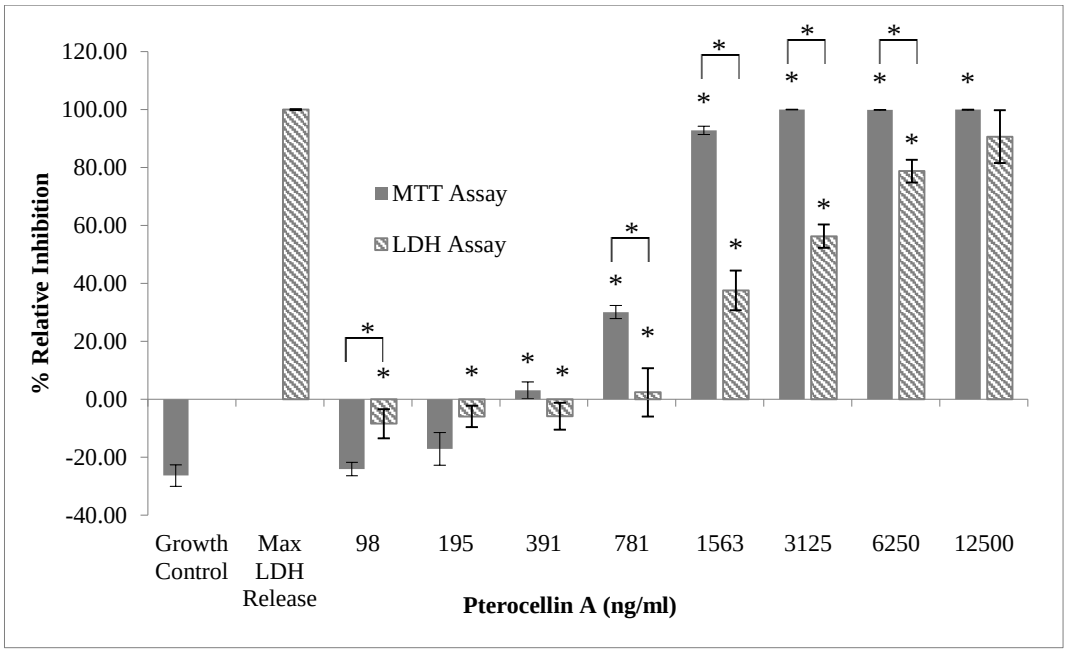

Figure 2.6 Pterocellin A toxicity against HeLa cells after 24 hours treatment, MTT and LDH assay. Bar graph showing the mean ± S.E.M. * = $p < 0.05$. N = 6.

Table 2.2 Relative Inhibition (%) by MTT and LDH assays relative to control.

Concentration (ng/mL)	Mean % Relative Inhibition (to solvent control)	
	MTT	**LDH**
Growth Control	-26.30	-
98	-24.06	-8.38
195	-17.12	-5.89
391	3.09	-5.83
781	30.10	2.41
1563	92.82	37.60
3125	99.97	56.28
6250	99.92	78.76
12500	99.94	90.66

Further experiments were carried out with a lower concentration range (Table 2.3). Based on the MTT assay, it was found that there was a steady increase in relative inhibition as the concentration increased, however the level of detected

LDH remained relatively low (Figure 2.7). All cells were killed at 2000 ng/mL after 24 hours and the amount of LDH released was 29.54%.

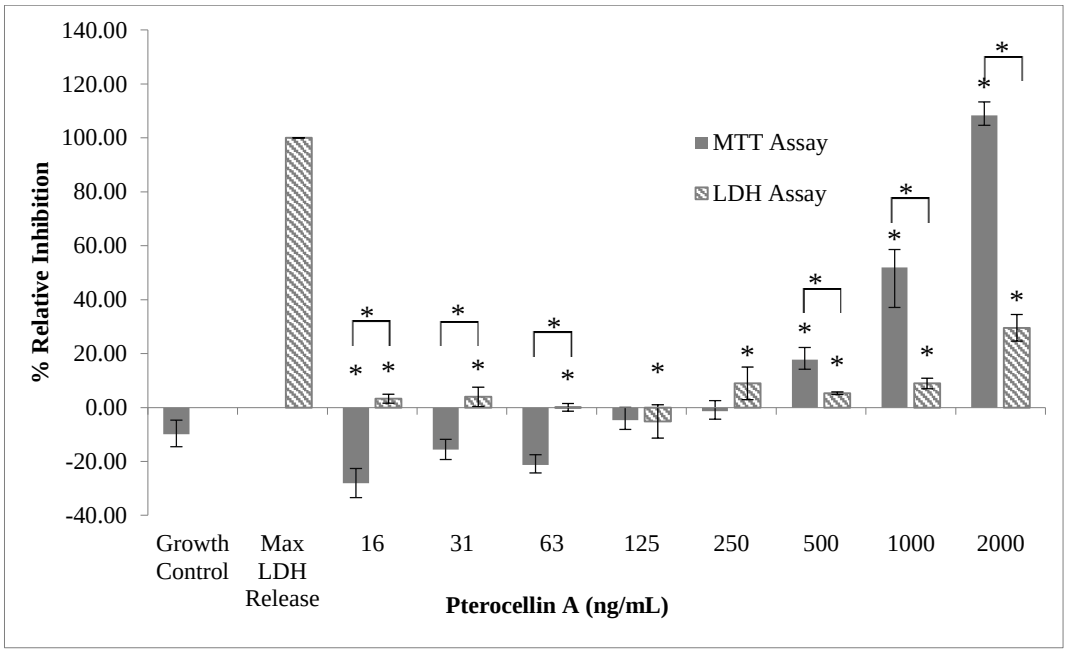

Figure 2.7 Pterocellin A toxicity against HeLa cells at 24 hours treatment, MTT and LDH assays. Bar graph showing the mean ± S.E.M. * = $p < 0.05$. N (MTT) = 12; N (LDH) = 6.

Table 2.3 Relative Inhibition (%) by MTT and LDH assays after 24 hours incubation.

Concentration (ng/mL)	Mean % Relative Inhibition (to solvent control)	
	MTT	LDH
Growth Control	-9.92	2.81
16	-28.05	3.30
31	-15.64	3.92
63	-21.30	0.07
125	-4.71	-5.19
250	-1.31	8.94
500	17.76	5.30
1000	51.89	8.92
2000	108.31	29.54

Time-course experiments at 3, 6 and 12 hours were carried out to determine the time at which the cytotoxic effects of pterocellin A began to affect HeLa cells. At the highest concentration (2000 ng/mL), cells started being affected after just 3 hours (Table 2.4), with no detectable LDH release. Similar observations were made after 6 hours (Figure 2.8, Figure 2.9, Table 2.5).

Table 2.4 Relative Inhibition (%) by MTT and LDH assays after 3 hours incubation.

Concentration (ng/mL)	Mean % Relative Inhibition (to solvent control)	
	MTT	LDH
Growth Control	-0.22	-
16	-10.83	-10.79
31	-14.01	-8.26
63	-21.40	-13.45
125	-14.91	-16.78
250	-16.80	-17.98
500	-12.36	-19.31
1000	-5.10	-16.42
2000	21.51	-14.25

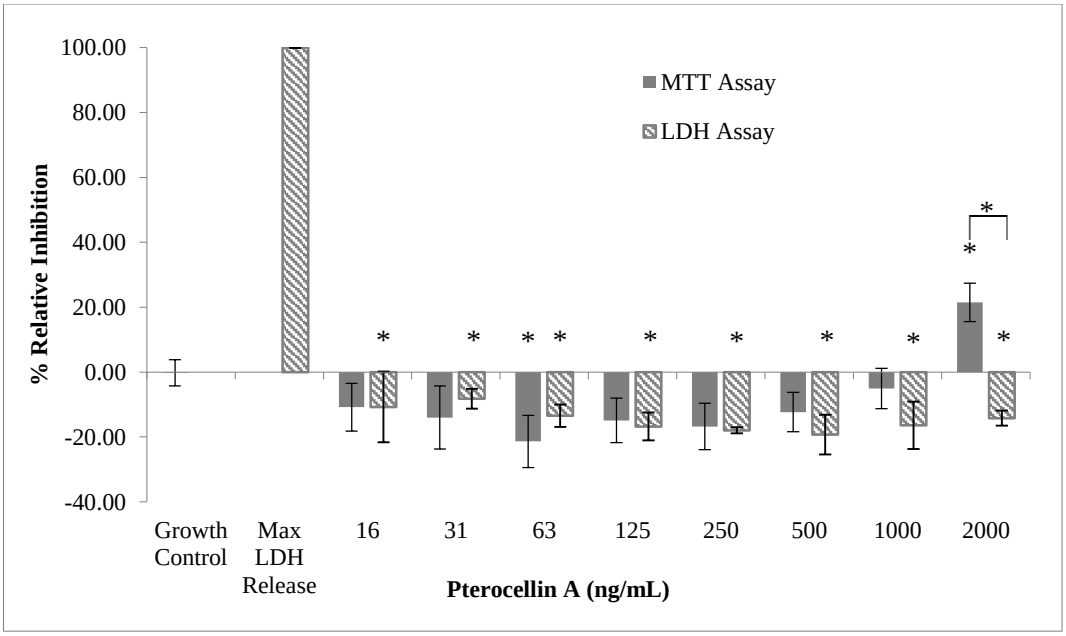

Figure 2.8 Pterocellin A toxicity against HeLa cells at 3 hours treatment, MTT and LDH assays. Bar graph showing the mean ± S.E.M. * = $p < 0.05$. N (MTT) = 9; N (LDH) = 3.

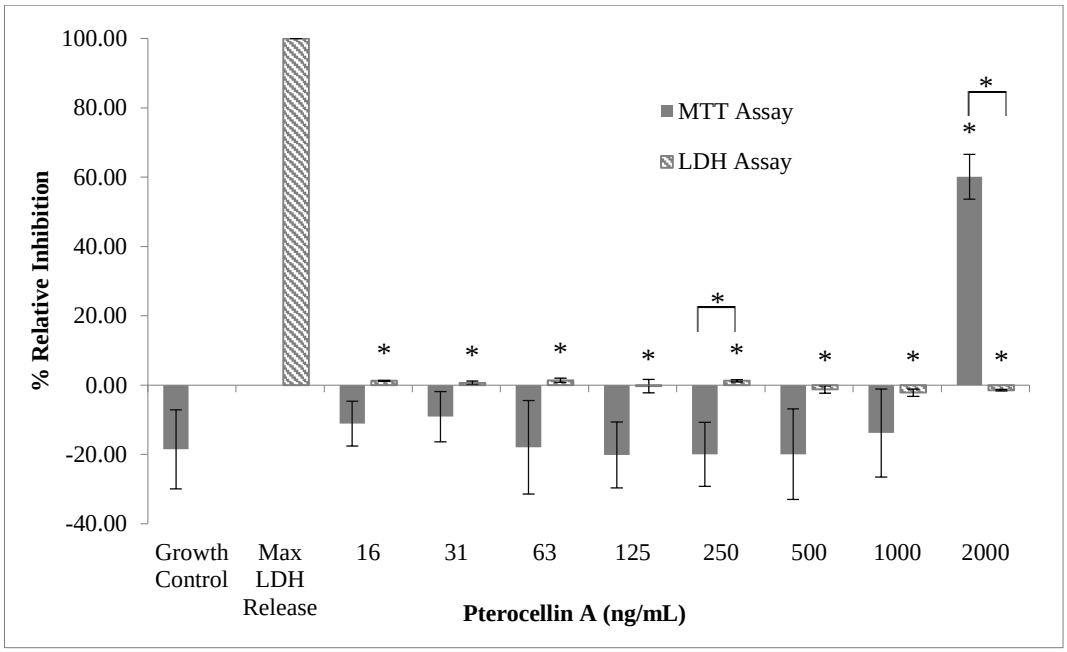

Figure 2.9 Pterocellin A toxicity against HeLa cells at 6 hours treatment, MTT and LDH assays. Bar graph showing the mean ± S.E.M. * = $p < 0.05$. N (MTT) = 9; N (LDH) = 6.

Table 2.5 Relative Inhibition (%) by MTT and LDH assays after 6 hours incubation.

Concentration (ng/mL)	Mean % Relative Inhibition (to solvent control)	
	MTT	LDH
Growth Control	-18.51	-
16	-11.12	1.25
31	-9.07	0.65
63	-17.93	1.40
125	-20.13	-0.32
250	-19.97	1.25
500	-19.92	-1.25
1000	-13.80	-2.18
2000	60.14	-1.45

It was found that after 12 hours, the relative inhibition of cells treated with 1000 ng/mL was 39.39% while that of cells treated with 2000 ng/mL was 87.88% inhibition (Table 2.6). The level of LDH increased slightly at approximately 20%

at these concentrations, however it did not correlate with the relative inhibition values by MTT (Figure 2.10).

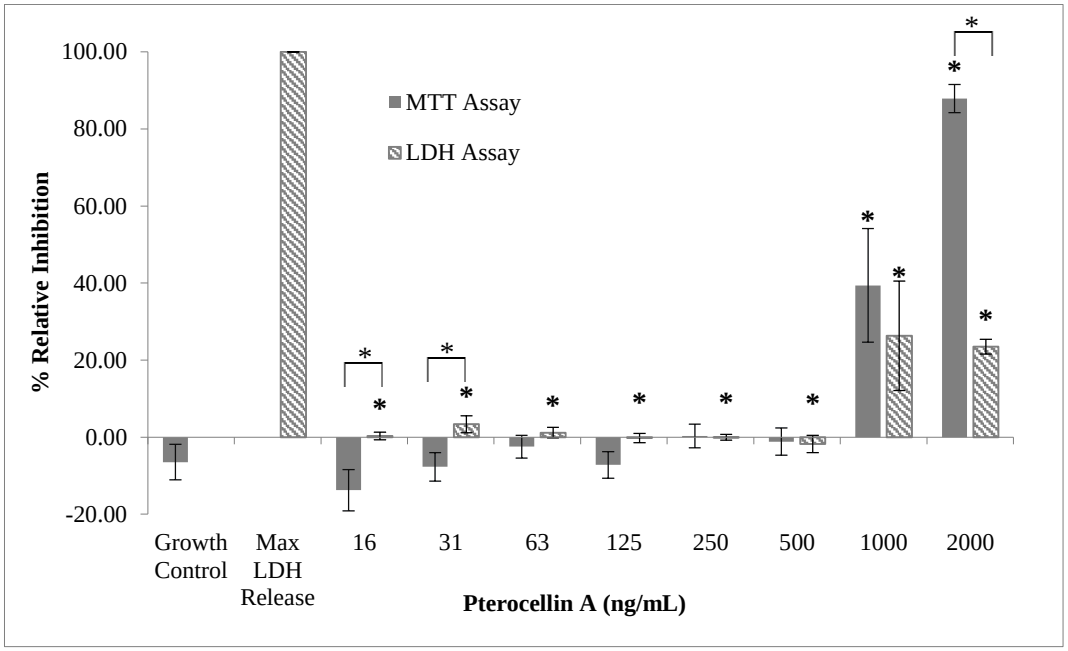

Figure 2.10 Pterocellin A toxicity against HeLa cells at 12 hours treatment, MTT and LDH assays. Bar graph showing the mean ± S.E.M. * = $p < 0.05$. N (MTT) = 9; N (LDH) = 6.

Table 2.6 Relative Inhibition (%) by MTT and LDH assays after 12 hours incubation.

Concentration (ng/mL)	Mean % Relative Inhibition (to solvent control)	
	MTT	LDH
Growth Control	-6.48	-
16	-13.75	0.28
31	-7.69	3.36
63	-2.46	1.15
125	-7.20	-0.21
250	0.29	-0.01
500	-1.15	-1.76
1000	39.39	26.32
2000	87.88	23.48

2.2.5 Trypan Blue Exclusion

A basic trypan blue exclusion cell count can distinguish between dead and live cells. Stained cells observed under the microscope would indicate a cell with a compromised plasma membrane. A trypan blue exclusion cell count was carried out after treating cells with different concentrations of pterocellin A for 24 hours. The calculated results are shown in Table 2.7. It was found that no stained cells were observed after treatment. The cell number steadily decreased as the concentration of pterocellin A increased (Figure 2.11).

Table 2.7 Trypan blue exclusion results and calculations

Trypan blue 24 hr Treatment	Cell Count	Mean % Relative Viability	Mean % Stained (dead) Cells
Solvent Control	2.75E+05	100.00	0.00
Growth Control	2.88E+05	111.67	0.00
62.5	2.48E+05	91.67	0.00
125	2.72E+05	103.53	0.60
250	2.45E+05	94.57	0.00
500	1.85E+05	71.45	0.81
1000	9.17E+04	35.45	0.00
2000	1.67E+03	0.56	0.00

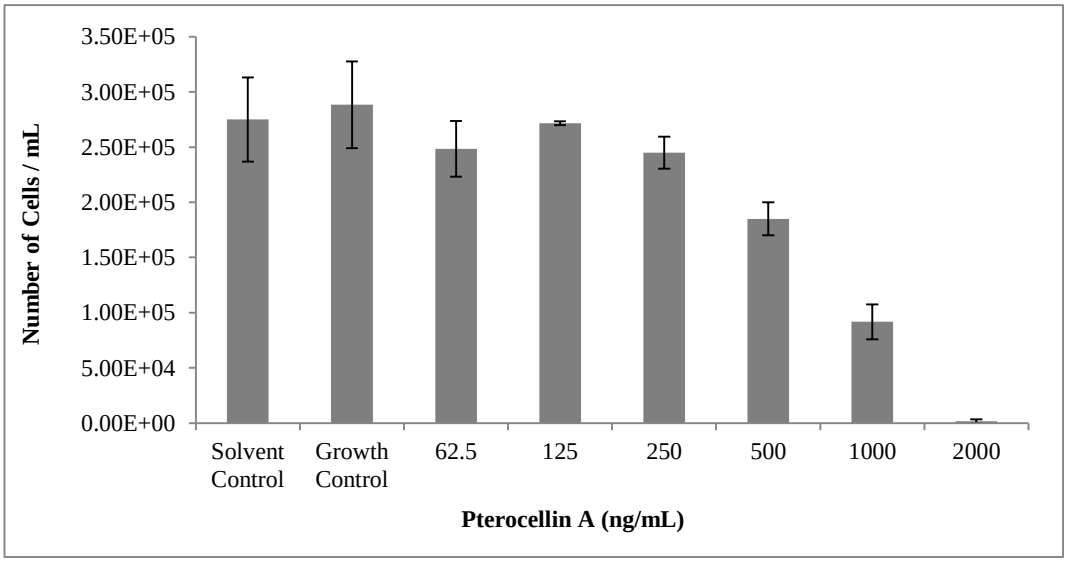

Figure 2.11 Trypan blue exclusion cell count after 24 hour treatment.
Bar graph showing the mean ± S.E.M. N = 3.

2.2.6 Changes in Cell Morphology

Changes in cell morphology were observed after treatment with pterocellin A. Figure 2.12 shows the images of cells treated by different concentrations of pterocellin A taken at the end of each incubation period.

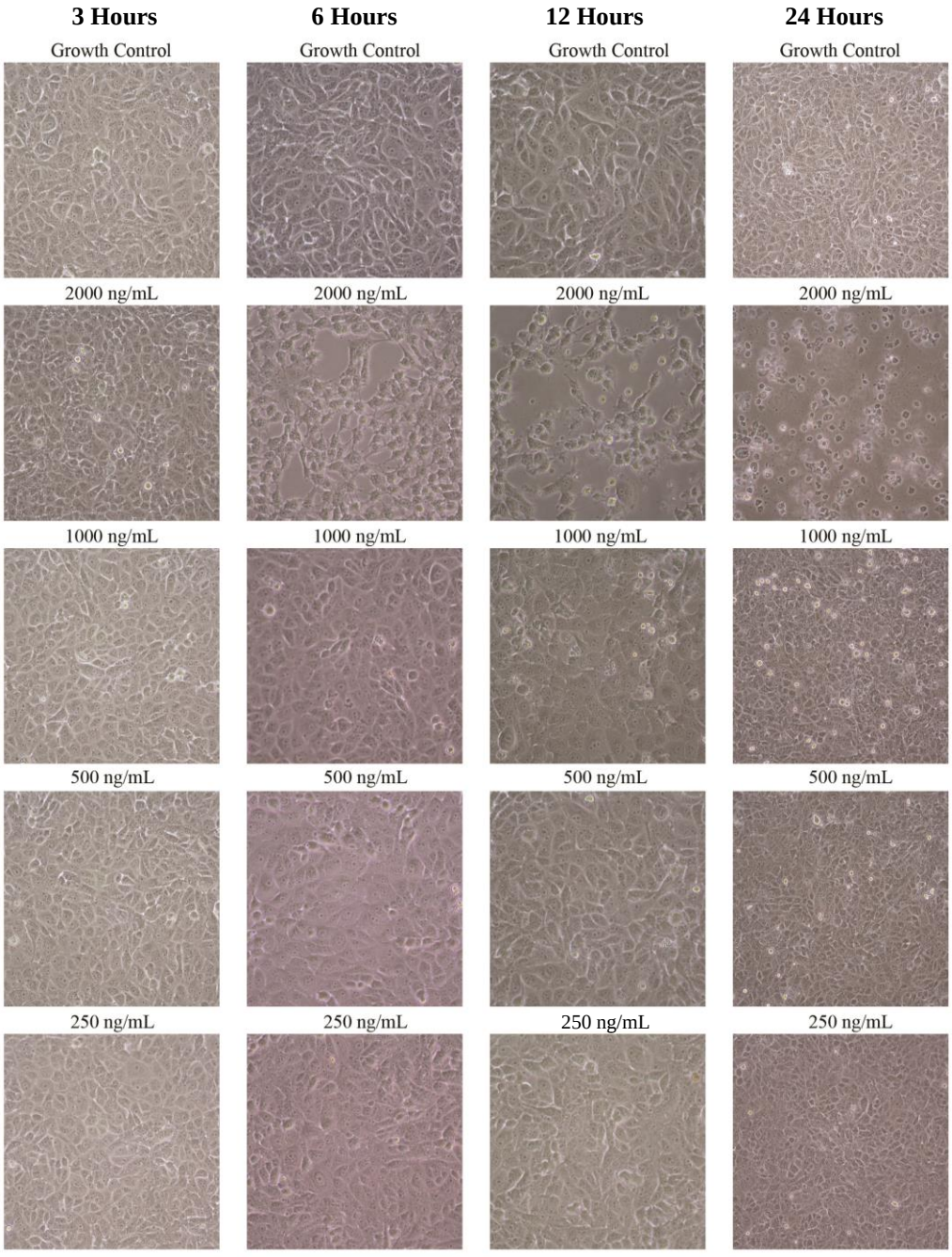

Figure 2.12 Images of cells treated at different concentrations of pterocellin A at different times. (Photos taken at 200X magnification using an inverted Nikon eclipse TS100 microscope with a Nikon COOLPIX 4500 camera.)

The morphology of the cells started to change after 6 hours of incubation from 1000 ng/mL. At the highest concentration (2000 ng/mL), the changes in cell morphology were obvious. Compared to the normal cells which appeared elongated and had contact with neighbouring cells, cells treated with pterocellin A appeared to have lost the contact and became round. The nuclei became condensed and were no longer visible. Cells also appeared more three-dimensional, and membrane blebbing, a characteristic of cells undergoing apoptosis could be seen. Some cells appeared to be 'shrinking' and apoptotic 'spikes' were also observed. After 24 hours treatment, cells were completely detached.

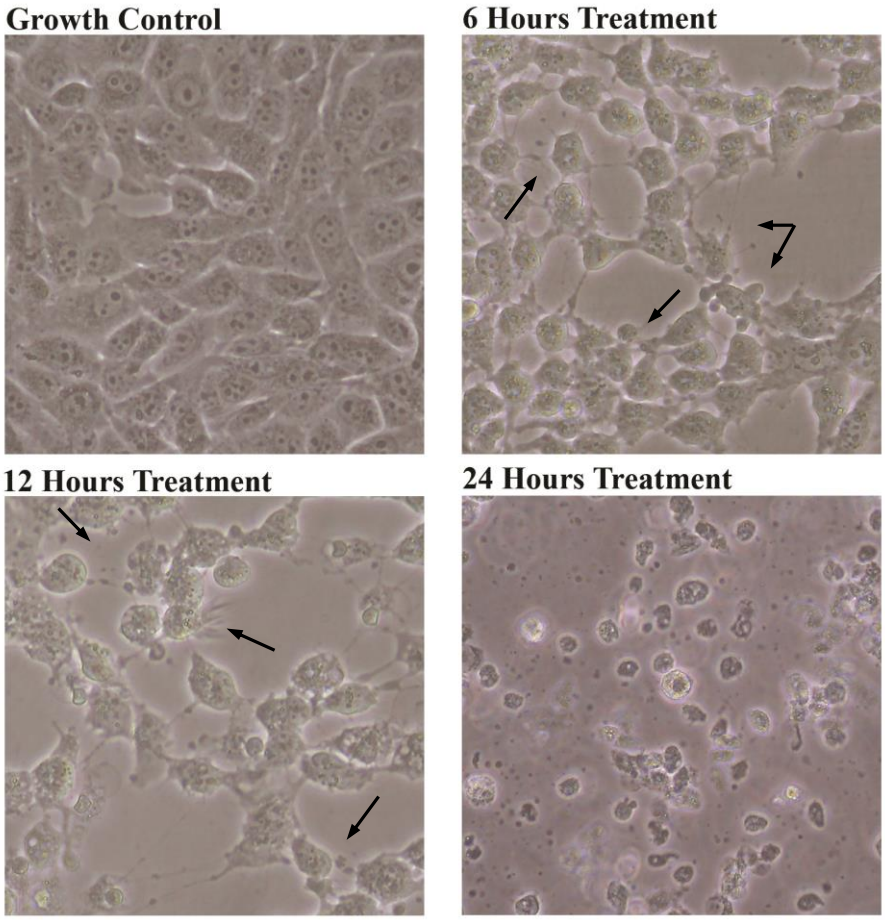

Figure 2.13 Changes in cell morphology after treatment with pterocellin A at 2000 ng/mL. Black arrows pointing at examples of apoptotic features. (Photos taken at 200X magnification using an inverted Nikon eclipse TS100 microscope with a Nikon COOLPIX 4500 camera.)

The presence of apoptotic cells was evident when observed under differential interference contrast (DIC) of a confocal microscope. Figure 2.14 shows cells undergoing late stage apoptosis; the membrane blebbing is clearly visible. A series of time-lapse photos was taken of a single cell undergoing apoptosis. Each image shows the movement of the apoptotic blebs.

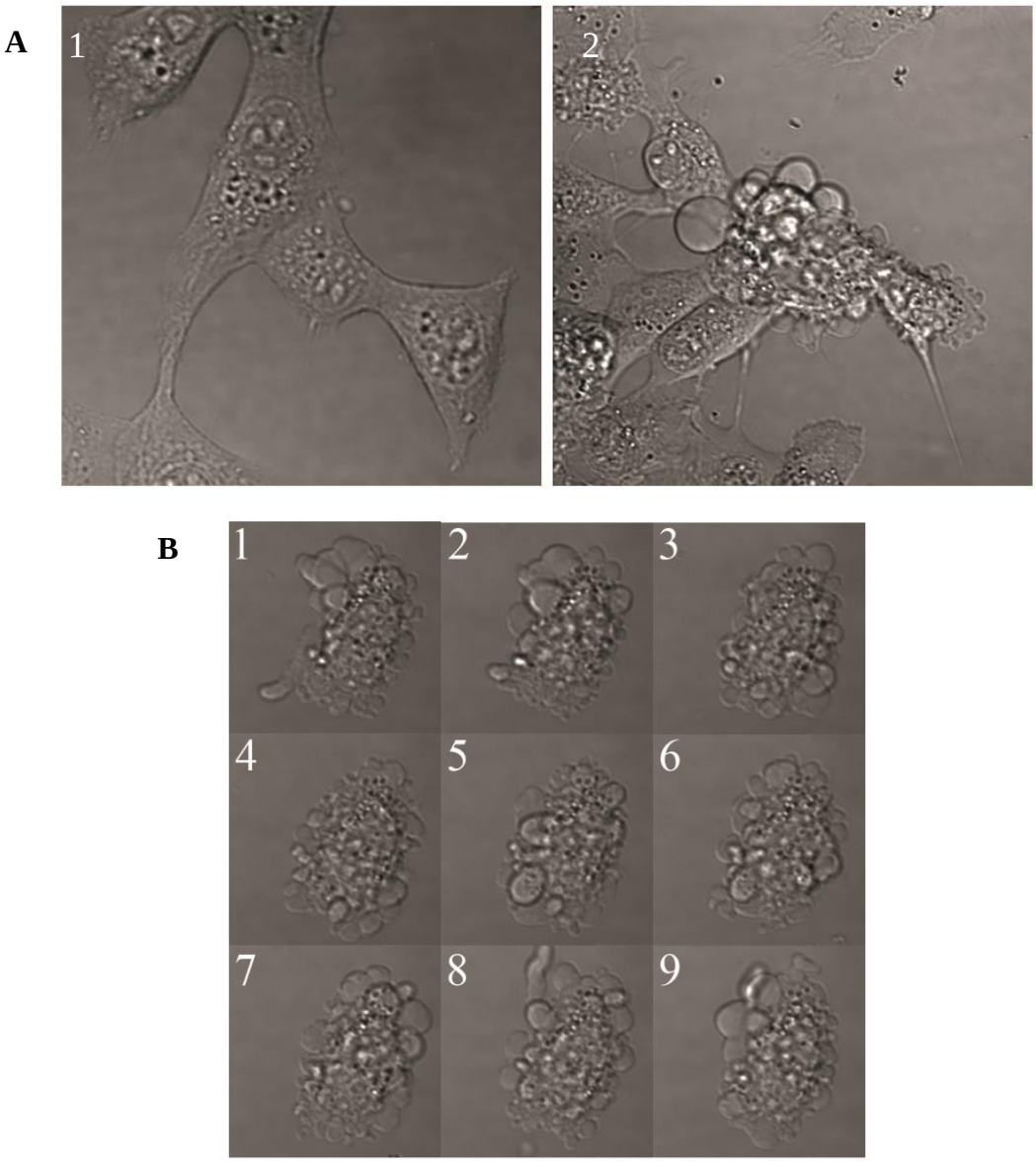

Figure 2.14 DIC images of a single apoptotic cell from the same experiment. **(A).** 1. Growth control. 2. Cells treated at 1000ng/mL for 6 hours. **(B).** 1-9. Timelapse images of membrane blebbing of a single cell undergoing apoptosis. (Photos were obtained from an Olympus FV1000 confocal microscope at 400X magnification.)

2.2.7 Changes in Mitochondria Morphology and Location

To investigate the effects of pterocellin A on mitochondria, cells were stained with MitoTracker Red CMXRos and visualised by a laser confocal fluorescent microscope. MitoTracker Red CMXRos is a membrane-permeable fluorescent dye used to label mitochondria. It contains a mildly thiol-reactive chloromethyl moiety that reacts with thiol groups of the proteins in the mitochondria.[104]

To determine the staining concentration, normal cells grown in a fluoro dish (WPI) were first stained with 100 nM MitoTracker Red CXRos, however non-specific staining was observed. The cells were then stained with 50 nM MitoTracker Red CMXRos to achieve specific staining of the mitochondria only with no background staining.

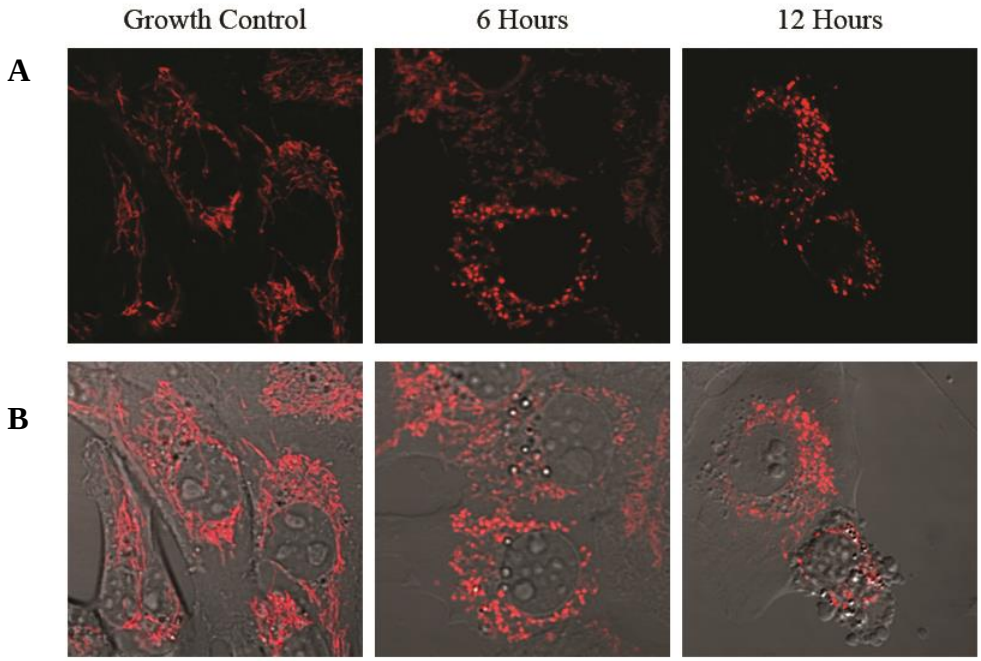

Figure 2.15 Changes in mitochondrial morphology after pterocellin A treatment at 1000ng/mL after 6 and 12 hours.
(A). Mitochondria stained with 50nM MitoTracker Red CMXRos (Em. 599 nm).
(B). Overlay of stained mitochondria and phase contrast images. Photos obtained from the Olympus FV1000 laser scanning confocal microscope at 400X magnification.

After treatment with pterocellin A (1000 ng/mL), the location of mitochondria re-distributed from the cell cytoplasm to the peri-nuclear region after six hours. This localisation took place before any notable changes in cell morphology and cell death as shown in the overlay images. Compared to healthy mitochondria that have an elongated tubular formation, the mitochondria of treated cells appeared to be fragmented and 'swollen' or 'grain-like' (Figure 2.15).

2.2.8 Caspase-3 Activation

The activity of caspase-3 was measured by FITC fluorescent staining. The original manufacturer's protocol was adapted and modified for adherent HeLa cells. The fold-increase calculation was based on blank-corrected samples. Although the change in fluorescence between control and treatment seemed minimal, the change was more noticeable after each sample was blank corrected. Cells treated with pterocellin A (at both 500 ng/mL and 1000 ng/mL) had an approximate 2.5-fold increase in caspase-3 activity compared to the control (Figure 2.16).

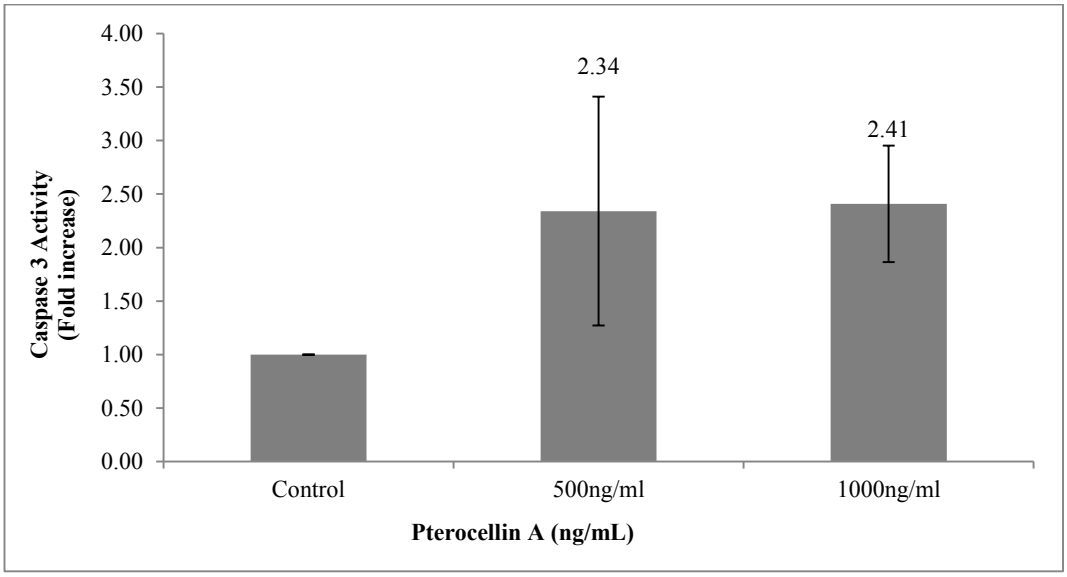

Figure 2.16 Caspase-3 activity of treated cells compared to control.
Bar graph showing the mean ± S.E.M. N = 6.

However due to the small sample size the results were not statistically significant with the p values greater than 0.05. Cells were also visualised under the fluorescent microscope with a FITC filter, however fluorescence in treated cells could not be observed.

2.2.9 DNA Fragmentation Studies

Many attempts were made to visualise any DNA fragmentation from apoptotic cells. The first attempt to extract genomic DNA using the TRIzol reagent according to the manufacturer's protocol was unsuccessful and the quality of DNA was poor when measured on a NanoDrop 2000 spectrophotometer (NanoDrop). The NanoDrop measures the amount of DNA which has a peak absorbance at 260 nm; it can detect impurities such as phenol or protein contaminations which have peak absorbance at 270 nm and 280 nm respectively. The ideal ratio should be above 1.8, however the NanoDrop readings for the TRIzol extractions were very low, ranging from 1.48 to 1.69. This suggested either phenol or protein contamination in the sample. When the samples were analysed on an agarose gel, the DNA bands did not move beyond the well which suggested large molecules of proteins trapped in the wells of the agarose gel. Attempts to remove the contamination by a proteinase-K digest and re-precipitation of the DNA were also unsuccessful.

The second attempt was to extract DNA using the Quick-gDNA™ MiniPrep Kit (Zymo). The quality of DNA improved dramatically with improved NanoDrop

readings closer to the ideal ratio of 1.8. However, when the extracted DNA was visualised on a 2% agarose gel, no fragmentation could be seen (Figure 2.17).

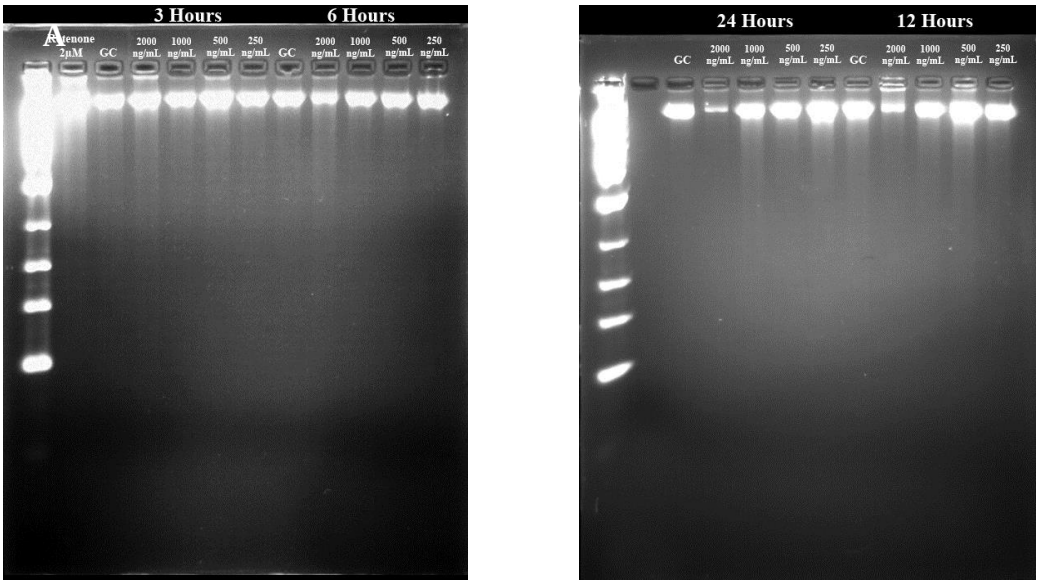

Figure 2.17 Genomic DNA visualised on a 2% agarose gel, run at 35 V for 4 hours. **(A, B)** DNA extracted at different treatment concentrations at various time points using the Quick-gDNA™ MiniPrep DNA Extraction Kit (Zymo).

A positive control was included with cells treated with rotenone (2 µM), a known inducer of apoptosis in HeLa cells.[105] However, no DNA laddering could be seen in this either.

Another attempt was made to extract the genomic DNA from treated cells. The experiment was up-scaled by growing cells in a T-25 culture flask instead of a 6-well plate. This was to ensure that a sufficient amount of DNA was extracted. Cells were treated with 2000 ng/mL pterocellin A for 3 and 6 hours, and 1000 ng/mL for 24 hours. Another batch of cells was treated with rotenone (5 µM) and the DNA was extracted at each time point. One flask of cells was starved for 24 hours, and grown in DMEM with no FBS. DNA was then extracted and visualised on an agarose gel (2% agarose, 35 V). Unfortunately, due to the pre-existing

loading dye in the DNA Suspension Buffer, NanoDrop readings could not be obtained even after blanking with the solution. A faint ladder was finally observed in Lane 3 (Figure 2.18, A) in cells treated with 2000 ng/mL pterocellin A for 6 hours.

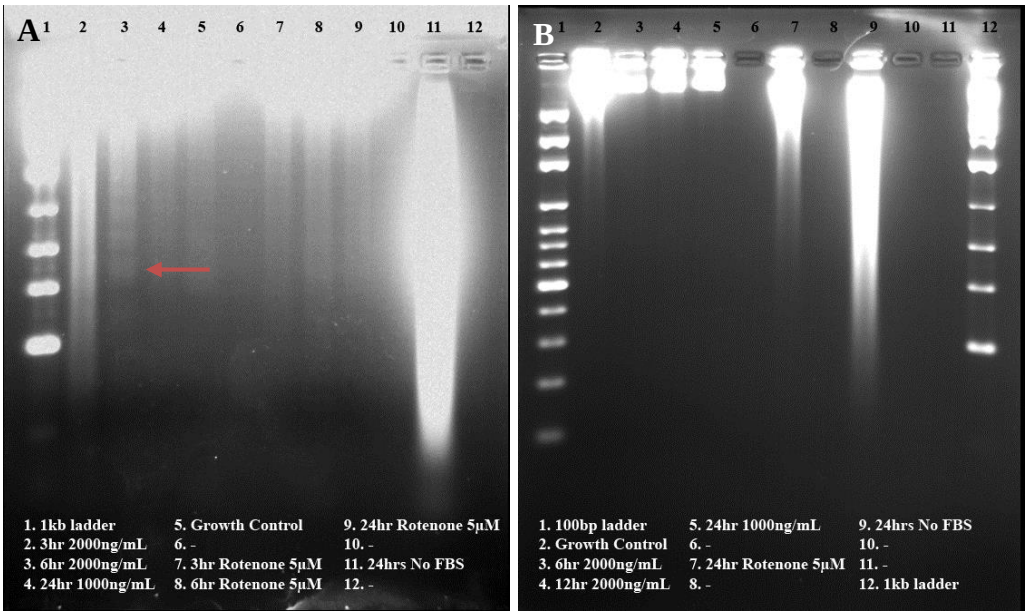

Figure 2.18 Genomic DNA visualised on a 2% agarose gel, run at 35 V for 4 hours. **(A, B).** DNA extracted at different treatment concentrations at various time points using the Apoptotic DNA Ladder Detection Kit (Abcam). Red arrow in **(A)** showing faint laddering in lane 3.

No laddering could be seen in other lanes, including the positive rotenone positive control. When the experiment was repeated again with an added 12-hour time point, the laddering effect could no longer be seen.

In order to assess whether rotenone was the right candidate for a positive apoptosis control, images of each flask were taken before and after treatment to compare morphology changes between pterocellin A and rotenone treated cells. The changes in morphology of rotenone treated cells can be seen in Figure 2.19 after 24 hours, and apoptotic bodies were also present.

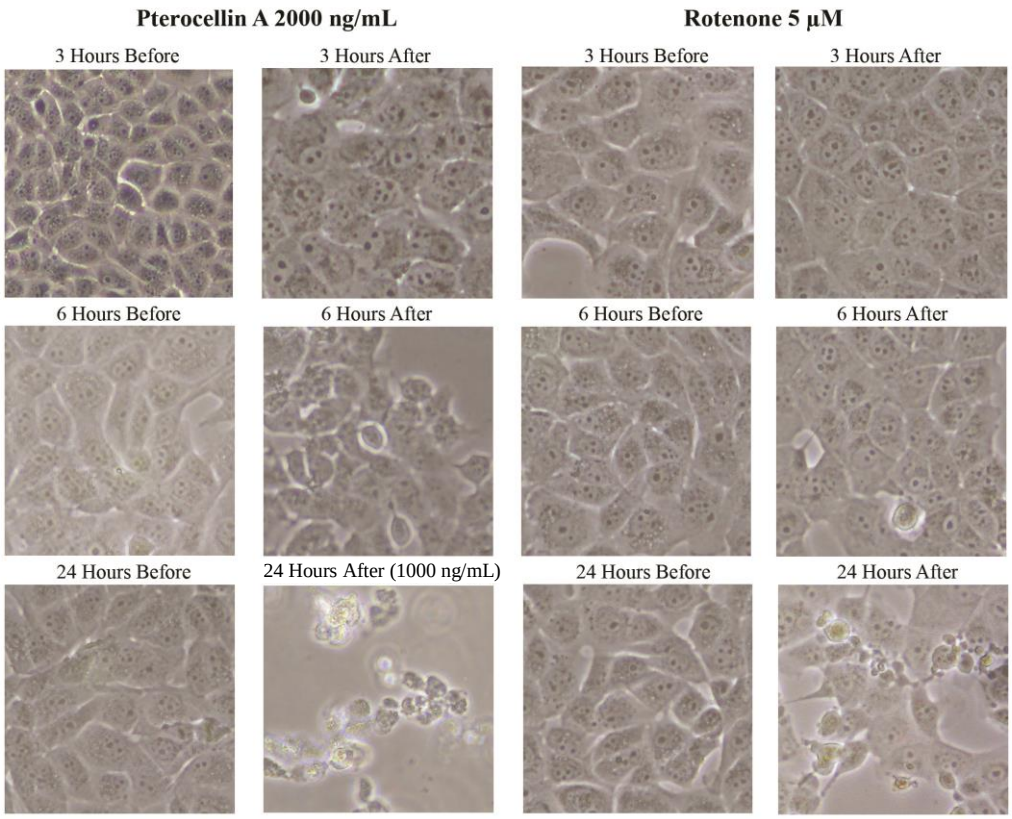

Figure 2.19 Comparison of cell morphology between cells treated with pterocellin A and rotenone. (Photos taken at 200X magnification using an inverted Nikon eclipse TS100 microscope with a Nikon COOLPIX 4500 camera.)

MTT and LDH assays were also carried out to see if there was any loss in membrane integrity. It was found that cells maintained membrane integrity in rotenone treated cells. Cells treated with pterocellin A only had a slightly elevated level of LDH after all cells were killed, which was consistent with experiments mentioned in Section 2.2.4. It is interesting to note that the cytotoxicity of pterocellin A seems to be more potent than that of rotenone. This combined with the apoptotic cells observed after treatment indicated that rotenone was indeed an apoptotic inducer. However for unknown reasons, no DNA laddering was observed despite various attempts.

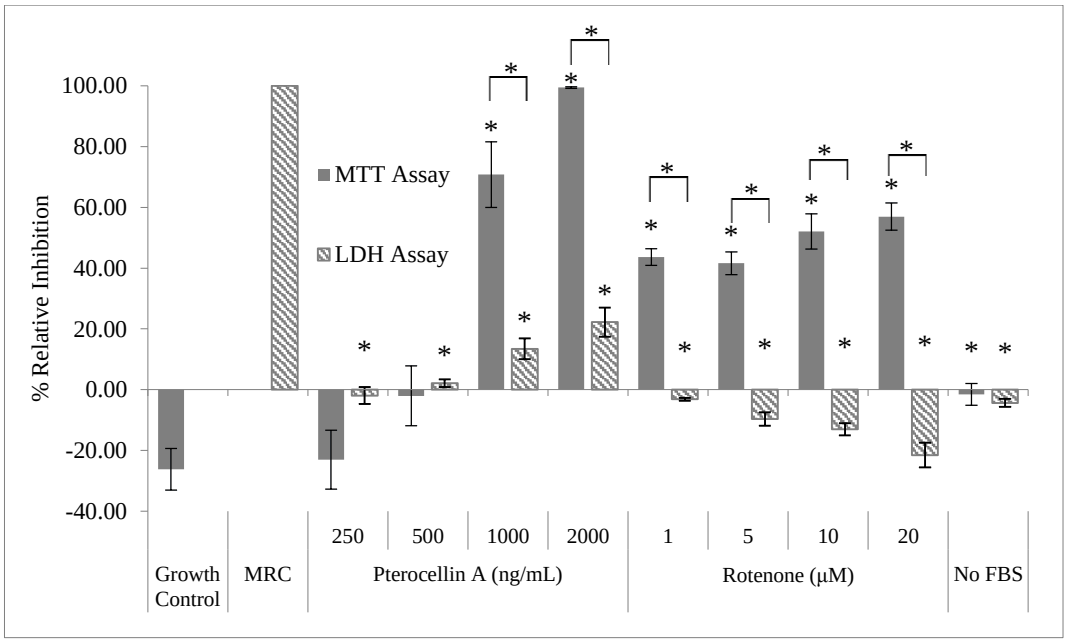

Figure 2.20 Pterocellin A and rotenone toxicity after 24 hours treatment by MTT and LDH. Bar graph showing the mean ± S.E.M. N = 3.

2.3 Discussion

The objective of this section of the study was to elucidate the mechanism of cytotoxicity induced by the antitumour metabolite pterocellin A against HeLa cells. In order to assess the mechanisms of cell death, a number of detection methods were utilised to determine whether the HeLa cells were undergoing apoptosis or necrosis in the presence of pterocellin A.

A number of MTT and LDH assays were performed during this study. The MTT assay was used to determine the cell viability after treatment with pterocellin A. The MTT cell viability assay measures the reduction of MTT, a water-soluble tetrazolium dye, to insoluble formazan crystals. This reduction reaction is dependent on the activity of functioning cellular dehydrogenases in living cells, thus is an indicator of cell viability and mitochondria activity.[106] The LDH assay

is a colorimetric assay that detects the loss of cell membrane integrity by measuring the release of cytosolic enzyme LDH into extracellular space upon cell lysis. Similar to the MTT assay, the LDH assay involves the enzymatic conversion of a tetrazolium salt, INT [2-(4-iodophenyl)-3-(4-nitrophenyl)-5-phenyl-2H-tetrazolium chloride], into a water-soluble red formazan product. The amount of colour formation is proportional to the amount of cell lysis.[92]

Initial experimental data showed that pterocellin A affected cell viability significantly ($p<0.05$) within 24 hours of treatment in HeLa cells. A longer treatment period did not increase the cytotoxicity, as 100% of the cells were no longer viable at concentrations above 3125 ng/mL. Interestingly, cells that survived the first 24 hours at the lower concentration range had lower relative inhibition values after 48 and 72 hours as demonstrated by the IC_{50} values. This suggests that the cells were able to proliferate and overcome the cytotoxic effects after the first 24 hours. It was not known how the cells had the ability to adapt and overcome the cytotoxicity after prolonged exposure; perhaps it could be due to an up-regulation in the expression of the multi-drug resistant gene and associated proteins such as P-glycoprotein.[107] It would be interesting for future research to carry out dose-response studies on HeLa cells treated with low concentrations of pterocellin A and examine the expression of proteins associated with multi-drug resistance.

The first evidence that suggested that the cells were undergoing apoptosis was demonstrated by the difference in the relative inhibition from the MTT and LDH assays. These assays showed that after 24 hours, all cells were killed at 2000 ng/mL according to the MTT data and also by visual observation. However, the

LDH data showed only a small increase in the level of detected LDH. The elevated LDH was likely due to a process known as secondary necrosis which occurs when the apoptotic cells have died but were not eliminated.[108] It would have been ideal to utilise annexin-v/PI staining by FACS in this project to distinguish between apoptosis and primary necrosis, however this was not done due to limited resources and time constraints. It would definitely be of interest in future cell death studies to utilise this method for detecting early stages of apoptosis.

In order to investigate apoptosis, a timeline would need to be established to ensure the experiments were carried out at the right time. Time-course experiments of pterocellin A showed that changes in HeLa cells after exposure to pterocellin A were detectable in just over three hours. Although visually the cell morphology displayed no change, detectable changes were observed in the MTT data. Since MTT is also an indicator of mitochondrial function, this suggests that there was a degree of mitochondria impairment attributed to the cytotoxicity of pterocellin A. Elevated LDH release was only apparent after 12 hours treatment at 2000 ng/mL when the cells were almost 90% inhibited. This further suggests that secondary necrosis took place to some extent after the apoptotic cells had already died.

The trypan blue exclusion experiment indicated that neighbouring cells were indeed taking up apoptotic cells after death as no cells were observed in the cell count, even after collecting supernatant during harvest. However, when observed under the microscope straight after treatment, cell debris could be seen floating in culture medium after 24 hours. These were just cell debris and not intact dead cells, as they did not show up during the trypan blue exclusion cell count.

Presence of cell debris indicated that some degree of cell lysis took place in the form of secondary necrosis after apoptotic cells have died.

Further evidence of HeLa cells undergoing apoptosis after exposure to pterocellin A was the morphological changes observed. After six hours treatment at 2000 ng/mL, it became obvious when observed under the microscope that cells were affected by the cytotoxicity. Treated cells were no longer attached to their neighbouring cells compared to the control, the nucleus was no longer visible and the cells also appeared to 'shrink'. This shrinking was due to condensation of the nucleus, another character of apoptosis. Additionally, apoptotic spikes and membrane blebbing were also observed within six hours of treatment. Time-lapse images taken under DIC on a confocal laser microscope displayed movement of the apoptotic blebs as the cells underwent apoptosis.

The MitoTracker staining of the mitochondria showed that the mitochondrial morphology changed after six hour of treatment. In healthy cells, the mitochondria appear elongated and filamentous; after exposure to pterocellin A, distinct changes were observed under a confocal laser microscope. Mitochondria are normally distributed throughout the cytoplasm, however it was found that the mitochondria redistributed from the cell periphery and localised around the nucleus after treatment with pterocellin A. This change took place before changes in cell morphology were observed. The overlay images showed that at 1000 ng/mL after six hours, the cells still appeared normal compared to the control, however changes in the mitochondria were obvious. This concentration was chosen for the ease of preparation and it was not too much higher than the IC_{50} value of 886 ng/mL. The individual morphology of the mitochondria went from

an elongated and filamentous appearance to spherical and ‘swollen’; it can also be described as a thread-grain transition.[109] These changes in the location and morphology of the mitochondria have been reported in the literature including in HeLa cells during UV-induced apoptosis and in pig kidney (PEK) cells after treatment with rotenone, an inhibitor of the respiratory complex I.[109-113] It was also found that the thread-grain transition occurred after the release of cyt *c* from the mitochondria upon induction of apoptosis.[110] These distinct morphological changes further supported the idea that pterocellin A was an inducer of apoptosis in HeLa cells.

It is hypothesised that pterocellin A could be acting on the mitochondria via the intrinsic pathway, however due to the complex nature of the signalling cascades, it is not yet known how the compound enters the cell and which pathway it is interacting with. Out of all the pterocellins, only those with no substitution at position 8, such as pterocellins A and B, exerted the highest antitumour activity against P388 cells. It could be that the biological interaction of pterocellins is size-dependent. The backbone ring structure could be intercalating with DNA and prompting apoptosis. It is also possible that if pterocellin A is able to target and enter the mitochondria, the mitochondrial DNA (mtDNA) could be more susceptible to damage due to the lack of histone proteins that are normally present in nuclear DNA as regulatory proteins.[114] However, until further information is available it is difficult to make such assumptions. Discussions on future research can be found in Chapter Five.

Another piece of evidence supporting this was the activation of caspase-3 detected after treatment by pterocellin A in HeLa cells. Activated caspase-3 is only present

upon the induction of apoptosis. Upon treatment by pterocellin A, the level of activated caspase-3 increased by approximately two-fold. However due to time constraint the caspase-3 assay was only performed after 24 hours incubation. It would have been ideal to carry out the assay on a time-course like the MTT and LDH assays.

Despite the other evidence pointing towards apoptosis as the mechanism of cell death, one of the most well-known characteristics of apoptosis, DNA fragmentation, could not be detected using 2% agarose gel-electrophoresis. DNA extractions were carried out after treatment on a time-course and a positive control of a known inducer of apoptosis, rotenone, was used in these experiment. Unfortunately, there was no success at visualising the laddering effect from DNA fragmentation. Different extraction methods were carried out as it was initially thought that using the spin-column DNA extraction kit (Zymo) might have washed away the small fragments of DNA. However even with the other extraction kit (Abcam), no obvious laddering could be seen. Interestingly, after many attempts to visualise the DNA ladder, a very faint ladder was observed after six hours treatment by pterocellin A at 2000 ng/mL only after over-exposure of the agarose gel. However this was only visible in one sample and not in the others, including the positive rotenone control. A repeat was carried out in an attempt to visualise this again but was not successful. It was unknown whether this was due to experimental errors, or whether there are some unknown underlying biochemical mechanisms affecting the detection of DNA fragmentation. Internucleosomal DNA fragmentation is a late event of apoptosis and has been found not to be essential in the execution of apoptosis. Furthermore, it has been found that difference cell types have different susceptibility to DNA

laddering despite similar responses in the cell viability assays so this could likely be the case in this study.[95, 115-116]

The gathered evidence to now support the notion that pterocellin A is an inducer of apoptosis in HeLa cells. The presented evidence includes the retainment of plasma membrane integrity upon cell death, morphological changes such as nucleus condensation, formation of apoptotic bodies and membrane blebbing, mitochondria relocation and thread-grain transition and caspase activation.

3. Bioassay Development using MTT and LDH Assays

3.1 Introduction

For the purpose of drug discovery, bioactivity screening is an important aspect of natural products research. One of the aims of this project was to develop an in-house bioassay screening system to be utilised alongside the isolation process as guidance. This would be useful in research of natural products at the University of Waikato as previous bioassay experiments were carried out elsewhere. Bioassays for natural products work previously performed at the University of Waikato were mostly tested against the murine leukaemia P388 cell line.

The objective of this section of the study was to develop a bioassay using the human cervical cancer cell line, HeLa and to utilise the MTT and LDH biochemical assays to assess cell viability and to gather any useful information on the possible mechanism of cell death. These assays were used extensively in the study of the pure compound pterocellin A on HeLa cells, with the intention being to demonstrate if the same approach could be applied to relatively crude fractions in the isolation process.

3.2 Results

3.2.1 Establishing Experimental Conditions

Much of the bioassay development was focused on determining the experimental conditions of the biochemical assays using HeLa cells. It was important that the protocols for the MTT and LDH assays were reproducible and robust. The process of determining the ideal conditions for each assay was described in Chapter Two.

3.2.2 MTT Bioassay: C_{18} Fractions

A crude extract of *P. vesiculosa* was obtained by bulk extraction as described in Chapter Six. Fractions (AW1.115.2 – 14) from the *P. vesiculosa* crude extract separated by reversed phase C_{18} column chromatography were screened to find out if the bioactivity of the pterocellins could be detected in the early stages of the isolation process. The fractions were then subjected to LC-MS to see if the presence of pterocellin A corresponded to the activity observed from the bioassay. MTT assay was used as the endpoint measurement of cell viability. The bioassay was carried out on a 96-well plate in triplicate with a range of four concentrations for each fraction, 0.025, 0.05, 0.1 and 0.2 mg/mL. The incubation period was 24 hours in standard incubation conditions. The results are shown in Figure 3.1 and Figure 3.2. The standard errors of the mean were calculated and the student t-test was used to determine any statistical significance. Statistically significant results were labelled with '*' ($p<0.05$). Fractions AW1.115.5 and AW1.115.6 displayed statistically significant strong inhibitory effects at the highest concentration (0.2 mg/mL). AW1.115.5 was able to kill 70.86% of the cells at 0.2 mg/mL relative to

the control and 99.97% of the cells were killed at 0.2 mg/mL in the fraction AW1.115.6.

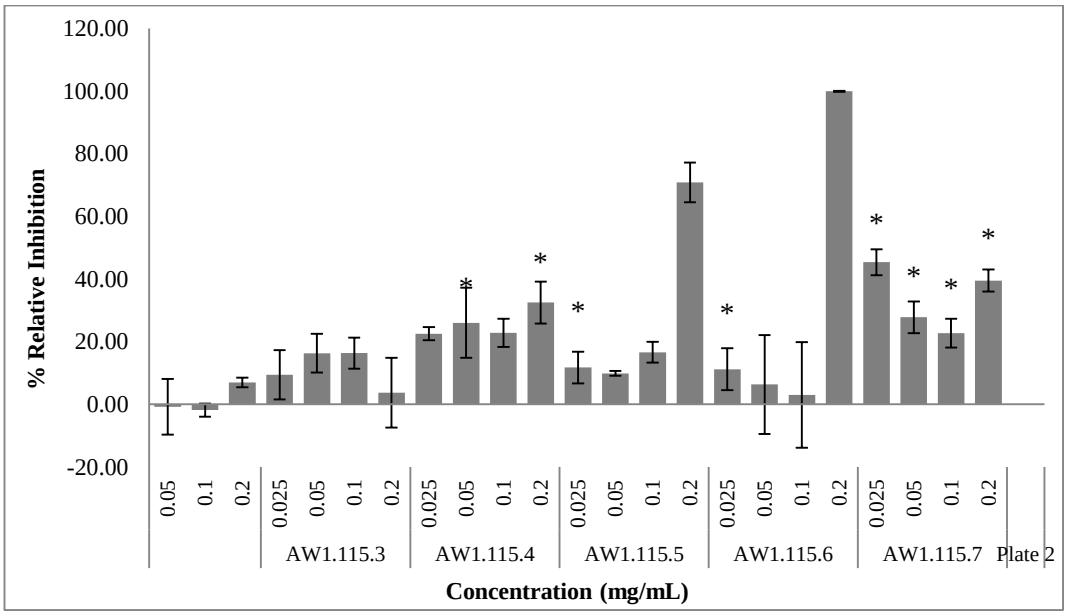

Figure 3.1 Bioassay (AW1.115.2 – 7) against HeLa cells at 24 hours treatment, MTT. Bar graph showing the mean ± S.E.M. * = $p < 0.05$ N = 3.

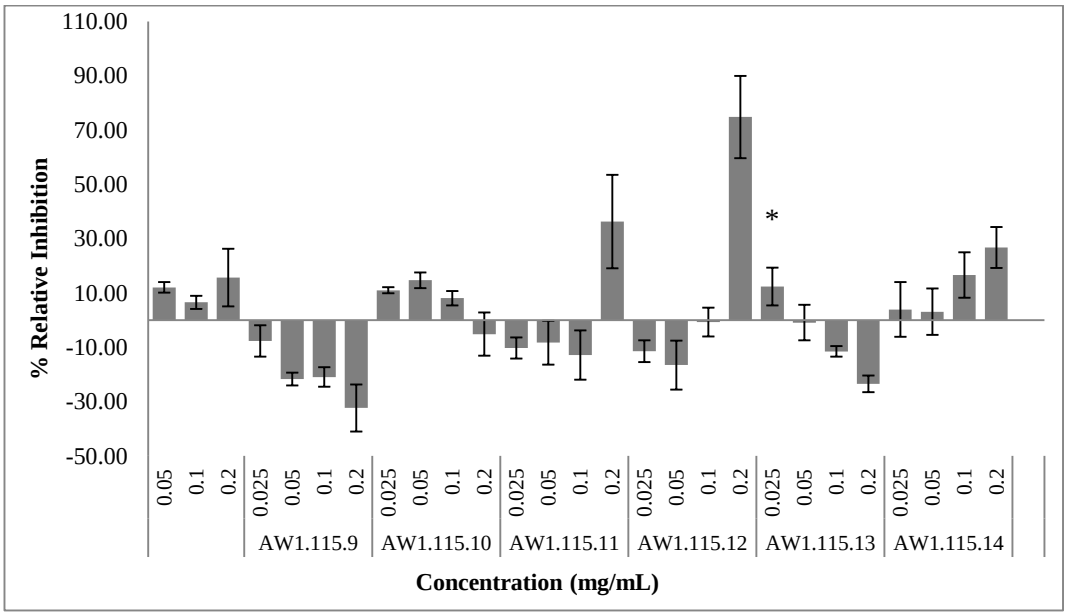

Figure 3.2 Bioassay (AW1.115.8 – 14) against HeLa cells at 24 hours treatment, MTT. Bar graph showing the mean ± S.E.M. * = $p < 0.05$ N = 3.

Fractions AW1.115.4 and AW1.115.7 displayed moderate activity across the concentration range when compared with other fractions and these observations

were also statistically significant. The moderately high activity displayed by the fractions AW1.115.11 and AW1.115.12 at 0.2 mg/mL was unlikely due to bioactive compounds. The test solutions were found to have precipitated out of the culture media and an insoluble mass was found at the bottom of the wells. The inhibitory effects were likely due to shock as the cell monolayer was covered by this insoluble mass and could not proliferate. The IC_{50} values were high (>125000 ng/mL) as these fractions were very crude.

3.2.3 MTT and LDH Bioassays: LH-20 Fractions

Based on the bioactivity, the metabolite composition and the amount of material available, fraction AW1.115.6 was chosen to be further separated by a size exclusion LH-20 column. Although pterocellins A and B were present in AW1.115.5 in higher quantities than in AW1.115.6, AW1.115.6 also contained a number of brominated β-carboline alkaloids as determined by LC-MS (Section 4.2.2). The main purpose for the LH-20 column was to separate the pterocellin alkaloids and the β-carboline alkaloids to determine whether the activities were contributed to the pterocellin alkaloids, β-carboline compounds, or combinations of both. An LDH assay was also carried out alongside the MTT assay to detect any loss of membrane integrity and therefore give an indication of the mechanism of cell death. It was found that fractions AW1.140.7 – 10 displayed significantly strong activities against the HeLa cells as determined by the MTT assay.

Figure 3.3 shows the endpoint of the MTT assay whereby purple formazan crystals were formed in viable cells. Visually, it is clear that the cells in

AW1.140.7 – 10 were affected by the cytotoxicity of the fractions. The wells at the highest concentration (0.1 mg/mL) of the four fractions were colourless, indicating that all the cells were killed at that concentration. The colour intensity directly correlates to the absorbance reading and therefore determines the cell viability.

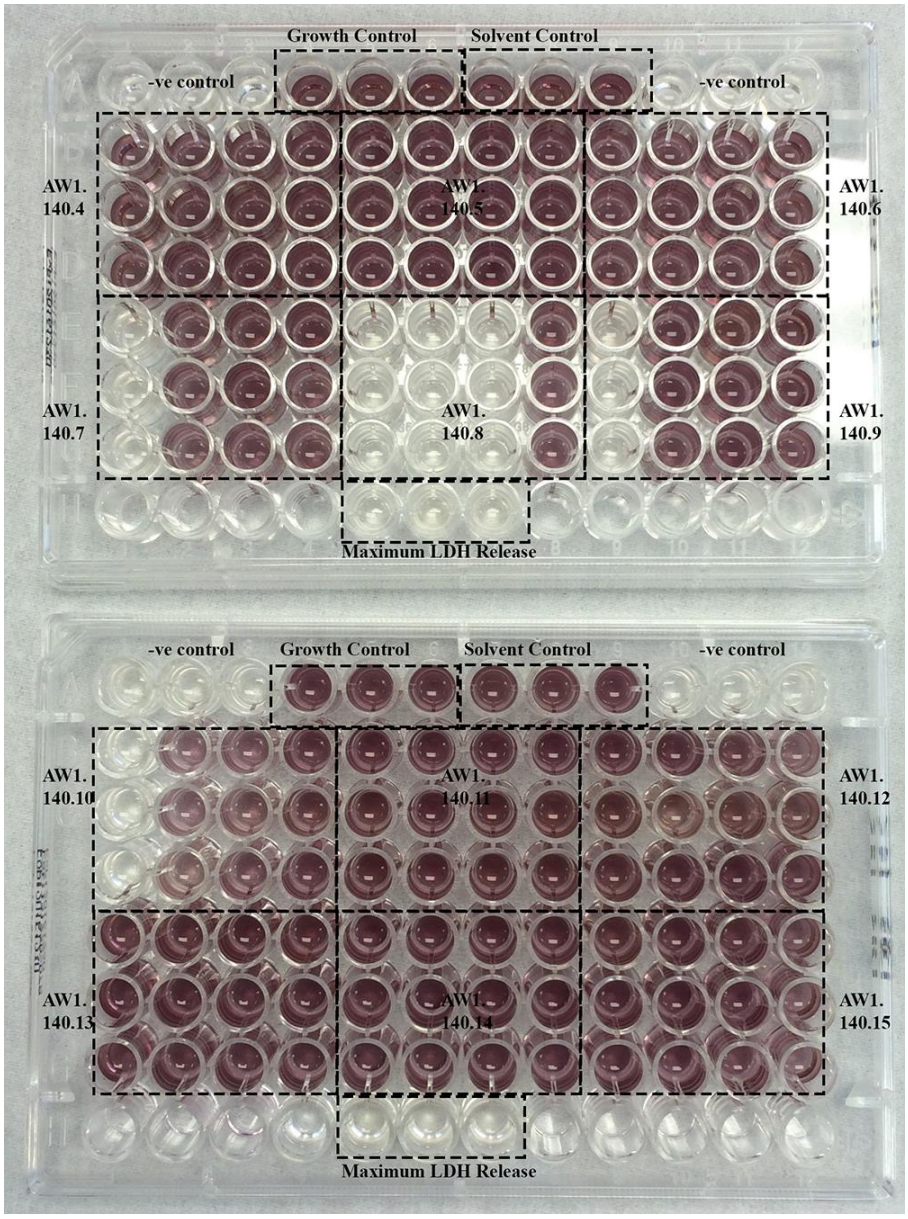

Figure 3.3 MTT assay plate layout showing the endpoint of the experiment. Each fraction was tested in triplicate in four concentrations; highest concentration on the left.

The calculated results were consistent with the visual observation of the MTT assay plate, with strong activity in fractions AW1.140.7 – 10 (Figure 3.4 and Figure 3.5).

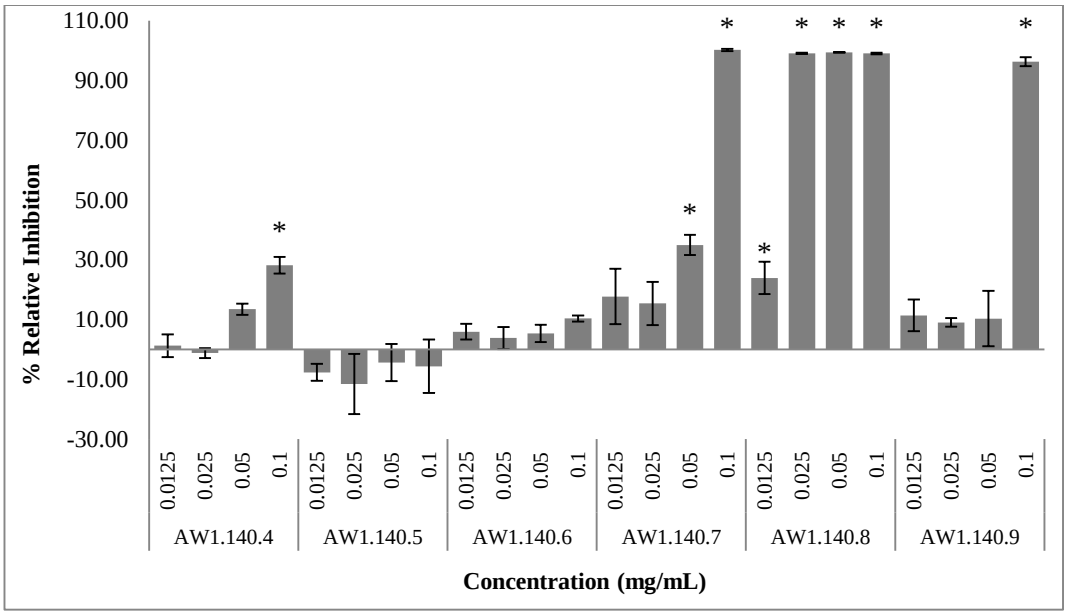

Figure 3.4 Bioassay (AW1.140.4 – 9) against HeLa cells at 24 hours treatment, MTT. Bar graph showing the mean ± S.E.M. * = $p < 0.05$ N = 3.

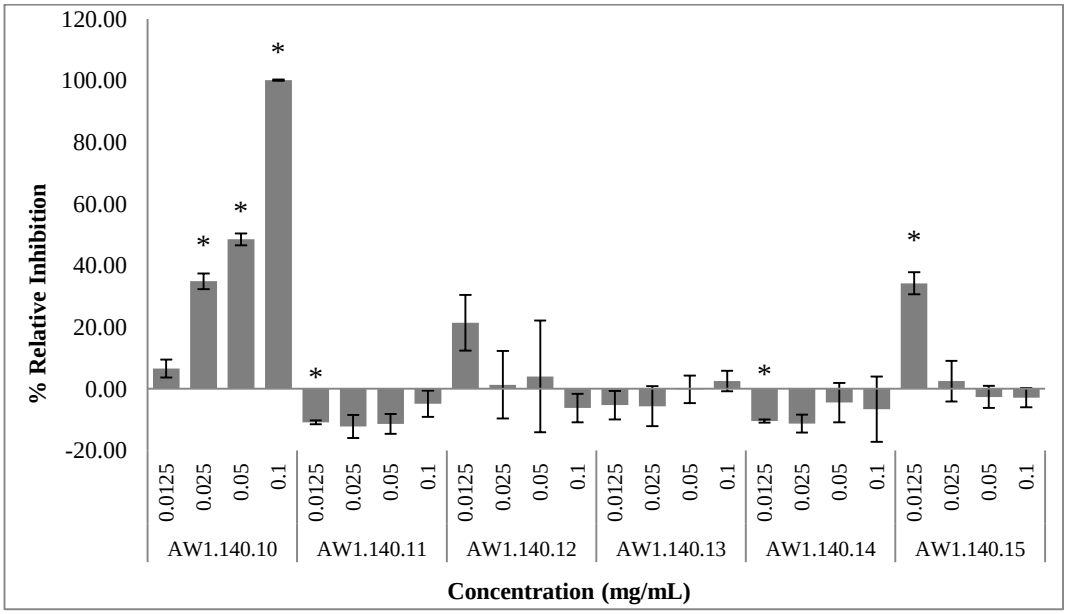

Figure 3.5 Bioassay (AW1.140.10 – 15) against HeLa cells at 24 hours treatment, MTT. Bar graph showing the mean ± S.E.M. * = $p < 0.05$ N = 3.

Fraction AW1.140.8 displayed the highest activity with an IC_{50} value of 0.0132 mg/mL; all the cells were killed at 0.025 mg/mL. The IC_{50} values for the other three bioactive fractions are listed in Table 3.1. The observed ions corresponded with the presence of pterocellin alkaloids in these fractions (Section 4.2.3). Interestingly however, no known pterocellins were detected in the relatively bioactive fraction AW1.140.10 and the fractions that follow.

Table 3.1 IC_{50} values of fractions AW1.140.7 – 10

Fraction #	HeLa IC_{50} (mg/mL)
AW1.140.7	0.0557
AW1.140.8	0.0132
AW1.140.9	0.0940
AW1.140.10	0.0211

To gather information on the possible mechanism of cell death in the early stages of the screening process, an LDH assay was carried out simultaneously to the MTT assay. The LDH assay detects the release of cytosolic LDH from a cell after the loss of membrane integrity, a characteristic of necrotic cell death. The plate layout of the LDH assay is shown in Figure 3.6.

Similar to the MTT assay, the intensity of the colour directly correlates to the absorbance readings. Three controls were used in this experiment: the growth control which accounted for the basal levels of LDH release; the maximum release control which represented the complete lysis of the cell and the maximum amount of LDH release; and culture medium control to account for the serum in the medium that can affect the absorbance readings.

As shown in Figure 3.6, the wells containing the maximum release control have a deeper red colour compared to the growth control with only basal level release of LDH.

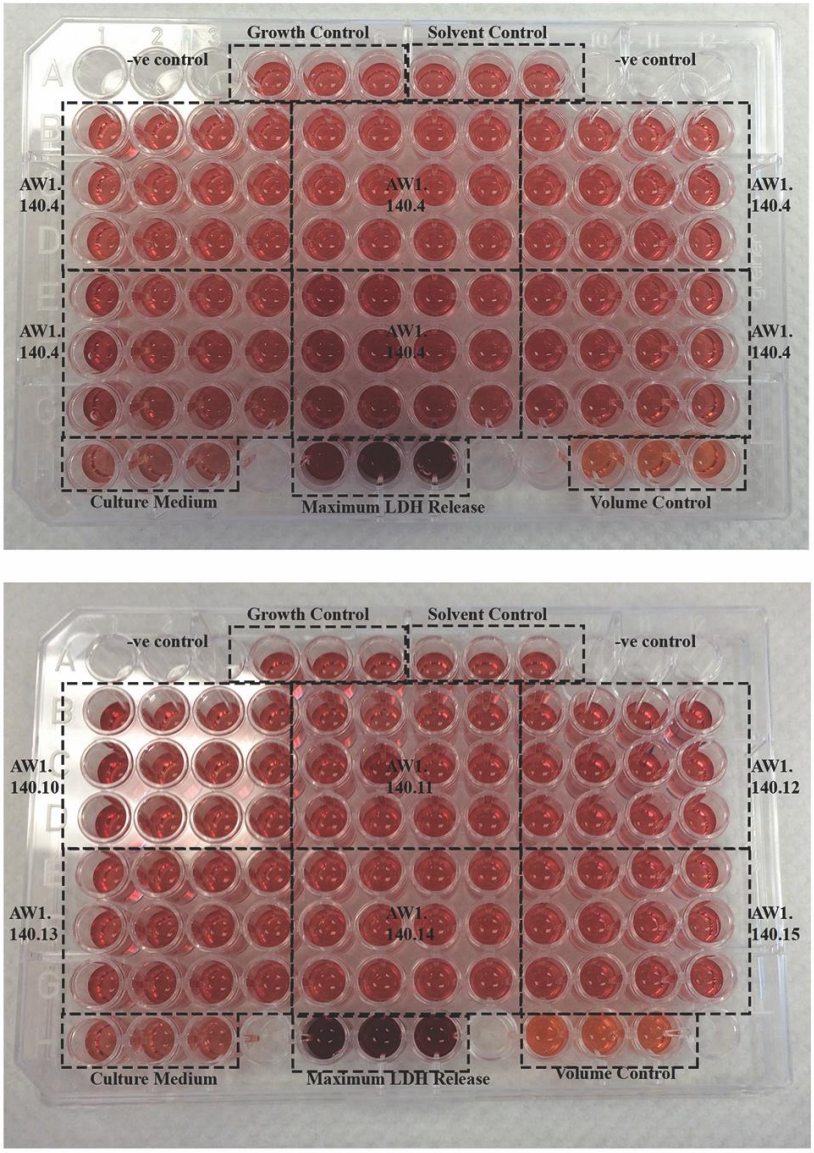

Figure 3.6 LDH assay plate layout showing the endpoint of the experiment.

It was found that the results from the LDH assay showed similar patterns to the work described in Section 2.2.4 where the cell viability calculated from the LDH assay did not align with the results from the MTT assay. In the MTT assay, 100% of the cells were killed at the highest concentration in AW1.140.7 – 10. However,

in the LDH assay, the highest calculated value for loss of membrane integrity and therefore cell death, was 20.2% in AW1.140.8 (Figure 3.7 and Figure 3.8). The inhibition values for the selected fractions for each assay are compared and listed in Table 3.2.

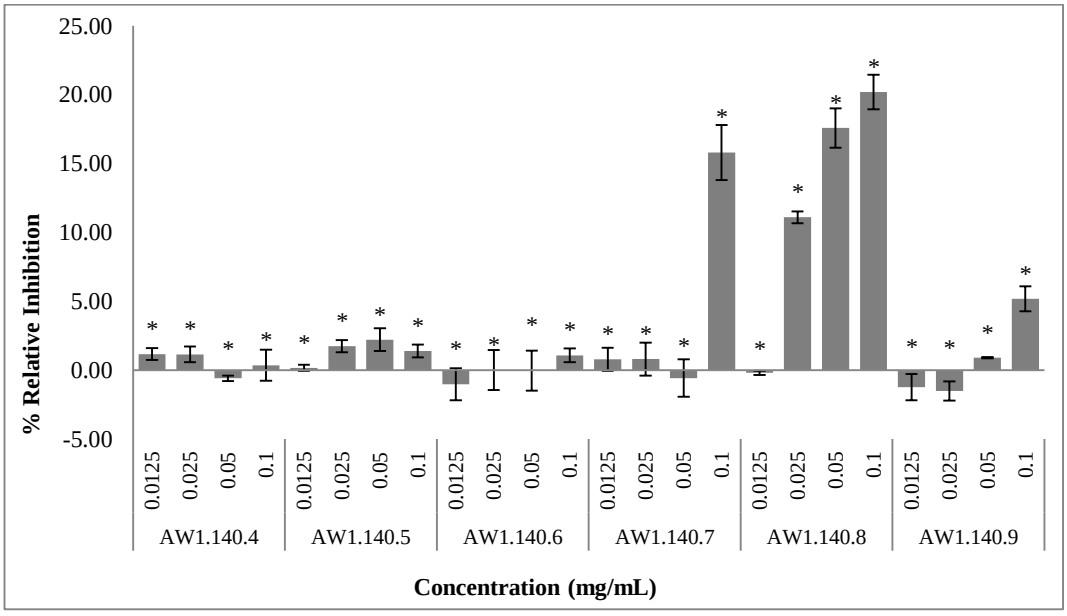

Figure 3.7 Bioassay (AW1.140.4 – 9) against HeLa cells at 24 hours treatment, LDH. Bar graph showing the mean ± S.E.M. * = $p < 0.05$ N = 3.

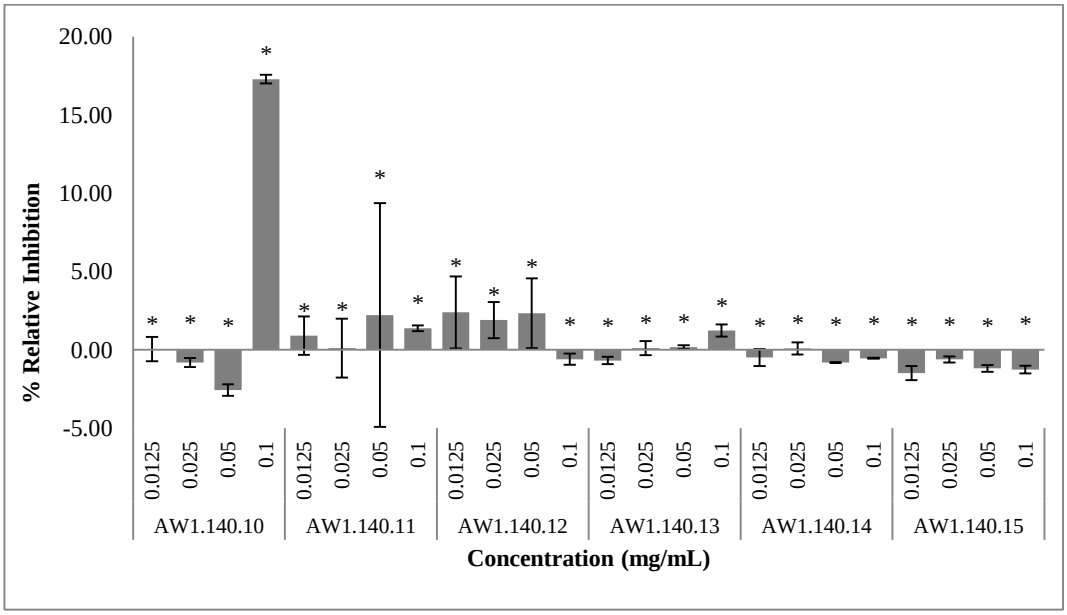

Figure 3.8 Bioassay (AW1.140.10 – 15) against HeLa cells at 24 hours treatment, LDH. Bar graph showing the mean ± S.E.M. * = $p < 0.05$ N = 3.

Table 3.2 Inhibition (%) by MTT and LDH assays relative to the control in selected fractions

Fraction #	Concentrations (µg/mL)	Mean % Relative Inhibition	
		MTT Assay	LDH Assay
AW1.140.7	12.5	17.7	0.8
	25	15.4	0.8
	50	34.9	-0.6
	100	100.3	15.8
AW1.140.8	12.5	23.9	-0.2
	25	99.1	11.1
	50	99.4	17.6
	100	99.1	20.2
AW1.140.9	12.5	11.4	-1.3
	25	9.0	-1.5
	50	10.3	0.9
	100	96.3	5.2
AW1.140.10	12.5	6.6	0.1
	25	34.9	-0.8
	50	48.5	-2.6
	100	100.2	17.3

3.3 Discussion

The objective of this section was to develop a bioassay screening system using HeLa cells and utilising MTT and LDH biochemical assays to guide the isolation process. The ideal experimental conditions for the MTT and LDH assays were established based on work described in Chapter Two. The idea was to use MTT and LDH assays simultaneously to detect any signs of necrotic cell death in crude fractions at the early stages of the isolation process. Any notable bioactivity would be useful in guiding the isolation of the bioactive compounds. The MTT assay measures the cell viability and also the mitochondrial activity of the cells and is commonly used in bioassay screening. The LDH assay is able to measure the release of LDH due to loss of membrane integrity caused by necrotic cell death. Necrotic cell death is an unwanted trait in drug discovery as it results in the

induction of an inflammatory response when cell contents are released into their surroundings. A high level of cell death with a corresponding low level of detected LDH would suggest cells are dying by apoptosis as the cell contents are retained after cell death. The approach taken to study pure compounds against HeLa cells as described in Chapter Two was applied to crude fractions and the bioassays performed successfully.

The first bioassay was able to detect the known cytotoxic effects of presumably pterocellin A or B in HeLa cells, as these two compounds are the most bioactive of the group. Two relatively crude fractions AW1.115.5 and AW1.115.6 displayed strong activities against HeLa cells with IC_{50} values of 148.6 mg/mL and.3 mg/mL respectively; and the corresponding pterocellins A and B ions were observed in the LC-MS spectra (Appendix 2.4 and Appendix 2.5). Examining the LC-MS spectra alone would not have predicted the bioactivity as both fractions contained an abundance of other peaks at higher quantities than pterocellin A. These peaks were attributed to pterocellins H and I and a number of brominated β-carboline related compounds (See Chapter Four).

Even though pterocellins A and B were present in AW1.115.11, the high levels of relative inhibition observed in fractions AW1.115.11 and AW1.115.12 were likely due to the precipitation of the test solution smothering the cells underneath; this was possibly caused by the salts or sterols in the solution (Appendix 2.12).

The second bioassay was carried out on fractions obtained from the LH-20 column separation of AW1.115.6. This fraction was chosen due to the presence of both pterocellin alkaloids and β-carboline alkaloids. The objective was to determine whether the observed activity was due to the action of either group of

compounds or perhaps a combination of both. The presence of pterocellin alkaloids contributed to the cytotoxicity in three of the four most active fractions. The cytotoxicity was likely contributed to both pterocellins A and B. In AW1.140.7, the concentration of pterocellin A was higher than B according to the LC-MS data (Appendix 2.8). In AW1.140.8 and AW1.140.9, the concentration of pterocellin B was higher than pterocellin A. Pterocellins H and I were also present in these fractions, however previous work by Masters student Marisa Till.[73] showed that they were not bioactive and therefore it is assumed they did not contribute to the observed effects. The fourth bioactive fraction, AW1.140.10 interestingly contained no traces of pterocellin alkaloids according to the LC-MS data. Instead a number of previously reported and unknown β-carboline compounds were observed (See Chapter Four).

A LDH assay was carried out alongside the MTT assay in this experiment to detect any loss of membrane integrity. It was found that the calculated values of inhibition in the LDH assay did not correspond to the inhibition values in the MTT assay. This pattern is similar to the work on pure pterocellin A described in Chapter Two. The slight increase in LDH levels seen in the bioactive fractions were likely due to secondary necrosis of apoptotic cells as discussed in Chapter Two. This experiment showed that the LDH assay can be used with crude fractions and changes can be detected at this stage of the isolation process.

One of the concerns with using crude fractions for bioassay was whether the salt and solvent contents would interfere with the assay performance. This was taken into consideration when evaluating the results, however no significant adverse effects were observed as demonstrated by the solvent control. Another matter of

concern was the solubility of the crude fractions. One must ensure that the samples are sufficiently dissolved in methanol, and also make sure that the final solvent concentration does not exceed 2% of the overall volume. The insoluble material observed in AW1.115.11 and AW1.115.12 was likely due to be sterols which are non-polar, as these were collected from DCM fractions. The bioassay preparations used MeOH to dissolve each sample. This use of polar solvent could explain the insoluble mass observed. This problem could be addressed by using a mixture of MeOH and small amount of DCM and also adjusting the solvent control using the same mixture.

The bioassay itself was a time consuming process. The preparation process involved growing HeLa cells to the optimum log phase, preparing test solutions and dilutions, treating the cells for a period of 24 hours and carrying out biochemical assays. Due to this, it was decided that four concentrations of each fraction prepared by serial dilution were sufficient for the bioassay. However, this was problematic when calculating the IC_{50} value. Due to the lack of data points along the X-axis (concentration), some IC_{50} values could not be calculated. The development of the bioassay protocol used in this study is not complete but good progress has been made. There are improvements needed for future research and these recommendations are discussed in Chapter Five.

4. Investigation of bioactive metabolites from *Pterocella vesiculosa*

4.1 Introduction

In the process of developing the bioassay, a number of fractions of the *P. vesiculosa* crude extract were analysed to investigate the metabolite composition. The specimen used in this study was collected from the Alderman Islands, New Zealand.

Fractions of interest were defined as those: that displayed statistically significant bioactivity from the developed bioassay; containing peaks with moderate to high relative signal intensity in the base peak chromatogram and with a retention time of 15 – 30 minutes.

A number of unknown metabolites were observed; they were grouped into either the pterocellins or the β-carboline alkaloids based on thin layer chromatography (TLC), LC-MS, and UV analyses. Some peaks of interest have been previously reported, however they are yet to be isolated and characterised to confirm the structures.

4.2 Results and Discussion

4.2.1 Preparation of the *Pterocella vesiculosa* crude extract

The crude extract (4.2 g) was prepared from the bulk extraction (MeOH:DCM (3:1)) of a *P. vesiculosa* sample (201 g) obtained from the Alderman Islands (See Chapter Six).

4.2.2 Reversed Phase Chromatography of the *P. vesiculosa* Crude Extract

The crude extract was separated by reversed phase (C_{18}) column chromatography and 15 fractions were collected (Figure 4.1). The solvent scheme and the mass of each fraction are listed in Table 4.1.

A

B

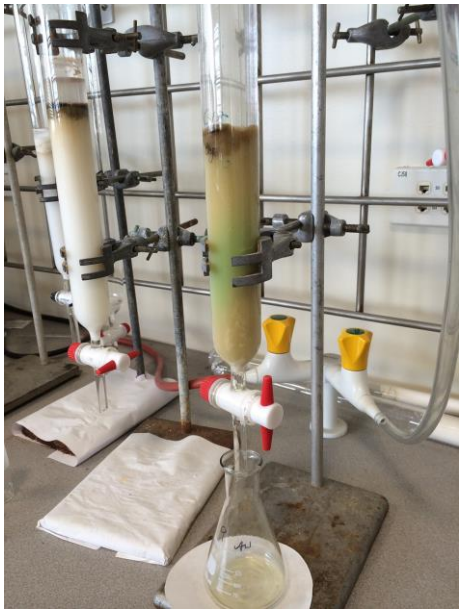

C

Figure 4.1 Separation of the crude extract by reversed phase C_{18} column chromatography. **(A).** Elution of the early polar fractions with the distinctive red colour indicative of the pterocellins. **(B).** Elution of fractions in the non-polar region. **(C).** Fractions collected from the C_{18} column.

Table 4.1 C_{18} fractions of AW1.115 and the recorded dry mass

Fraction #	Solvent	Mass (mg)
1	H_2O	-
2, 3, 4	H_2O/MeOH (1:1)	682.3, 215.8, 161.7
5	H_2O/MeOH (3:7)	125.7
6	H_2O/MeOH (1:9)	223.0
7, 8	MeOH	151.1, 131.1
9	MeOH/DCM (9:1)	274.3
10, 11,	MeOH/DCM (1:1)	33.7, 80.7
12	DCM	130.7
13	MeOH	2.4
14	H_2O/MeOH (1:1)	0.4
15	H_2O	-
	Total mass:	2.2 g

The LC-MS spectra of the crude extract AW1.116 (Appendix 2.2) contained peaks of known pterocellin and β-carboline alkaloids that have been characterised previously (Table 4.2), as well as a number of related compounds that have been reported by previous Masters students Marisa Till and Aaron Anderson.[73-74]

Separation of the crude extract by C_{18} reverse phase column chromatography resulted in two moderately active fractions (AW1.115.4, AW1.115.7) and two highly active fractions (AW1.115.5 – 6) against HeLa cells as described in Chapter Three.

Fractions (AW1.115) were analysed by TLC and LC-MS focusing on the four bioactive fractions (AW1.115.4 – 7). TLC of the bioactive fractions (Figure 4.2) showed pink spots in each fraction with R_f values of ~ 0.7 that were UV active at 254 nm; the pink spots indicated the presence of pterocellin-like metabolites. Two

other spots were present in AW1.115.6 – 7 and these were also visible at 312 nm; the R_f values were 0.75 and 0.85 respectively.

Table 4.2 Previously characterised metabolites from *P.vesiculosa* in the crude extract

Compounds	Observed ions (*m/z*, $[M+H]^+$)	LC-MS retention time (minutes)
Pterocellin A[68]	295	23.1
Pterocellin B[68]	319	24.1
Pterocellin F[69]	581	27.8
Pterocellin H[74]	343	19.0
Pterocellin I[74]	377	19.8
5-Bromo-8-methoxy-1-methyl-β-carboline[76]	291/293	20.5

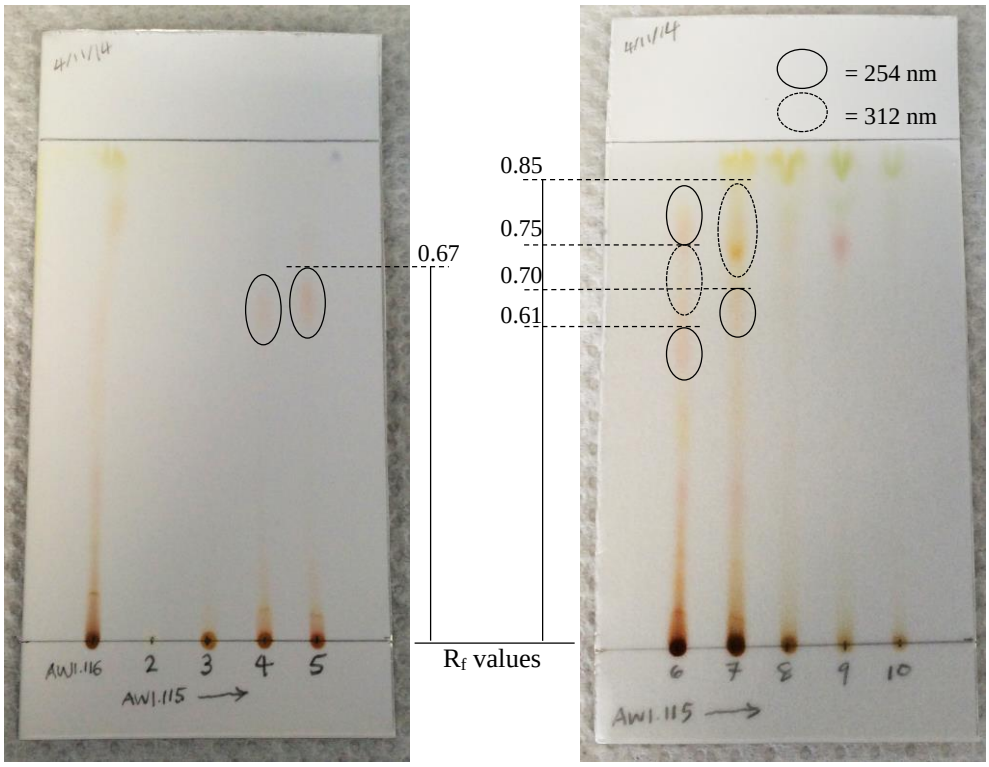

Figure 4.2 TLC analysis and R_f values of the bioactive AW1.115 fractions

The base peak chromatograms of AW1.115.4 and AW1.115.5 revealed significant quantities of *m/z* 343 and *m/z* 377 which corresponded to pterocellins H and I respectively. AW1.115.4 also contained a significant peak of an unknown ion with *m/z* 345, likely to be a pterocellin related compound due to its similarity in the UV spectrum with pterocellin H. The odd number of the mass to charge ratio (*m/z* = $[M+H]^+$) is also indicative of an even number of nitrogens which is typical of the pterocellins. AW1.115.5 also contained the *m/z* 345 ion, as well as a number of other unknown ions with their UV spectra closely resembling to those of the known pterocellins (Figure 4.3).

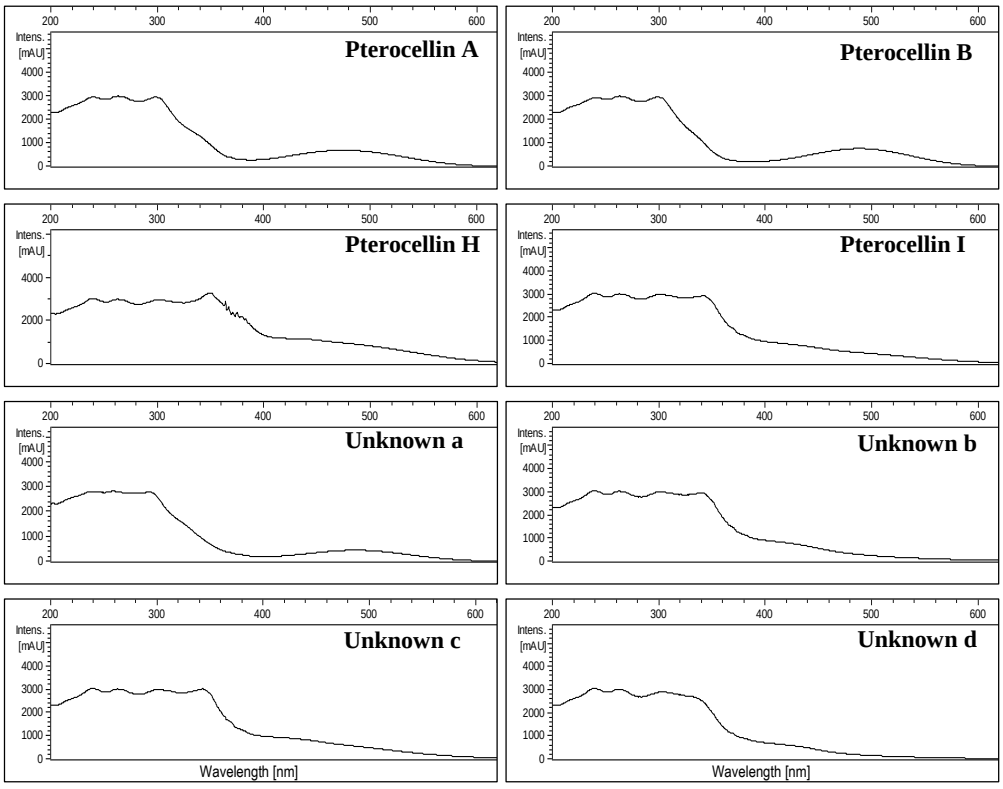

Figure 4.3 UV chromatograms of pterocellin alkaloids and related unknown compounds from the fractions AW1.115.4 – 5

(a) = *m/z* 501 **(b)** = *m/z* 345 **(c)** = *m/z* 379 **(d)** = *m/z* 415

Although the pterocellin alkaloids were present in AW1.115.6, the fraction that managed to kill ~100% of the cells at 0.2 mg/mL, there were also multiple brominated metabolites observed including the previously characterised 5-bromo-

8-methoxy-1-methyl-β-carboline (Appendix 2.1). The two isotopes of bromine, ^{79}Br and ^{81}Br, occur naturally at approximately 1:1 ratio. The isotope patterns observed were typical of monobrominated compounds, indicating these metabolites were likely to be related to the group of monobrominated β-carboline alkaloids. The moderately active AW1.115.7 only contained minor quantities of pterocellin alkaloids, however the brominated compounds observed in AW1.115.6 were also present.

Table 4.3 Significant ions observed in the bioactive fractions AW1.115.4 – 7

Potential Compounds	Observed ions (*m/z*)	LC-MS retention time (minutes)	Fractions containing the observed ions
Pterocellin related metabolites	345	18.1	AW1.115.4, AW1.115.5, AW1.115.6, AW1.115.7
	352	21.2	AW1.115.4, AW1.115.5
	379	19.7	AW1.115.4, AW1.115.5
	415	17.6	AW1.115.4, AW1.115.5, AW1.115.6
	449	18.6	AW1.115.6
	501	23.6	AW1.115.5
β-carboline related metabolites	199	18.0	AW1.115.6
	213	19.2	AW1.115.6
	261/263	20.3	AW1.115.6, AW1.115.7
	275/277	20.8	AW1.115.7
	277/279	19.4	AW1.115.6, AW1.115.7
	303/305	22.2	AW1.115.7
	305/307	20.1	AW1.115.7
	337/339	22.8	AW1.115.7

Interestingly, based on the LC-MS spectra, AW1.115.5 contained four times the quantity of pterocellins A and B than AW1.115.6, however the bioassay data

showed that AW1.115.6 was slightly more bioactive. It was not known at this stage whether the bioactivity was solely attributed to pterocellins A and B, or whether the presence of the β-carboline alkaloids affected cell growth. These unknown brominated β-carboline alkaloids could possess bioactivities yet to be elucidated. Previously isolated 5-bromo-8-methoxy-1-methyl-β-carboline from *P. vesiculosa* was found to have moderate bioactivity with an IC_{50} value of 5089 ng/mL.[76] Another interesting observation was that pterocellins A and B were present in the later fractions (AW1.115.8 – 11) but that these fractions were not bioactive. Questions were raised as to whether the pterocellins were responsible for the high activity in the earlier fractions. This led to further separation by LH-20 size-exclusion column chromatography of the bioactive fraction AW1.115.6 that contained a mixture of pterocellin and β-carboline compounds.

4.2.3 Size Exclusion Chromatography of the Bioactive Fraction

AW1.115.6 was fractionated into 19 fractions by LH-20 size exclusion column (Figure 4.4). Bioassay of these fractions resulted in four active fractions (Table 4.4), AW1.140.7 – 10 as discussed in Chapter Three.

Table 4.4 Bioactive fractions from the LH-20 size exclusion column.

Fraction #	Volume (mL)	Mass (mg)
AW1.140.7	50	2.2
AW1.140.8	50	0.9
AW1.140.9	50	2.2
AW1.140.10	50	0.4

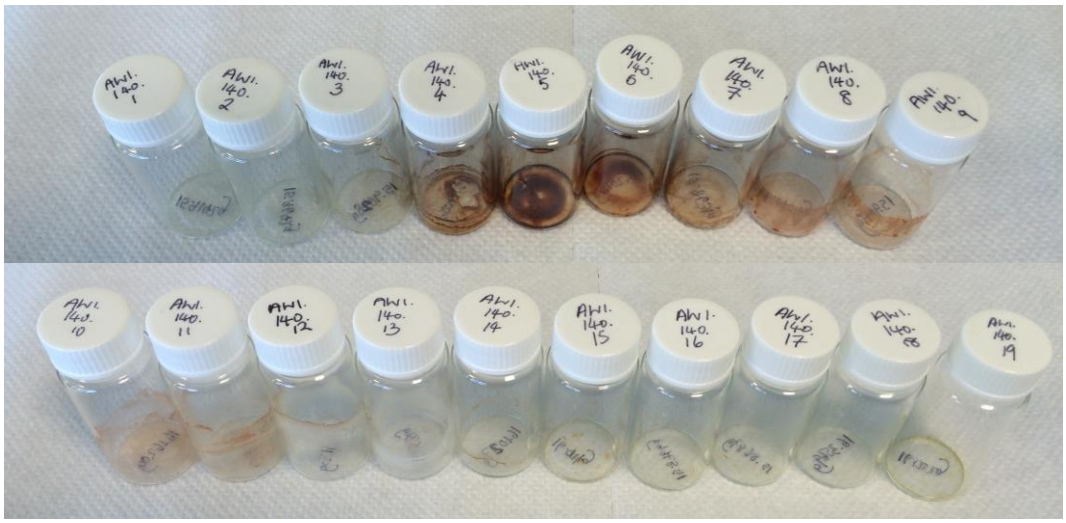

Figure 4.4 Dried fractions from the LH-20 size exclusion column

TLC analyses were carried out on all fractions. The highly pigmented fractions AW1.140.5 – 6 had higher masses than most of the other fractions. These fractions were presumed to contain high quantities of pterocellins A and B due to the distinctive red colour. However, the typical red spot of the pterocellins with R_f ~0.7 was not present on the TLC (Appendix 2.7). Instead, these fractions barely moved from the baseline of the TLC plate in solvent (EtOAc:MeOH, 5:1) which suggest they were quite polar. The LC-MS spectra showed that these fractions contained a mixture of metabolites of similar quantities with no significant peak, whichcould explain the lack of bioactivity observed in the bioassay despite the presence of pterocellins A and B.

In contrast, the fractions that displayed strong bioactivity did not have a large mass which could be due to the fractions being purer than the others. TLC analysis of the bioactive fractions showed a number of spots that were UV active at 254 nm and 312 nm. Although these fractions were not entirely pure, the distinct red spots of the pterocellins A and B at R_f ~0.7 were visible on the TLC plate (Figure 4.5).

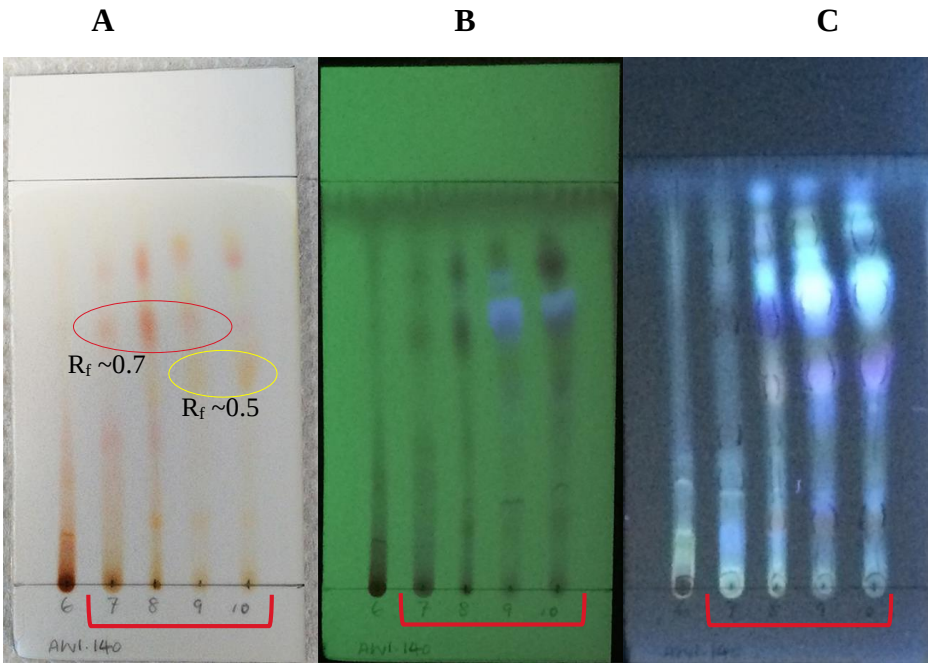

Figure 4.5 TLC analysis of the bioactive fractions AW1.140.7 – 10.
(A). TLC plate in normal lighting. **(B).** TLC plate at 254 nm. **(C).** TLC plate at 312 nm.

Another interesting observation from the TLC analysis was that the yellow spots at R_f ~0.5 and the colourless spots around R_f ~0.8 appeared to fluoresce at 312 nm in fractions AW1.140.9 and AW1.140.10; these were characteristics of the β-carboline alkaloids.

Dereplication of known bryozoan metabolites was carried out on the LC-MS data of the bioactive fractions to separate known and unknown metabolites (Table 4.5). LC-MS analysis indicated that the separation of the pterocellins and the β-carboline alkaloids was mostly successful. A noticeable quantity of pterocellin B was present in AW1.140.9 but no pterocellins were detected in the fractions following. A number of unknown ions were interest after analysing the LC-MS and bioassay data. These include pterocellin-related ions observed in the C_{18} fractionation and the multiple numbers of monobrominated compounds likely to be related to the β-carboline alkaloids due to their similarity in the UV spectra. A

list of significant ions observed in the bioactive fractions can be found in Table 4.6.

Table 4.5 Dereplication of the bioactive fractions AW1.140.7 – 10

Compounds	Observed ions (*m/z*, $[M+H]^+$)	Bioactive fractions containing the known compounds
Pterocellin A	295	AW1.140.7, AW1.140.8,
Pterocellin B	319	AW1.140.7, AW1.140.8, AW1.140.9
Pterocellin F	581	AW1.140.7
Pterocellin H	343	AW1.140.7
Pterocellin I	377	AW1.140.7, AW1.140.8
1-methyl-β-carboline (Harman)	183	AW1.140.9, AW1.140.10
5-Bromo-8-methoxy-1-methyl-β-carboline	291/293	Not present in the bioactive fractions, but present in AW1.140.11 – 12.

Table 4.6 Significant ions observed in the bioactive fractions AW1.140.7 – 10

Potential Compounds	Observed ions (*m/z*)	LC-MS retention time (minutes)	Fractions containing the observed ions
Pterocellin related metabolites	359	24.8	AW1.140.8, AW1.140.9,
	389	28.3	AW1.140.8
β-carboline related metabolites	199	18.0	AW1.140.10
	213	19.3	AW1.140.9, AW1.140.10
	227	19.8	AW1.140.9,
	261/263	20.3	AW1.140.9, AW1.140.10
	275/277	20.8	AW1.140.10
Unknown	403/405	22.5	AW1.140.9, AW1.140.10
	415	17.8	AW1.140.7
	417/419	23.1	AW1.140.9, AW1.140.10
	449	19.1	AW1.140.8

Pterocellin alkaloids generally display a distinctive UV spectrum which assists in identifying any similar metabolites in the isolation process. From the above bioactive fractions, there were not many peaks with such a UV pattern. Two ions, *m/z* 359 and *m/z* 389 had prominent peaks in the LC-MS spectra. They also shared a similar UV pattern to the pterocellins, however they were not an identical match. It was not known whether these two ions are truly related to the pterocellin alkaloids (Figure 4.6).

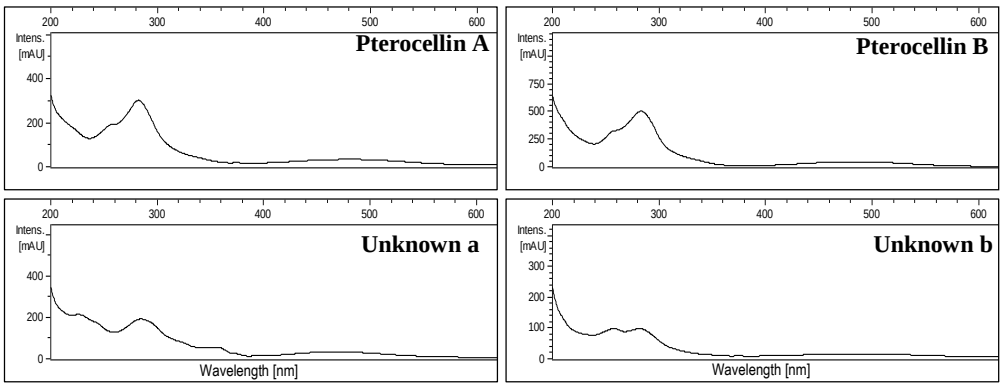

Figure 4.6 UV chromatograms of possible pterocellin alkaloids from fractions AW1.140.8 – 9
(a) = *m/z* 359 **(b)** = *m/z* 389

A number of β-carboline-related metabolites were observed in the bioactive fractions AW1.140.9 – 10. These were confirmed by comparing the UV chromatograms to a known compound, the previously characterised 5-bromo-8-methoxy-1-methyl-β-carboline (Figure 4.7). It is not known what the quantities of the brominated β-carboline alkaloids are, as brominated compounds are easily ionised and may give intense peaks even at low concentration. AW1.140.9 contained a large amount of the known metabolite 1-methyl-β-carboline **(49)** (harman). This could have contributed to the activity observed. However it was previously found that harman was not bioactive against the P388 cell line. It is not known if harman is bioactive against HeLa cells.

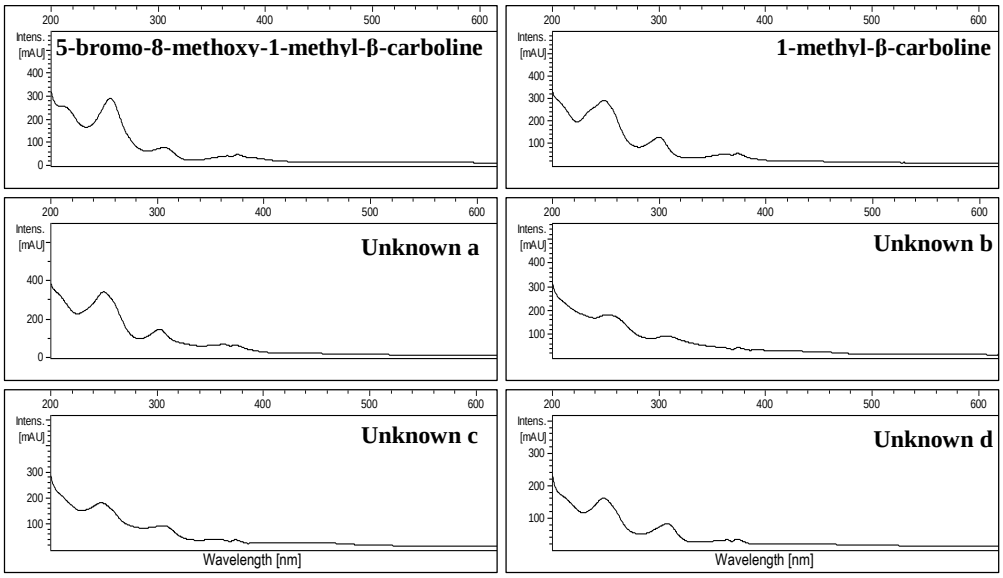

Figure 4.7 UV chromatograms of as before possible β-carboline alkaloids from fractions AW1.140.9 – 10

(a) = *m/z* 199 **(b)** = *m/z* 227 **(c)** = *m/z* 261/263 **(d)** = *m/z* 275/277

The previously observed ions *m/z* 277/279, 303/305, 305/307 and 337/339 from the bioactive C_{18} fractionation were not observed in these bioactive LH-20 fractions which suggests they were not representative of biologically active compounds.

Due to time constraints of the project, further analyses of these fractions were not carried out. Although the scope of the project was not solely focused on the surveying of natural products, it would have been ideal to perform additional analyses such as tandem mass spectrometry and NMR spectroscopy on these fractions to obtain structural information. However, most of these observed ions have been reported previously, so an attempt was made to hypothesise the corresponding structures based on current knowledge.

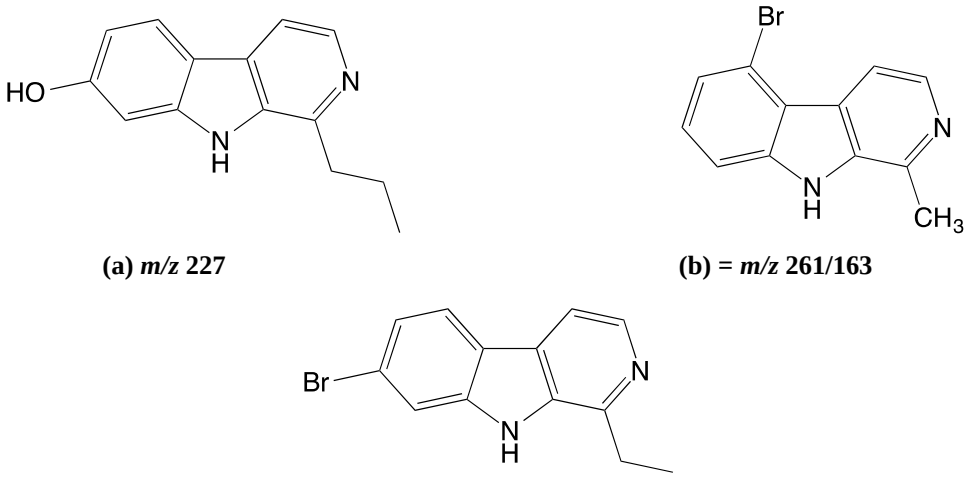

(a) *m/z* 227 **(b) = *m/z* 261/163**

(c) = *m/z* 275/277

Figure 4.8 Proposed corresponding structures.[73]

The *m/z* 199 ion is 31 Da more than that of the β-carboline nucleus (168 Da). This could correspond to a methoxy substitution on the β-carboline core structure. If this were a methoxy-β-carboline alkaloid, then the tandem mass spectra would show a fragment of 15 Da from the loss of the methyl group. The *m/z* 227 ion could either correspond to an ethyl-methoxy-β-carboline or a propyl-hydroxy-β-carboline alkaloid. It was previously reported by Aaron Anderson that the tandem mass spectra did not show a fragmentation of 15 Da, which would be characteristic of a methoxy substituent. Therefore this was likely to be the previously noted 7-hydroxy-1-propyl-β-carboline (Figure 4.8, a).**[73]** The *m/z* 261/263 ion could correspond to the demethoxy- counterpart (Figure 4.8, b) of the 5-bromo-8-methoxy-1-methyl-β-carboline with a mass difference of 31 Da. The final unknown ion from the bioactive fractions *m/z* 275/277 is likely to be the previously reported 7-bromo-1-ethyl-β-carboline (Figure 4.8, c).[73]

5. Concluding Remarks and Future Directions

5.1 Concluding Remarks

This project investigated the mechanism of cytotoxicity of pterocellin A against HeLa cells. Pterocellin A exhibited similar cytotoxicity against HeLa cells with an IC_{50} value of 886 ng/mL compared to the published IC_{50} value against P388 cells of 477 ng/mL. In this study, HeLa cells were incubated with up to 2000 ng/mL of pure pterocellin A and characteristic markers of apoptotic and necrotic cell death were assessed using several *in vitro* biochemistry techniques. The results from the time-course MTT and LDH assays showed only a low level of cytosolic LDH was detected in the supernatant after all the cells have died from pterocellin A at 2000 ng/mL. This indicated the cells maintained plasma membrane integrity upon cell death suggesting apoptotic cell death. The slight increase in LDH levels after all the cells were killed was likely due to secondary necrosis, the final stage of apoptosis when phagocytes are absent. Additionally, morphological changes were observed after six hours of treatment at 2000 ng/mL. Cell shrinkage and nucleus condensation were observed, as well as apparent membrane blebbing, a key feature of apoptosis. The MTT data was also indicative of mitochondria impairment as the conversion of MTT to formazan relied on active mitochondrial dehydrogenases, suggesting that pterocellin A could be targeting the mitochondria. This hypothesis was supported by the observed changes in the morphology and location of the mitochondria after just six hours of exposure to pterocellin A at 1000 ng/mL; thread-grain transition of the mitochondria were observed. Furthermore, these changes to the mitochondria occurred before the

changes in cell morphology were observed. Although no DNA fragmentation was readily observed, the level of activated caspase-3 in HeLa cells increased after treatment with pterocellin A. Activated caspase-3 can only be detected after a series of signalling events following the induction of apoptosis. These data supported the notion that pterocellin A is an inducer of apoptosis in HeLa cells.

This project also utilised biochemical assays and developed a systematic bioassay screening system at the University of Waikato, and further investigated the bioactive metabolites of *P. vesiculosa.* Although there are improvements that need to be implemented, good progress was made on the development of the bioassay system. The bioassays using HeLa cells and MTT/LDH assays were successfully carried out and demonstrated that the same approach taken to study pure compound in HeLa cells could be successfully applied to the bioassay development. Analysis of the bioactive fractions from the bioassay revealed several unknown metabolites that could be pterocellin alkaloids. It was not known which metabolite was responsible for the bioactivity shown in AW1.140.10 and further investigation is required in the future.

5.2 Future Research

There are still a number of areas of interest that remain unexplored and could form the basis of future research. To confirm that the mechanism of cell death is indeed attributed to apoptosis, additional information on apoptotic markers is required. These include the analysis of intracellular markers such as the release of cyt *c* from the mitochondria and other pro-apoptotic proteins assessed by Western

blot; DNA fragmentation using the PI stain analysed by FACS; and carrying out annexin-v staining to detect the presence of phosphatidylserine on the cell surface in the early stages of apoptosis. Since the MTT and MitoTracker data suggested impairment of the mitochondria after exposure to pterocellin A, other properties such as the disruption of the mitochondria membrane potential and an increased level of stress protein HSP60 could provide insight into the modes of action of pterocellin A. Although the findings from this study provided some good evidence that pterocellin A induces apoptosis in HeLa cells, the mechanisms for the initiation processes are not known. Some questions were raised during this study: how does pterocellin A enter a cell? What intracellular components is it targeting and interacting with? How is pterocellin A metabolised within the cell? Is the cytotoxicity activated by the parent compound or its metabolites? Perhaps future research could explore synthetic analogues of pterocellin A and determine the essential functional groups for cytotoxicity. Kinetic studies could also be explored to study the movement of pterocellin A into a cell. It would be interesting to investigate pterocellin A against human melanoma cells as the published data suggested that pterocellin A was selective cytotoxic against five melanoma cell lines. Future research could also explore the cytotoxicity of pterocellin A against non-cancerous cell lines to determine if the compound is selectively toxic to cancer cells. If found not to be cytotoxic, there could be great potential for pterocellin A as a lead compound for pharmaceutical development.

Due to limited time associated with this project, a number of fractions of interest from *P. vesiculosa* were not explored further. Future research could include exploring the polar metabolites from the pterocellin fractions and identifying any further pterocellin alkaloids yet to be discovered. Another area of research to

pursue further would be the isolation and characterisation of the β-carboline alkaloids mentioned above to confirm the proposed structures. It would be interesting to find out which β-carboline metabolite was responsible for the strong bioactivity observed in the fraction that contained no pterocellins or the 5-bromo-8-methoxy-1-methyl-β-carboline.

The bioassay screening system developed in this study can be greatly improved in the future. Future work could include increasing data points for IC_{50} calculations and also to include a known positive control for each plate used in an experiment to eliminate errors. It is important for future improvements to develop a method that is robust, reproducible, and can be scaled for high throughput screening. Intra- and inter-assay variability should also be determined during future validations. Another recommendation for future research is to produce a flow-chart protocol upon validated development of the bioassay system. This would ensure consistency across all the users of the bioassay system and therefore more precise data can be collected.

6. Materials and Methods

6.1 Materials

6.1.1 Commercial Kits

6.1.1.1 CytoTox 96® Non-Radioactive Cytotoxicity Assay

This kit was used to quantitatively measure lactate dehydrogenase (LDH), a stable cytosolic enzyme that is released upon cell lysis. The kit was supplied by Promega, Madison, Wisconsin, USA. The contents are listed in Table 6.1.

Table 6.1 CytoTox 96® Non-Radioactive Cytotoxicity Assay Kit.

Kit Contents	
Item	**Quantity**
Substrate Mix	5 vials
Assay Buffer	60 mL
LDH Positive Control	25 μL
Lysis Solution (10X)	5 mL
Stop Solution	65 mL

6.1.1.2 Caspase-3 (active) FITC Staining Kit

This fluorometric kit was used to measure caspase-3 activities in treated cells. The kit was supplied by Abcam, Cambridge, UK. The contents are listed in Table 6.2.

Table 6.2 Caspase-3 (active) FITC Staining Kit

Kit Contents	
Item	**Quantity**
FITC-DEVD-FMK	100 μL
Wash Buffer	2 x 200 mL
Z-VAD-FMK	10 μL

6.1.1.3 Apoptotic DNA Ladder Detection Kit

This kit was used to isolate and detect any fragmentation of genomic DNA of treated cells. The supplier was Abcam, Cambridge, UK. The contents are listed in Table 6.3.

Table 6.3 Apoptotic DNA Ladder Detection Kit

Kit Contents	
Item	**Quantity**
Ammonium Acetate Solution	250 µL
DNA Suspension Buffer	2 mL
Enzyme A Solution	250 µL
Enzyme B (Lyophilised)	1 vial
TE Lysis Buffer	1.8 mL

6.1.1.4 Quick-gDNA™ MiniPrep DNA Extraction Kit

This kit was used to purify genomic DNA from cultured cells. The supplier was Zymo, Irvine, California, USA. The contents are listed in Table 6.4.

Table 6.4 Quick-gDNA™ MiniPrep DNA Extraction Kit

Kit Contents	
Item	**Quantity**
Genomic Lysis Buffer	50 mL
DNA Pre-Wash Buffer	15 mL
g-DNA Wash Buffer	50 mL
DNA Elution Buffer	10 mL
Zymo-Spin™ Columns	50
Collection Tubes	100

6.1.2 Common Solutions

Table 6.5 lists the compositions of media, reagents and common solutions routinely used in the laboratory.

Table 6.5 Common Solutions Used in the Laboratory

Solution	Composition
Complete DMEM (Dulbecco's Modified Eagle's Medium)	0.5 mL penicillin/streptomycin (100X units total). 5 mL foetal bovine serum (FBS). Make up to 50 mL in a Falcon tube with DMEM under sterile conditions. Store at 4°C.
5% DMSO Freezing Media	0.5 mL DMSO Make up to 10 mL in a Falcon tube with complete DMEM under sterile conditions. Store at 4°C protected from light.
Phosphate Buffer Saline (PBS)	8 g NaCl (137 mM) 0.2 g KCl (2.7 mM) 1.44 g Na_2HPO_4 (4.0 mM) 0.24 g KH_2PO_4 (1.7 mM) Dissolve in 800 mL MilliQ water and adjust to pH 7, make up to 1 L, and store at 4°C.
1 mg/mL Pterocellin A	1.8 mg pterocellin A (crystallised – synthetic sample supplied by T. Ross Kelly, E. F. Merkert Chemistry Centre, Boston College, Chestnut Hill, Massachusetts, U.S.A.) Dissolved in 1.8 mL methanol and store at 4°C.
5 mg/mL MTT Reagent	0.01 g MTT Dissolve in 2 mL complete DMEM then filter through a 0.2 µm filter with a syringe. Mix well and store in 1 mL aliquots protected from light. Store at 4°C for no more than 1 week.
MTT Solubilising Solution	1 mL HCl (1M) Make up to 10 mL with isopropanol. Store at 4°C.

1 μM MitoTracker Red CMXRos Stock Solution	50 μg MitoTracker Red CMXRos Dissolve in 94 μL DMSO to make 1mM MitoTracker Red CMXRos. Take 10 μL of 1 mM MitoTracker and make up to 10 mL with complete DMEM to make 1 μM solution. Store both solutions at -20°C.
50 nM MitoTracker Red CMXRos Working Solution	50 μL 1 μM MitoTracker. Make up to 1 mL with complete DMEM to make 50 nM solution. Use immediately.
0.5 M EDTA	14.61 g EDTA. Dissolve in 80 mL MilliQ water and adjust to pH 8. Make up to 100 mL.
5X Tris-borate Buffer (TBE)	54 g Tris base. 27.5 g boric acid. 20 mL 0.5 M EDTA. Make up to 1 L with MilliQ water.
1X Tris-borate Buffer (TBE)	200 mL 5X TBE buffer. Make up to 1 L with MilliQ water.
6X Loading Buffer	0.5 mL glycerol. 0.5 mL MilliQ water. 50 μL 1% bromophenol blue.
2% Agarose Gel in 1X TBE	2 g agarose. Dissolve in 100 mL 1X TBE. Heat in microwave on high for 1 minute. Stir contents gently. Heat in microwave on high for another 30 seconds. Make up to 100 mL with 1X TBE. Add 2 drops (approximately 90 μL) ethidium bromide

	Cool to 50°C and pour into casting tray, leave to set for 30 minutes. For short term storage, cover gel in 1X TBE and store at 4°C.
70% Ethanol	700 mL ethanol Make up to 1 L with MilliQ water
1 mM Rotenone Stock Solution	3.9 mg rotenone Dissolve in 10 mL DMSO, store at 4°C protected from light.

6.1.3 Common Laboratory Chemicals and Reagents

All water used in this project was deionised distilled water (≥ 18 MΩ-cm) purified on either an E-Pure (Barnstead) or a Direct-Q (Merck Millipore) ultrapure water system. Methanol and dichloromethane used in bench columns was distilled from drum grade before use. Common chemicals and reagents used and their sources are listed in Table 6.6.

Table 6.6 Common Laboratory Chemical or Reagents

Chemical or Reagent	Source
Trifluoroacetic acid	Acros Organics
Boric acid Disodium hydrogen phosphate dodecahydrate Ethyl acetate Hydrochloric acid Potassium chloride	Ajax
Agarose LE	AppliChem
Ethylenediaminetetra-acetic acid (EDTA) Glycerol Sodium chloride	BDH

Dichloromethane – drum grade	Dongyue
Isopropyl alcohol (IPA) – drum grade	Exxon Mobil Chemical
Dulbecco's Modified Eagle Medium (DMEM): [+] High glucose (4.5 g/L) [+] L-glutamine [+] Phenol red [+] Sodium pyruvate; Foetal Bovine Serum (FBS) Penicillin-Streptomycin: - Penicillin 10000 U/mL - Streptomycin 10000 μg/mL Trypsin/EDTA 0.05%	Gibco
MitoTracker Red CMXRos SYBR® DNA Gel Stain 10000 X	Invitrogen
Acetonitrile – HPLC grade Methanol – drum grade	Merck
Bromophenol blue	Park Scientific
LH-20 (Sephadex)	Pharmacia Fine Chemicals
Methanol – HPLC grade Potassium dihydrogen phosphate	Scharlau
Rotenone Thiazolyl Blue Tetrazolium Bromide (MTT) Trypan Blue (0.4% w/v in PBS)	Sigma
Dimethyl Sulfoxide (DMSO)	Sigma-Aldrich
DNA ladders (1 kb and 100 bp)	Solis BioDyne
Octadecyl Silane (C_{18})	YMC

6.2 Methods

6.2.1 Cell Culture

Cell culture work was carried out under sterile conditions inside a laminar flow cabinet (Heraeus HERAsafe™) within a physical containment facility (PC2) at the University of Waikato.

6.2.1.1 HeLa Cell Culture

The human cervical cancer cell line, HeLa, was purchased from the American Tissue Culture Collection (ATCC) (Number CCL-2). The cells were grown in DMEM (25 mM D-Glucose, 4 mM L-Glutamine, 1 mM sodium pyruvate, Gibco) supplemented with 100X units of penicillin/streptomycin (Gibco) and 10% foetal bovine serum (FBS) (Gibco). Unless specified otherwise, cells were grown in T-25 flasks (Biofil) in standard incubation conditions in a humidified incubator (Heraeus HERAcell™) at 37°C with 5% CO2. Cells were harvested and subcultured every four days at near confluency.

To harvest, existing media was discarded and the adherent cell monolayer was gently washed with pre-warmed PBS (2 mL) before the addition of trypsin/EDTA (1 mL). This was followed by a short incubation period to aid the detachment of cells from the flask. Once the cells were in suspension, pre-warmed complete DMEM (4 mL) was added to neutralise the effects of trypsin. An aliquot was then taken for cell counting and the remaining cells were added to a new flask at a desirable seeding density with fresh complete DMEM.

6.2.1.2 Freezing Cells

Cells were harvested as in Section 6.2.1.1 and centrifuged at 800 × *g* for five minutes. The supernatant was discarded and the cell pellet was re-suspended at a desirable cell density in freezing media, which consisted of complete DMEM with 5% DMSO as cryoprotectant. The cell suspension was then divided into aliquots in cryogenic vials (NUNC) and placed in a CoolCell® (Biocision) freezing apparatus overnight at -80°C. The CoolCell® freezing apparatus allowed the cells to freeze slowly by steadily decreasing the temperature at approximately 1°C per minute. The next day, cryogenic vials were transferred to a storage container at -80°C.

6.2.1.3 Thawing Cells

Cells were thawed quickly by placing the cryogenic vial in a 37°C water bath for one minute, then immediately transferred to a culture flask under sterile conditions. This was followed by the slow drop-wise addition of complete DMEM (4 mL) to the flask, and cells were left to recover overnight in standard incubation conditions. The media was changed the next day to remove traces of freezing media.

6.2.1.4 Cell Counting

Cell counts were carried out on a haemocytometer slide under the microscope at 100X magnification. A mixture of cell suspension (10 µL) with an equal amount of Trypan Blue (Sigma) was added to the slide and covered with a glass coverslip. Cells in the four large outer corner squares were counted and the cell concentration was calculated with the following formula:

$$Cells\ per\ mL = \frac{Cell\ Count\ of\ Outer\ Corners}{4} \times 2\ (Dilution\ Factor) \times 10^4$$

Equation 6.1 *Calculating cell concentration using a haemocytometer*

6.2.2 Biochemical Assays

6.2.2.1 MTT Assay

The Sigma thiazolyl blue tetrazolium bromide (MTT) reagent was used as per the manufacturer's protocol. The MTT solution was freshly prepared before each experiment by dissolving in complete DMEM at a concentration of 5 mg/mL, pre-warmed to 37°C and passed through a filter (0.2 µm) with a syringe. The solubilising solution was also freshly prepared to a final concentration of 0.1 M HCl in isopropanol.

Each experiment was carried out in triplicate samples in 96-well cell culture plates (Biofil). There were three controls in each experiment: growth control, negative control and solvent control. Growth control consisted of untreated cells in media; solvent control consisted of untreated cells in media, with the addition of MeOH equal to the solvent percentage of the highest treatment concentration and the negative control consisted of media plus solvent. The final solvent concentration did not exceed 2% of the total volume. Near confluent cells in log-phase were harvested and seeded at a density of $1x10^4$ cells per well, each well containing 150 µL cell culture. The cells were then incubated at standard conditions overnight to allow the cells to attach and recover from handling before treatment was added. To carry out the assay, existing media containing test compound were removed and replaced with fresh media (150 µL per well). This was followed by the addition of reconstituted MTT in an amount equal to 10% of the media

volume (15 µL) and incubate at standard conditions for two hours. The MTT media was then carefully removed and replaced with MTT solubilising solution in an amount equal to the original volume (150 µL) to dissolve the formazan crystals. The samples were then placed on a plate-shaker (IKA® MS 1) for fifteen minutes at room temperature protected from light. Occasionally, some samples required mixing by pipette for homogenisation. Once homogenised, the samples were spectrophotometrically measured on a plate reader (Bio-Rad 680) at an absorbance wavelength of 570 nm, with a background absorbance reading at 655 nm. Results were then blank corrected as per Equation 6.2.

$$Absorbance\ (corrected) = (Experimental\ Abs) - (Blank\ Abs)$$

Equation 6.2 *Blank correction for MTT assay*

Experimental values of relative growth inhibition were then calculated and expressed as percentage of solvent control, which is also indicative of mitochondrial dehydrogenase activity (Equation 6.3).

$$Relative\ Inhibition\ (\%) = 100\% - \frac{Experimental\ Absorbance\ (corrected) \times 100\%}{Solvent\ Control\ Absorbance\ (corrected)}$$

Equation 6.3 *Relative growth inhibition calculations*

6.2.2.2 LDH Assay

The LDH assays were carried out simultaneously to MTT assays using a CytoTox 96® Non-Radioactive Cytotoxicity Assay commercial kit (Promega) as per the manufacturer's protocol. The assay involved taking supernatant from treated cells without disturbing the cell population for MTT assay. The substrate mix used in the assay was reconstituted with assay buffer (12 mL) and stored at -20°C for no more than six to eight weeks protected from light. There were several controls included in these experiments: spontaneous release control (SRC), maximum

release control (MRC), and culture medium background control (CM). Spontaneous control corrected for the spontaneous release of LDH from cells; maximum control represented 100% release of LDH upon cell lysis and culture medium background control corrected for any LDH activity contributed by FBS in the DMEM, and the varying amounts of phenol red in the media. Cells were seeded as described in Section 6.2.2.1. The growth control from MTT assays served the same purpose as the spontaneous control in LDH assays.

Cells were incubated with test compound as per experimental protocol. Prior to harvesting supernatant, 15 μL of lysis solution (10X) was added to the maximum release control. This allowed total cell lysis and therefore the release of total LDH into the supernatant. After incubating for forty-five minutes, the maximum release control was checked under the microscope to confirm complete lysis. The culture plate was then centrifuged (Heraeus™ Multifuge™ X3) at 250 × g at room temperature for four minutes to pellet any cell debris.

To carry out the assay, 50 μL supernatant from each sample of the culture plate was transferred to a new assay plate (Greiner Bio-One). The reconstituted Substrate Mix was then brought to room temperature and 50 μL was added to each sample. This was incubated for thirty minutes at room temperature protected from light using foil, followed by the addition of Stop Solution (50 μL) to each sample. The samples were measured on a plate reader (Bio-Rad 680) at an absorbance of 490 nm within an hour of adding the stop solution. A syringe needle was used to remove any bubbles in the samples before measurements were taken.

To calculate the percentage of LDH release relative to the maximum release control (Equation 6.4), each set of data was blank corrected by subtracting the average of control background readings. The percentage of LDH release is also demonstrative of loss of membrane integrity due to necrotic cell death.

$$Loss\ of\ Membrane\ Integrity\ (\%) = \frac{Experimental - SRC}{MRC - SRC} \times 100\ (\%)$$

Equation 6.4 *Calculating loss of membrane integrity*

6.2.3 Statistical Analysis

$$Standard\ Deviation\ (\sigma) = \sqrt{\frac{\sum(x - \bar{x})^2}{n - 1}}$$

$\Sigma = sum\ of$
$x = each\ sample\ in\ the\ data\ set$
$\bar{x} = mean\ of\ all\ samples\ in\ the\ data\ set$
$n = number\ of\ samples\ in\ the\ data\ set$

Equation 6.5 *Standard deviation calculation*

$$Standard\ Error\ (SE) = \frac{\sigma}{\sqrt{n}}$$

$\sigma = standard\ deviation$
$n = number\ of\ samples\ in\ the\ data\ set$

Equation 6.6 *Standard error calculation*

6.2.4 Work Described in Chapter Two

All MTT assays mentioned in this chapter were carried out in triplicate in 96-well plates. LDH assays were always carried out simultaneously to the MTT assay.

6.2.4.1 HeLa Cell Growth Curve

The growth curve experiment was set up as shown in Figure 6.1. Each well was seeded with the same number of cells ($2x10^4$ in 1 mL) and grown for eight days

under standard incubation conditions. Media was changed after three days. At the same time each day, corresponding cells were harvested with PBS (100 μL), trypsin/EDTA (100 μL) and complete DMEM (900 μL). Cell count was carried out as described in Section 6.2.1.4 in triplicate per well to allow for any counting errors. The results were plotted on a graph to identify the log growth phase of HeLa cells. The calculated cell concentration (cells/mL) was equivalent to the number of cells in each sample with the volume being 1mL.

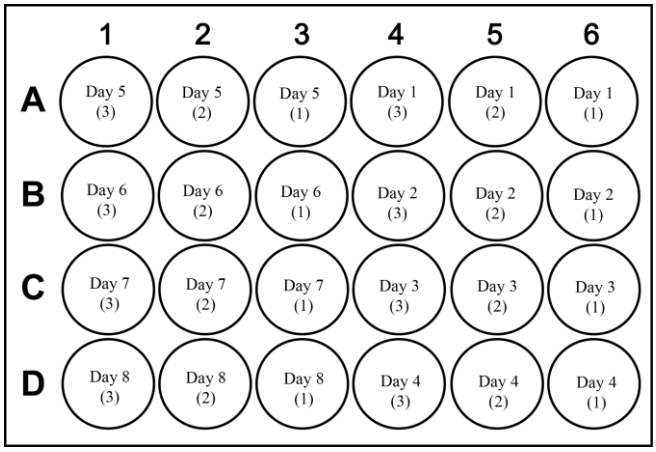

Figure 6.1 Plate layout for the HeLa cell growth curve experiment

6.2.4.2 Determining Optimal Cell Counts for MTT and LDH Assays

In order to accurately quantify any changes in the rate of cell proliferation, a linear relationship between cell number and signal produced was established. For the MTT assay, cells were seeded at a range of densities ($1x10^2$, $5x10^2$, $1x10^3$, $5x10^3$, $1x10^4$, $5x10^4$, and $1x10^5$ cells per 100 μL well) and left to attach overnight in standard incubation conditions. A blank containing no cells and only DMEM was also included. The MTT assay was carried out the next day as per the protocol described in Section 6.2.2.1. The absorbance was plotted against cell density and the linear region of the graph indicated the optimal cell counts for MTT experiments. The optimal cell count for the LDH assay was obtained in a

similar manner with cells seeded at $1x10^2$, $5x10^2$, $1x10^3$, $5x10^3$, $1x10^4$, $5x10^4$ and $1x10^5$ cells per 100 µL well). After the cells were attached overnight, 10 µL of 10X lysis solution (1X) was added to each well and incubated for forty-five minutes under standard conditions. The plate was then centrifuged at 250 × *g* for four minutes at room temperature, and the LDH assay was carried out as per the protocol described in Section 6.2.2.2.

6.2.4.3 Time-Course and Dose Response Experiment

In order to obtain information on optimal experimental conditions, time course and dose response experiments were carried out. Following the suggestion of a generic protocol from previous bioassay work on the P388 cell line at the University of Canterbury, a 1 in 80 dilution (12500 ng/mL) of the pterocellin A stock solution (1 mg/mL) was prepared and a further seven concentrations were made by serial dilution (Table 6.7).

Table 6.7 Pterocellin A concentrations used in initial time-course experiments

Sample #	Concentration (ng/mL)
1 (lowest)	98
2	195
3	391
4	781
5	1563
6	3125
7	6250
8 (highest)	12500

Cells were seeded in triplicate as described in Section 6.2.2.1 and treatment of test compound was prepared by serial dilution (Figure 6.2) in the layout shown in

(Figure 6.3). This was incubated for initial time periods of 24, 48 and 72 hours. MTT and LDH assays were utilised at the end of each incubation period to measure cell viability and cell lysis (if any).

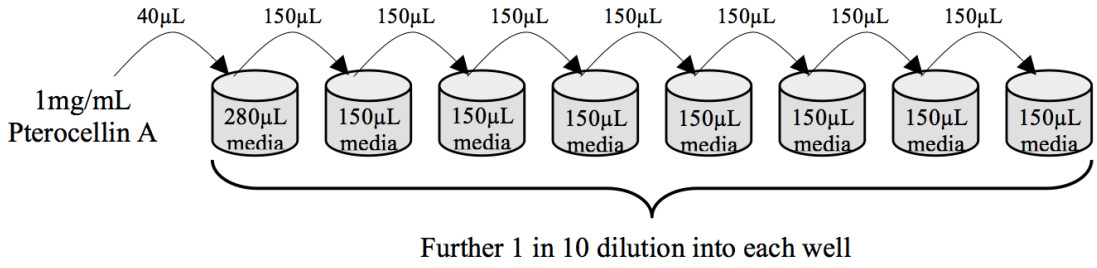

Figure 6.2 Dilution series of the initial time-course dose response experiments

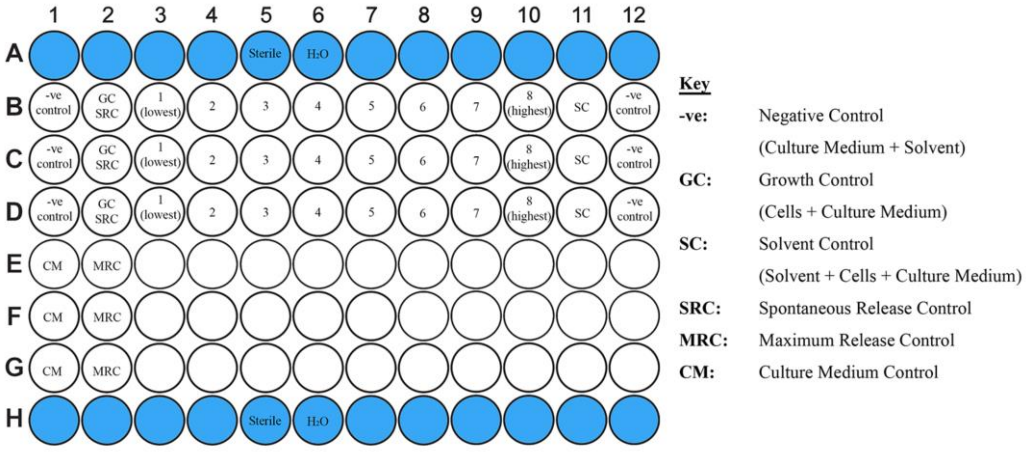

Figure 6.3 Plate layout for MTT and LDH assays

Further time-course and dose response experiments were carried out. Treatment with test compound was carried out at 3, 6, 12 and 24 hours with a much narrower range of concentrations (Table 6.8) prepared by serial dilution shown in Figure 6.4.

Table 6.8 Pterocellin A concentrations used in later time-course experiments

Sample #	Concentration (ng/mL)
1 (lowest)	16
2	31
3	63
4	125
5	250
6	500
7	1000
8 (highest)	2000

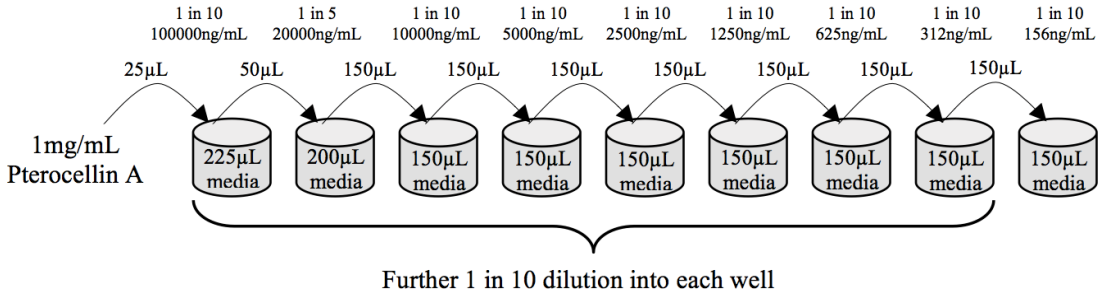

Figure 6.4 Dilution series of the later time-course dose response experiments

6.2.4.4 Trypan Blue Exclusion Experiment

This experiment was carried out in triplicate. Cells were seeded in a 24-well plate at $5x10^4$ cells per well (100 µL) and left to attach overnight. Two controls were used in this experiment: growth control and solvent control. Six concentrations of pterocellin A treatment were prepared (Table 6.9) and cells were incubated in standard incubation conditions for 24 hours.

To harvest the cells after treatment, culture media was transferred to Eppendorf tubes (1.5 mL) from each well to collect detached cells. The collected cells were then centrifuged at 800 × *g* for five minutes and the supernatant was removed.

While the collected cells were being centrifuged, those remaining were washed with pre-warmed PBS (0.5 mL) and harvested by adding trypsin/EDTA (0.2 mL).

Table 6.9 Sample concentrations in trypan blue exclusion

Sample #	Concentration (ng/mL)
Growth Control	Cells + Media
Solvent Control	Cells + Media + MeOH
1 (lowest)	62.5
2	125
3	250
4	500
5	1000
6 (highest)	2000

Once cells were in suspension, pre-warmed media (0.8 mL) was added to neutralise the effects of trypsin. This was then combined with the cells in Eppendorf tubes and cells were counted by trypan blue exclusion as an end point measurement. The numbers of excluded (live) cells and stained (dead) cells were recorded, and the cell viability relative to the solvent control was calculated. The calculated cell concentration (cells/mL) was equivalent to the number of cells in each sample with the volume being 1 mL.

6.2.4.5 Caspase-3 Activation Assay

This assay was carried out using a commercial kit Caspase-3 (active) FITC Staining Kit (Abcam) as per the manufacturer's protocol with small modifications. Near confluent cells in log-phase were harvested and seeded at a density of $3x10^5$ in a 6-well cell culture plate (Greiner Bio-One). The cells were then incubated at standard incubation conditions overnight to allow the cells to

attach and recover from handling before treatment was added. After treatment, the media from each well was transferred to Falcon tubes (15 mL) to collect any detached cells from treatment. The remaining cells were harvested by washing with pre-warmed PBS (1 mL) followed by the addition of trypsin/EDTA (0.5 mL). Once detached, pre-warmed DMEM (1.5 mL) was added to each well to neutralise trypsin before being transferred to the corresponding Falcon tubes. An aliquot (100 μL) was then taken from each sample for a cell count. The remaining cells were centrifuged at 800 × *g* for five minutes, and the cell pellets were re-suspended in pre-warmed DMEM (1 mL). To measure the fluorescent activity of caspase-3, FITC-DEVD-FMK (1 μL) was added to aliquots (300 μL) of each sample in Eppendorf tubes (1.5 mL) and incubated at standard incubation conditions for 1 hour. After incubation, the cells were centrifuged at 3000rpm for 5 minutes and the supernatant was removed. Wash Buffer (0.5 mL) was then added followed by centrifugation; and this step was repeated again. Finally, the cell pellet was re-suspended in Wash Buffer (100 μL) then transferred to a black microtitre plate (Greiner Bio-One). The fluorescence intensity was measured on a plate reader (BMG Fluostar Optima) at excitation and emission wavelengths of 485 nm and 520 nm respectively.

6.2.4.6 Confocal Fluorescent Microscopy

Fluorescent microscopy work was carried out on an Olympus FV1000 laser scanning confocal microscope. The staining and visualisation of the mitochondria utilised a fluorescent dye MitoTracker Red CMXRos which has peak absorption and emission at 578 nm and 599 nm respectively, producing a red fluorescence.

A stock solution (1 mM) was made up according to the manufacturer's manual by adding DMSO (94 μL) to a vial (50 μg) of MitoTracker Red CMXRos at room temperature. An aliquot (10 μL) was made up to 1 μM with complete DMEM (9.99 mL) and stored at -20°C protected from light. The working solutions (50 nM) were prepared fresh from the 1 μM stock solution before each experiment.

To visualise mitochondria under fluorescence, cells were grown in a Fluorodish™ (WPI) and stained with working solution under standard conditions for twenty minutes. The staining media was then replaced with fresh media and cells were incubated for a further ten minutes to wash away unincorporated dye. Treatment of pterocellin A was applied after staining.

6.2.4.7 DNA Extraction and DNA Agarose Gel Electrophoresis

DNA extractions were carried out according to manufacturer's protocol using either the Apoptotic DNA Ladder Detection Kit (Abcam) or the Quick-gDNA™ MiniPrep DNA Extraction Kit (Zymo). Cells were seeded in a 6-well plate (Greiner Bio-One) at 0.5 – $1x10^6$ cells per well, and left to attach overnight and treatment was added the next day.

DNA extraction using the Quick-gDNA™ MiniPrep DNA Extraction Kit (Zymo) was carried out as follows. Cells were harvested by directly adding the Genomic Lysis Buffer (1 mL) to each well after removing the media. This was then left for ten minutes at room temperature before being transferred to a Zymo-spin column in a collection tube. The column was then centrifuged at 10000 × *g* for one minute and the collection tube was discarded, and replaced with a new one. DNA Pre-wash Buffer (200 μL) was added to the spin column and centrifuged again at 1000 × *g* for one minute. This was followed by the addition of gDNA Wash Buffer

(500 μL) and further centrifugation. The collection tube was then discarded and the spin-column was placed in an Eppendorf tube with added Elution Buffer (150 μL). This was incubated for five minutes at room temperature before centrifugation at 16000 × *g* for thirty seconds. The eluted DNA was then used for gel electrophoresis and the rest was frozen at -20°C.

DNA extraction using the Apoptotic DNA Ladder Detection Kit (Abcam) was carried out as follows. Cells were harvested and pelleted as per normal; the supernatant was also collected to collect any detached cells. The cell pellet was washed by PBS and centrifuged at 500 × *g* for five minutes then the supernatant was removed. TE Lysis Buffer (35 μL) was then added and mixed by gentle pipetting to lyse the cells. This was followed by the addition of Enzyme A Solution (5 μL), gentle mixing by vortex and incubation at 37°C for twenty minutes. Enzyme B Solution (5 μL) was then added and cells incubated at 37°C for at least two hours. Afterwards, ammonium acetate solution (5 μL) was added to each sample, mixed, then followed by the addition of isopropanol (50 μL). This was kept in the freezer at -20°C overnight. Samples were centrifuged the next day for ten minutes at maximum speed (16000 × *g*) to precipitate the DNA. After removing the supernatant, the DNA pellets were washed with cold 70% ethanol (0.5 mL), and air-dried at room temperature for 10 minutes after the removal of ethanol. Finally, the pellet was dissolved in DNA Suspension Buffer (30 μL).

To prepare for gel electrophoresis, 5 μL of each sample was mixed with a loading dye (2 μL) before being loaded into the gel. The gel was made by 2% agarose in 1X TBE buffer, with a either small amount of ethidium bromide or SYBR Safe

Stain (Invitrogen). The gels ran at a low voltage (35V) for four hours before being analysed on the MiniBIS Pro using GelCapture software.

6.2.5 Work Described in Chapter Three

6.2.5.1 Bioassay Protocol Using the HeLa Cell Line

Based on the biochemistry work carried out on pterocellin A using HeLa cells, a bioassay protocol was developed using MTT and LDH assays to guide the process of isolating bioactive natural products. The MTT and LDH assays followed the same protocol with the same controls as described in Section 6.2.2.1 and 6.2.2.2 respectively. Bioassays were carried out in the PC2 laboratory using HeLa cells. Four concentrations were prepared from each fraction and the experiments were carried out in triplicate.

The bioassay procedure for the C_{18} column fractions (AW1.115) was carried out as follows: a subsample (2 mg) was taken from each fraction (AW1.115.2 – AW1.115.14 and dissolved in MeOH to a stock concentration of 20 mg/mL. This was then further prepared into four working concentrations by serial dilution, and added to the corresponding wells on a 96-well plate containing $1x10^4$ cells. The total dilution factor was 1:100. The final concentrations for the bioassay were 0.025, 0.05, 0.1 and 0.2 mg/mL for each fraction. The plate was incubated in standard conditions for 24 hours and MTT assay was carried out at the end. The percentage of growth inhibition relative to the control was calculated using Equation 6.3.

The bioassay procedure for the LH-20 column fractions (AW1.140) was similar to the above. Four concentrations in triplicate were assayed for each fraction. A

stock solution of each fraction (AW1.140.4 – AW1.140.15) was standardised to 10 mg/mL. Final concentrations for the bioassay were 0.0125, 0.025, 0.05 and 0.1 mg/mL. MTT and LDH assays were carried out at the end of the 24 hour incubation period. The percentage of growth inhibition relative to the control for both MTT and LDH assays was calculated using Equation 6.3 and Equation 6.4

The IC_{50} values were calculated by plotting % inhibition vs. the logarithm of the sample concentration, and the antilog of the 50% value obtained was the IC_{50}. An alternative method of obtaining the IC_{50} values was by plotting the log (% inhibition / (100 - % inhibition)) vs. log (concentration) and calculating the linear region of the regression line that intercepts the x-axis. This is a more precise way of obtaining the IC_{50} values, however it requires a high number of data points.

6.2.6 Work Described in Chapter Four

6.2.6.1 Bulk Sample Extraction

Exhaustive bulk extraction was carried out on a proportion (201 g) of the *P. vesiculosa* (AI201-11, identified by sample voucher) sample. The extraction process began by soaking the sample in solvent (MeOH:DCM, 3:1) overnight at 4°C. The sample was then blended in small quantities and filtered through a Buchner funnel to collect the filtrate. The dried sample was then repeatedly blended with fresh solvent (MeOH:DCM; 3:1) six times until the filtrate became colourless. The filtrate was then dried by rotary evaporation (Büchi) and lyophilisation in liquid nitrogen to yield crude extract AW1.116 (4.2 g). The crude extract was then subjected to further separation and analysis.

6.2.6.2 Thin Layer Chromatography (TLC)

All fractions from each separation step were analysed by TLC using aluminium backed pates coated with silica gel (Merck TLC silica gel 60 F_{254}). TLC analyses were performed in a solvent mixture of ethyl acetate and methanol (EtOAc:MeOH; 5:1). Samples were dissolved in MeOH and applied to the plate using thinly drawn glass capillary tubes. The TLC plates were then visualised under a UV lamp (Uvitec) at wavelengths of 245 nm and 312 nm.

6.2.6.3 Reversed Phase C18 Column Chromatography

The reversed phase column was prepared by mixing C_{18} gel (YMC) and MeOH to produce a slurry, which was then packed into a glass column and equilibrated back to H_2O. The crude extract (AW1.111) was carefully loaded as solids and the chromatography followed a steep, stepped gradient from H_2O to MeOH to DCM, then back to H_2O (Table 6.10) under a gentle N_2 gas pressure.

Table 6.10 Solvent gradient for reverse phased chromatography

Solvent	Volume (mL)
H_2O	150
H_2O:MeOH (1:1)	335
H_2O:MeOH (3:7)	150
H_2O:MeOH (1:9)	150
MeOH	300
MeOH:DCM (9:1)	150
MeOH:DCM (1:1)	160
DCM	160
MeOH	150
H_2O:MeOH (1:1)	150
H_2O	150

The collected fractions (AW1.115.1-15) were then rotary evaporated to dryness and transferred to a pre-weighed glass vial, which was then placed in a heating block (Lab-line) at 36°C to be dried under a gentle N_2 stream.

6.2.6.4 Size Exclusion Chromatography

The size exclusion column was packed with Sephadex LH-20 (Pharmacia Fine Chemicals) into a glass column and eluted with MeOH. The sample (AW1.115.6) was loaded by dissolving in minimum MeOH and added to the column with a glass Pasteur pipette. Fractions (AW1.140.1-19) were collected (~ 50 mL each) and dried by rotary evaporation under N_2.

6.2.6.5 Liquid Chromatography – Mass Spectrometry (LC-MS)

All LC-MS experimental data were generated on an HPLC (UltiMate 3000; Dionex) coupled to a mass spectrometer (Bruker Daltonics amaZon X™) using electrospray ionisation in positive ion mode. The instrumental method utilised a standard solvent gradient with running conditions listed in Table 6.11.

All samples were prepared by dissolving in HPLC-grade MeOH (500 µL) and filtered (0.2 µm) into HPLC vials, followed by addition of MeOH (2 x 250 µL) into the vials.

Table 6.11 LC instrumental conditions for all LC-MS experiments

Flow Rate	0.2 mL/min
Column	Reversed Phase; Phenomenex, Luna 5 µ C_{18} 100 Å, 150 x 4.60 mm
Column Temperature	25°C
Mobile Phase Solvents	**Solvent A** 0.05% TFA in H_2O **Solvent B** 0.05% TFA in acetonitrile (ACN)

Detector	DIONEX UltiMate 3000 Diode Array Detector		
Run Time	50 minutes		
Gradient Programme	**Time (minutes)**	**Solvent A %**	**Solvent B %**
	0	95	5
	2	95	5
	27	0	100
	39	0	100
	45	95	5
	50	95	5

Appendices

Appendix 1: Bioassay Development Raw Data

Appendix 1.1: AW1.115 Bioassay Raw Data, MTT Assay

Appendix 1.2: AW1.140 Bioassay Raw Data, MTT Assay

Appendix 1.3: AW1.140 Bioassay Raw Data, LDH Assay

Appendix 1.1: AW1.115 Bioassay Raw Data, MTT Assay

Plate 1					
Sample #	**Crude Concentration (ug/ml)**	**Mean RI%**	**Standard Deviation RI%**	**Standard Error RI%**	**IC_{50} (mg/mL)**
Growth Control	0	-8.59	11.30	6.52	
AW1.115.2	0.025	6.47	5.06	2.92	0.4636
	0.05	-0.76	15.46	8.92	
	0.1	-1.82	3.67	2.12	
	0.2	6.97	2.61	1.51	
AW1.115.3	0.025	9.45	13.55	7.82	0.2194
	0.05	16.33	10.74	6.20	
	0.1	16.38	8.60	4.97	
	0.2	3.74	19.26	11.12	
AW1.115.4	0.025	22.54	3.64	2.10	0.2022
	0.05	26.03	19.37	11.19	
	0.1	22.85	7.74	4.47	
	0.2	32.50	11.54	6.66	
AW1.115.5	0.025	11.78	8.73	5.04	0.1486
	0.05	9.91	1.35	0.78	
	0.1	16.63	5.78	3.34	
	0.2	70.86	10.92	6.31	
AW1.115.6	0.025	11.22	11.62	6.71	0.1963
	0.05	6.37	27.38	15.81	
	0.1	3.03	29.18	16.85	
	0.2	99.97	0.30	0.18	
AW1.115.7	0.025	45.39	7.23	4.18	0.0229
	0.05	27.80	8.81	5.08	
	0.1	22.74	8.04	4.64	
	0.2	39.52	6.08	3.51	

Appendix 1.1 (Cont.): AW1.115 Bioassay Raw Data, MTT Assay

Plate 2					
Sample #	**Crude Concentration (mg/ml)**	**Mean RI%**	**Standard Deviation RI%**	**Standard Error RI%**	**IC50 (mg/mL)**
Growth Control	0	-15.17	13.43	7.76	
AW1.115.8	0.025	5.87	3.01	1.74	0.2728
	0.05	12.05	3.33	1.92	
	0.1	6.54	4.22	2.43	
	0.2	15.66	18.41	10.63	
AW1.115.9	0.025	-7.67	9.96	5.75	-
	0.05	-21.71	4.15	2.40	
	0.1	-20.94	6.26	3.61	
	0.2	-32.32	15.01	8.67	
AW1.115.10	0.025	11.01	1.90	1.10	-
	0.05	14.71	4.99	2.88	
	0.1	8.08	4.64	2.68	
	0.2	-5.15	13.73	7.93	
AW1.115.11	0.025	-10.25	6.71	3.87	0.1998
	0.05	-8.31	14.00	8.08	
	0.1	-12.82	15.74	9.09	
	0.2	36.33	29.80	17.20	
AW1.115.12	0.025	-11.42	6.98	4.03	0.1146
	0.05	-16.57	15.71	9.07	
	0.1	-0.68	9.22	5.32	
	0.2	74.84	26.28	15.17	
AW1.115.13	0.025	12.37	12.07	6.97	-
	0.05	-0.95	11.34	6.55	
	0.1	-11.55	3.36	1.94	
	0.2	-23.47	5.22	3.01	
AW1.115.14	0.025	3.93	17.48	10.09	-
	0.05	3.11	14.78	8.53	
	0.1	16.61	14.43	8.33	
	0.2	26.72	13.06	7.54	

	Plate 1		Plate 2	
	Mean	Blanked Corrected	Mean	Blanked Corrected
Solvent Control	0.668	0.660	0.744	0.739
Culture Medium (Blank)	0.009	-	0.006	-

Appendix 1.2: AW1.140 Bioassay Raw Data, MTT Assay

Plate 1					
Sample #	**Crude Concentration (mg/ml)**	**Mean RI%**	**Standard Deviation RI%**	**Standard Error RI%**	**IC_{50} (mg/mL)**
Growth Control	0	3.73	5.88	3.40	
AW1.140.4	0.0125	1.22	6.62	3.82	0.0502
	0.025	-1.22	2.89	1.67	
	0.05	13.43	3.22	1.86	
	0.1	28.15	4.83	2.79	
AW1.140.5	0.0125	-7.71	4.91	2.84	-
	0.025	-11.57	17.45	10.08	
	0.05	-4.43	10.75	6.21	
	0.1	-5.66	15.53	8.97	
AW1.140.6	0.0125	5.91	4.55	2.62	0.0635
	0.025	3.79	6.36	3.67	
	0.05	5.33	4.94	2.85	
	0.1	10.35	1.77	1.02	
AW1.140.7	0.0125	17.67	16.07	9.28	0.0557
	0.025	15.36	12.55	7.25	
	0.05	34.96	5.89	3.40	
	0.1	100.26	0.62	0.36	
AW1.140.8	0.0125	23.91	9.35	5.40	0.0132
	0.025	99.10	0.40	0.23	
	0.05	99.42	0.19	0.11	
	0.1	99.10	0.49	0.28	
AW1.140.9	0.0125	11.38	9.13	5.27	0.0940
	0.025	9.00	2.52	1.46	
	0.05	10.28	16.07	9.28	
	0.1	96.34	2.55	1.47	

Appendix 1.2 (Cont.): AW1.140 Bioassay Raw Data, MTT Assay

Plate 2					
Sample #	**Crude Concentration (mg/ml)**	**Mean RI%**	**Standard Deviation RI%**	**Standard Error RI%**	**IC_{50} (mg/mL)**
Growth Control	0	-3.28	2.39	1.38	
AW1.140.10	0.0125	6.57	5.07	2.92	0.0211
	0.025	34.88	4.35	2.51	
	0.05	48.47	3.35	1.94	
	0.1	100.16	0.34	0.20	
AW1.140.11	0.0125	-10.84	1.09	0.63	-
	0.025	-12.22	6.52	3.76	
	0.05	-11.43	5.57	3.22	
	0.1	-4.86	7.30	4.21	
AW1.140.12	0.0125	21.41	15.73	9.08	-
	0.025	1.31	19.00	10.97	
	0.05	4.01	31.38	18.12	
	0.1	-6.24	7.95	4.59	
AW1.140.13	0.0125	-5.32	8.08	4.66	-
	0.025	-5.65	11.28	6.51	
	0.05	-0.20	7.74	4.47	
	0.1	2.56	5.77	3.33	
AW1.140.14	0.0125	-10.51	0.89	0.51	-
	0.025	-11.30	4.95	2.86	
	0.05	-4.47	11.03	6.37	
	0.1	-6.63	18.33	10.58	
AW1.140.15	0.0125	34.22	6.21	3.59	-
	0.025	2.50	11.40	6.58	
	0.05	-2.63	6.26	3.61	
	0.1	-2.89	5.36	3.10	

	Plate 1		**Plate 2**	
	Mean	**Blanked Corrected**	**Mean**	**Blanked Corrected**
Solvent Control	0.528	0.519	0.515	0.508
Culture Medium (Blank)	0.009	-	0.008	-

Appendix 1.3: AW1.140 Bioassay Raw Data, LDH Assay

Plate 1				
Sample #	**Crude Concentration (mg/ml)**	**Mean Membrane Integrity Loss %**	**Standard Deviation %**	**Standard Error %**
AW1.140.4	0.0125	1.16	0.75	0.43
	0.025	1.14	0.99	0.57
	0.05	-0.60	0.33	0.19
	0.1	0.34	1.95	1.13
AW1.140.5	0.0125	0.16	0.38	0.22
	0.025	1.73	0.78	0.45
	0.05	2.20	1.43	0.82
	0.1	1.39	0.81	0.47
AW1.140.6	0.0125	-1.03	2.01	1.16
	0.025	0.00	2.52	1.46
	0.05	-0.04	2.52	1.45
	0.1	1.07	0.86	0.50
AW1.140.7	0.0125	0.78	1.45	0.83
	0.025	0.80	2.06	1.19
	0.05	-0.58	2.35	1.35
	0.1	15.81	3.46	2.00
AW1.140.8	0.0125	-0.20	0.27	0.16
	0.025	11.10	0.76	0.44
	0.05	17.58	2.49	1.44
	0.1	20.20	2.18	1.26
AW1.140.9	0.0125	-1.25	1.66	0.96
	0.025	-1.52	1.20	0.69
	0.05	0.90	0.08	0.05
	0.1	5.17	1.57	0.91

Appendix 1.3 (Cont.): AW1.140 Bioassay Raw Data, LDH Assay

Plate 2				
Sample #	**Crude Concentration (mg/ml)**	**Mean Membrane Integrity Loss %**	**Standard Deviation %**	**Standard %**
AW1.140.10	0.0125	0.05	1.35	0.78
	0.025	-0.82	0.49	0.28
	0.05	-2.56	0.64	0.37
	0.1	17.29	0.49	0.28
AW1.140.11	0.0125	0.91	2.12	1.22
	0.025	0.11	3.26	1.88
	0.05	2.22	12.39	7.16
	0.1	1.37	0.30	0.18
AW1.140.12	0.0125	2.39	3.99	2.30
	0.025	1.90	1.99	1.15
	0.05	2.33	3.86	2.23
	0.1	-0.60	0.63	0.36
AW1.140.13	0.0125	-0.68	0.39	0.23
	0.025	0.11	0.79	0.46
	0.05	0.17	0.20	0.12
	0.1	1.24	0.67	0.39
AW1.140.14	0.0125	-0.49	0.93	0.54
	0.025	0.09	0.67	0.39
	0.05	-0.80	0.00	0.00
	0.1	-0.54	0.05	0.03
AW1.140.15	0.0125	-1.48	0.79	0.45
	0.025	-0.62	0.35	0.20
	0.05	-1.19	0.37	0.21
	0.1	-1.27	0.42	0.25

	Plate 1		**Plate 2**	
	Mean	**Blanked Corrected**	**Mean**	**Blanked Corrected**
Spontaneous Release	0.851	0.225	0.873	0.202
Maximum Release	2.695	2.069	3.032	2.361
Culture Medium (Blank)	0.626	-	0.671	-

Appendix 2: Analysis of *Pterocella vesiculosa*

Appendix 2.1: LC-MS base peak chromatogram (BPC) of the P. vesiculosa crude extract

Appendix 2.2: BPC of the P. vesiculosa crude extract and mass spectra of known metabolites

Appendix 2.3: BPC of fraction AW1.115.4 and mass spectra of significant metabolites

Appendix 2.4: BPC of fraction AW1.115.5 and mass spectra of significant metabolites

Appendix 2.5: BPC of fraction AW1.115.6 and mass spectra of significant metabolites

Appendix 2.6: BPC of fraction AW1.115.7 and mass spectra of significant metabolites

Appendix 2.7: TLC analysis of the size-exclusion column fractions AW1.140.1– 19.

Appendix 2.8: BPC of fraction AW1.140.7 and mass spectra of significant metabolites

Appendix 2.9: BPC of fraction AW1.140.8 and mass spectra of significant metabolites

Appendix 2.10: BPC of fraction AW1.140.9 and mass spectra of significant metabolites

Appendix 2.11: BPC of fraction AW1.140.10 and mass spectra of significant metabolites

Appendix 2.12: Separation tree for the *Pterocella vesiculosa* extract

Appendix 2.1: LC-MS base peak chromatogram (BPC) of the *P. vesiculosa* crude extract

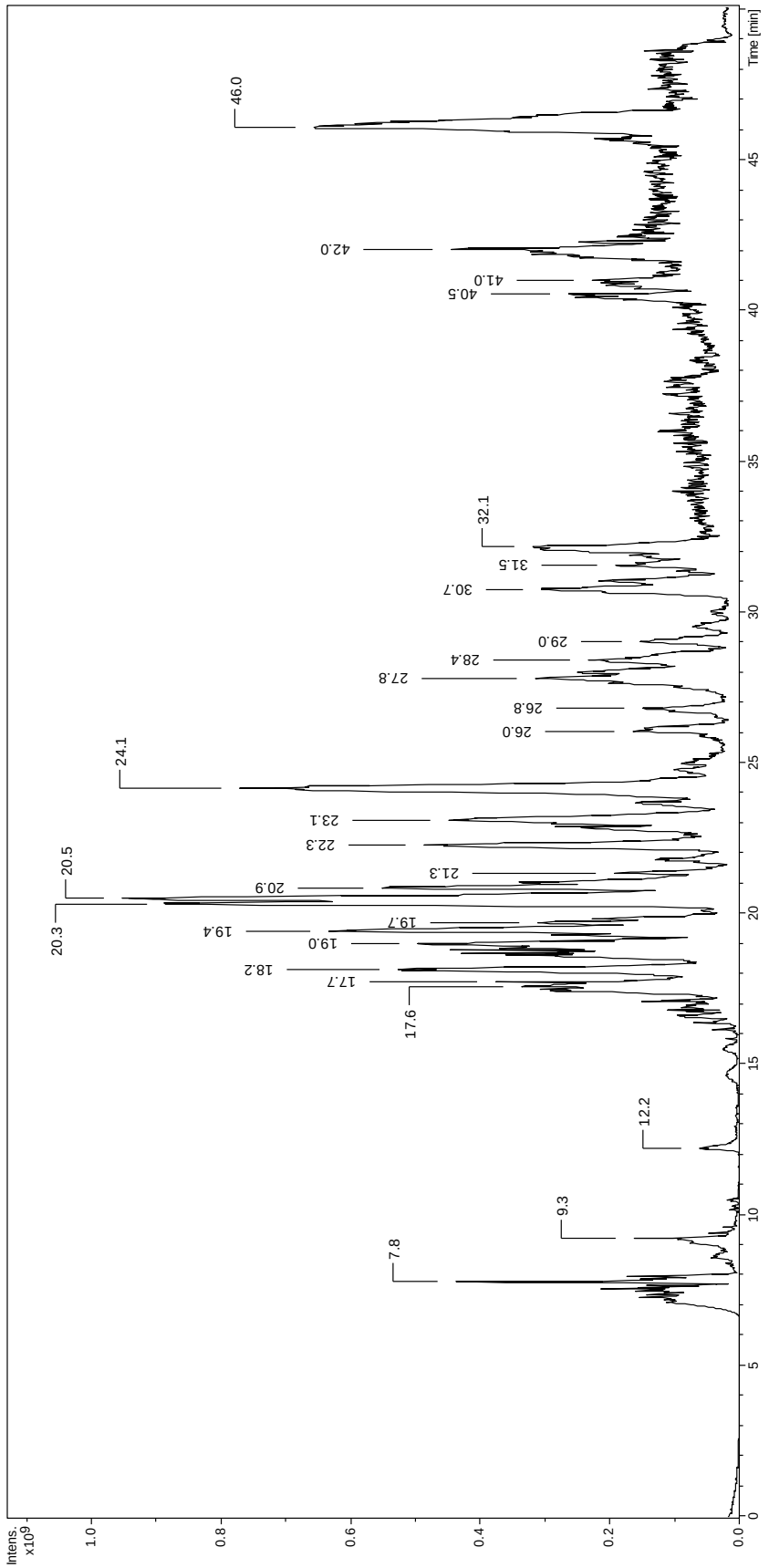

Appendix 2.2: BPC of the *P. vesiculosa* crude extract and mass spectra of known metabolites

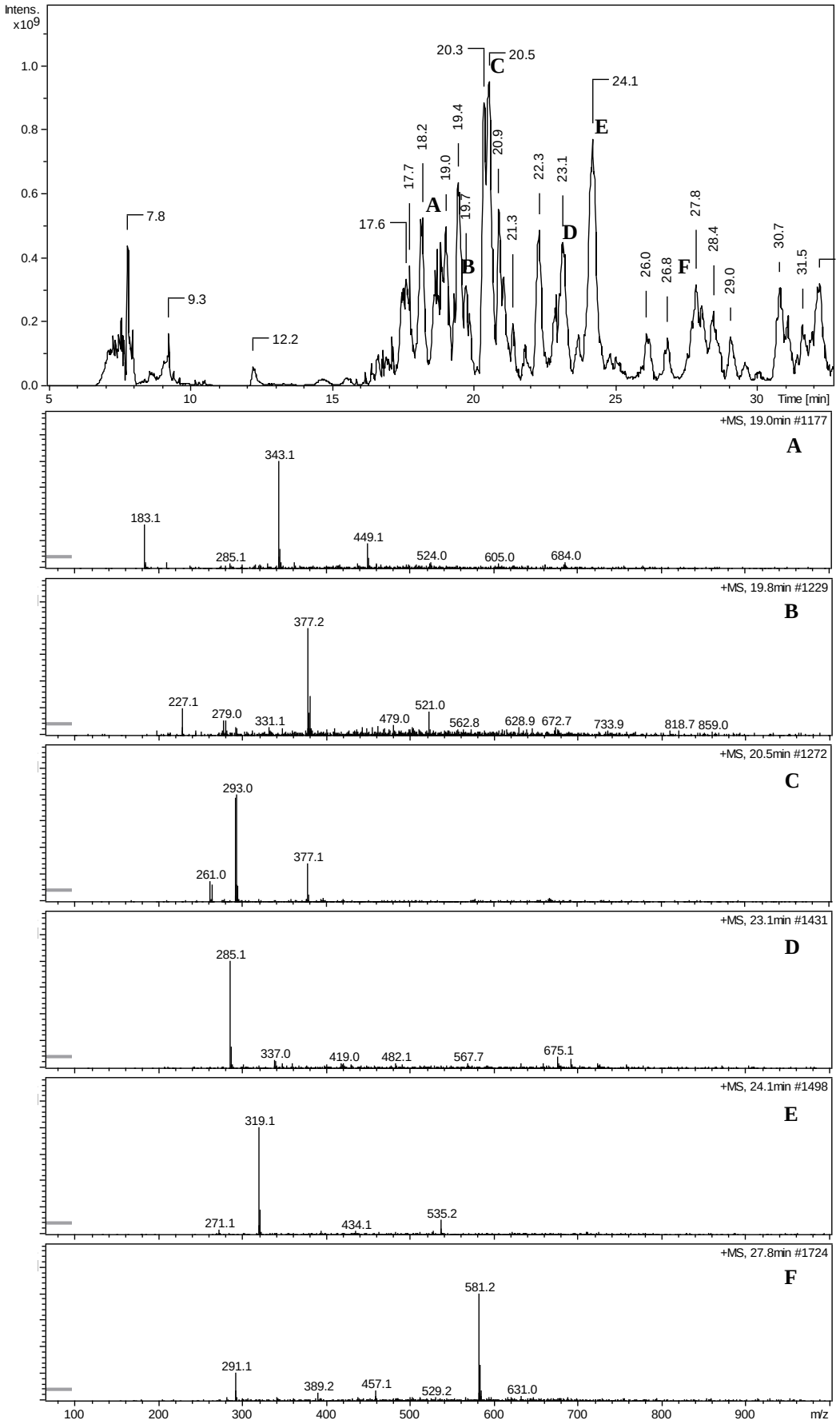

Appendix 2.3: BPC of fraction AW1.115.4 and mass spectra of significant metabolites

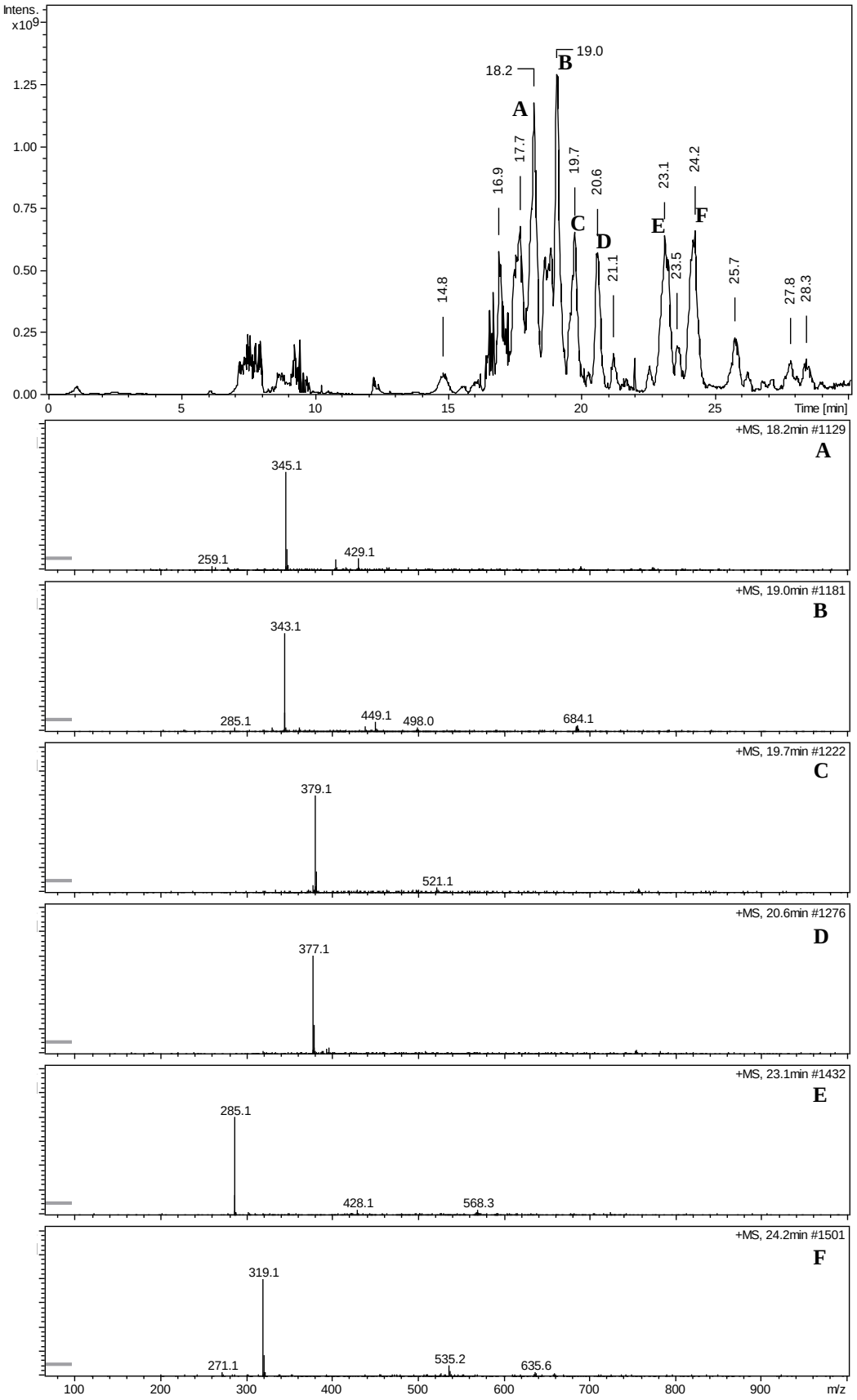

Appendix 2.4: BPC of fraction AW1.115.5 and mass spectra of significant metabolites

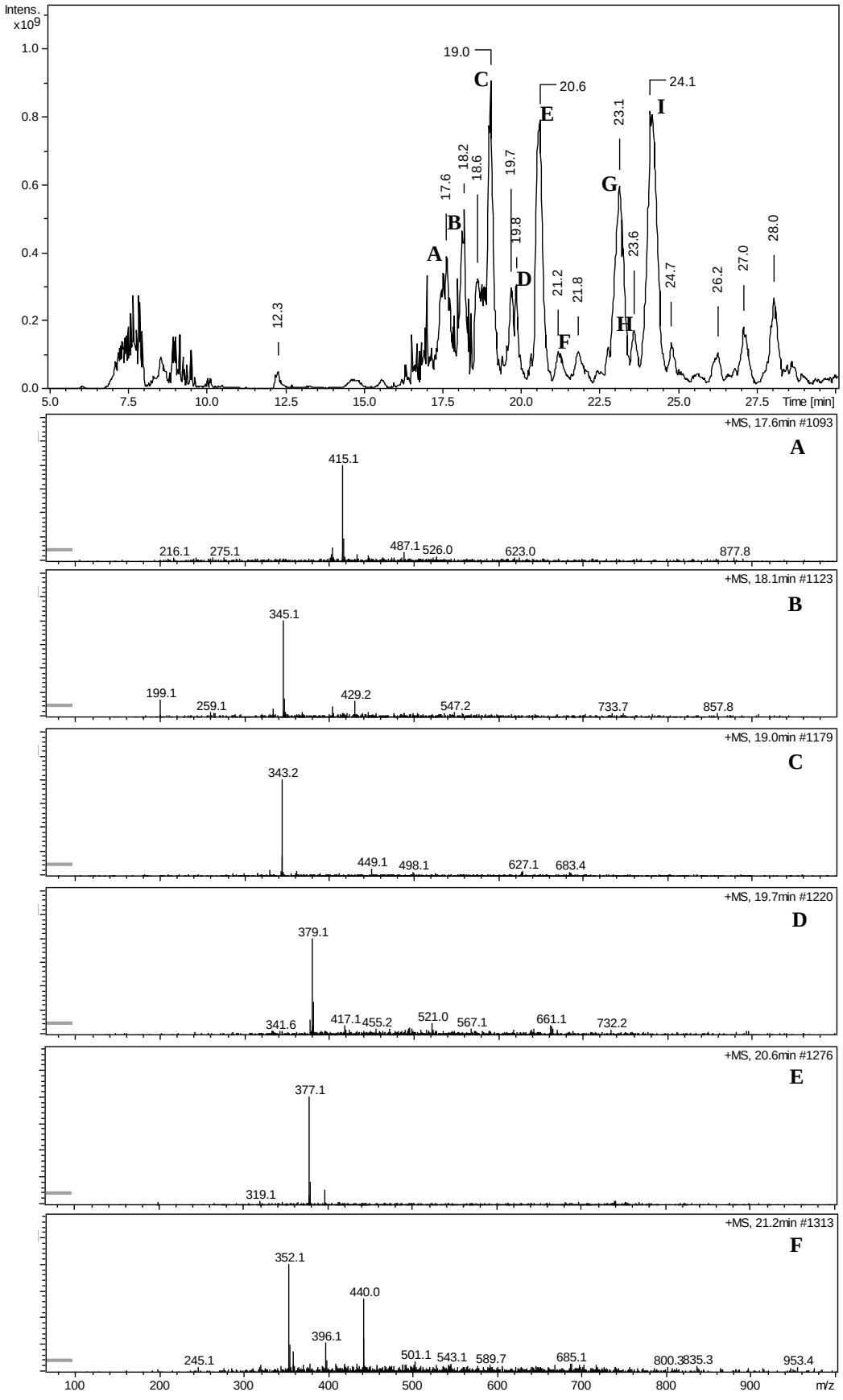

Appendix 2.4 (cont.): BPC of fraction AW1.115.5 and mass spectra of significant metabolites

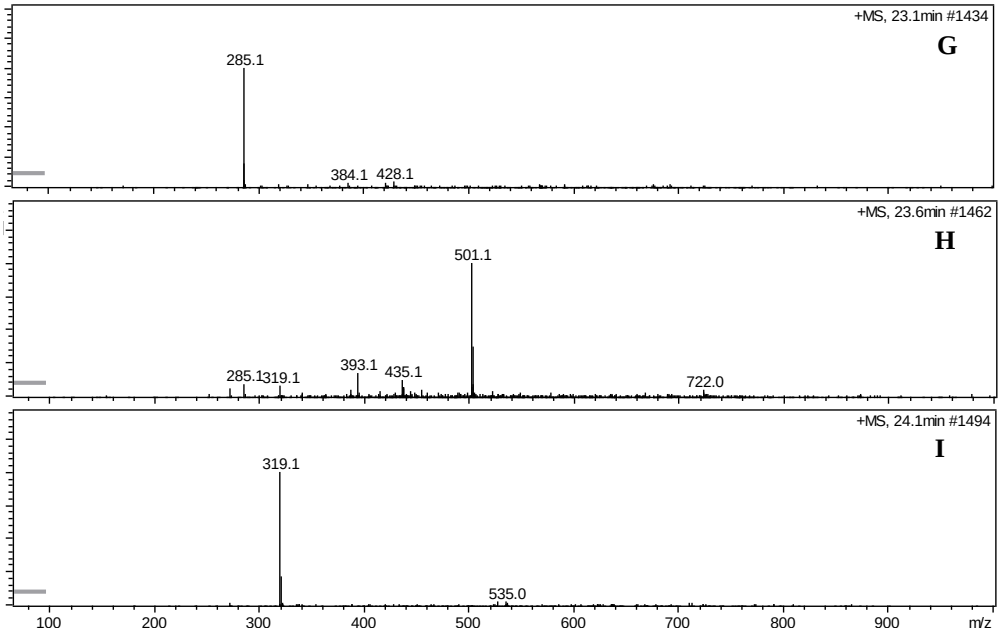

Appendix 2.5: BPC of fraction AW1.115.6 and mass spectra of significant metabolites

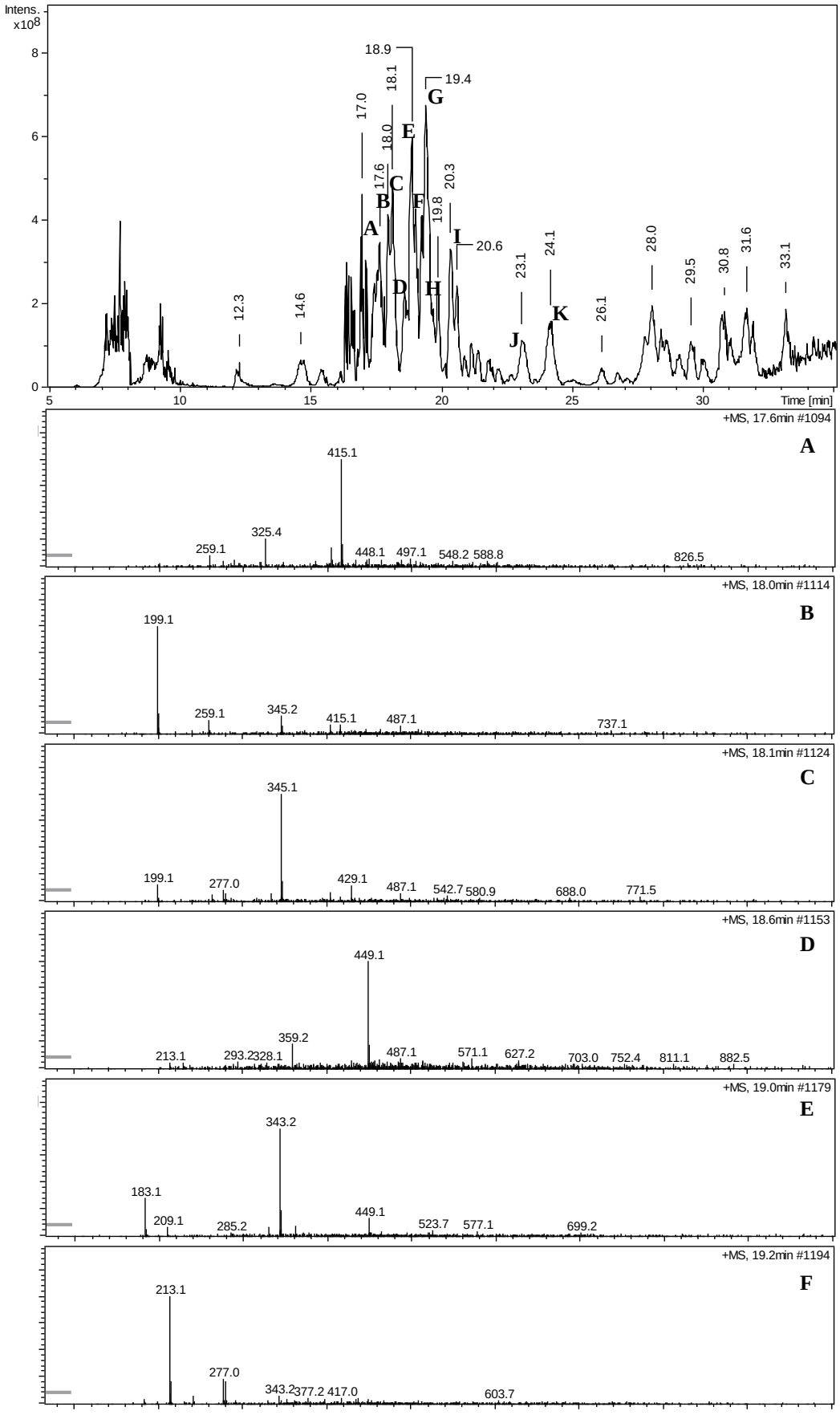

Appendix 2.5 (cont.): BPC of fraction AW1.115.6 and mass spectra of significant metabolites

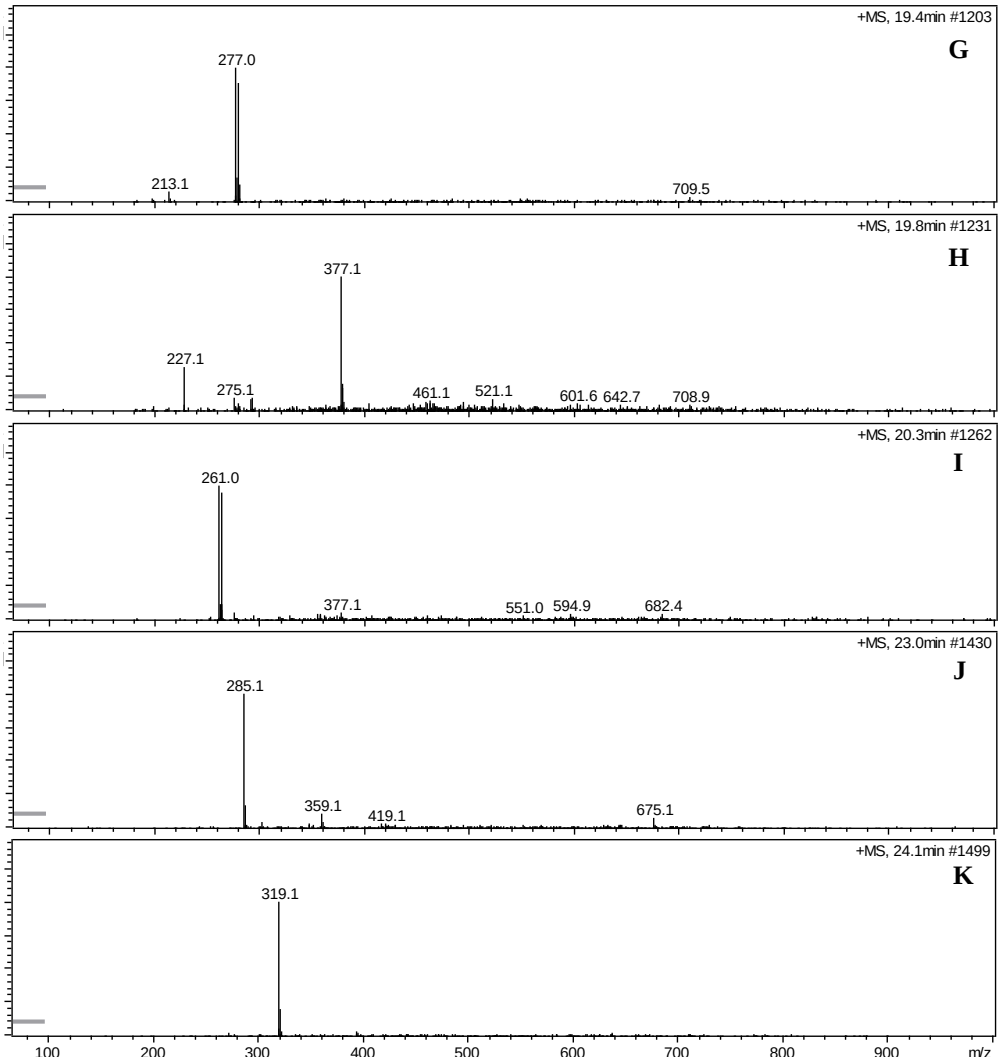

Appendix 2.6: BPC of fraction AW1.115.7 and mass spectra of significant metabolites

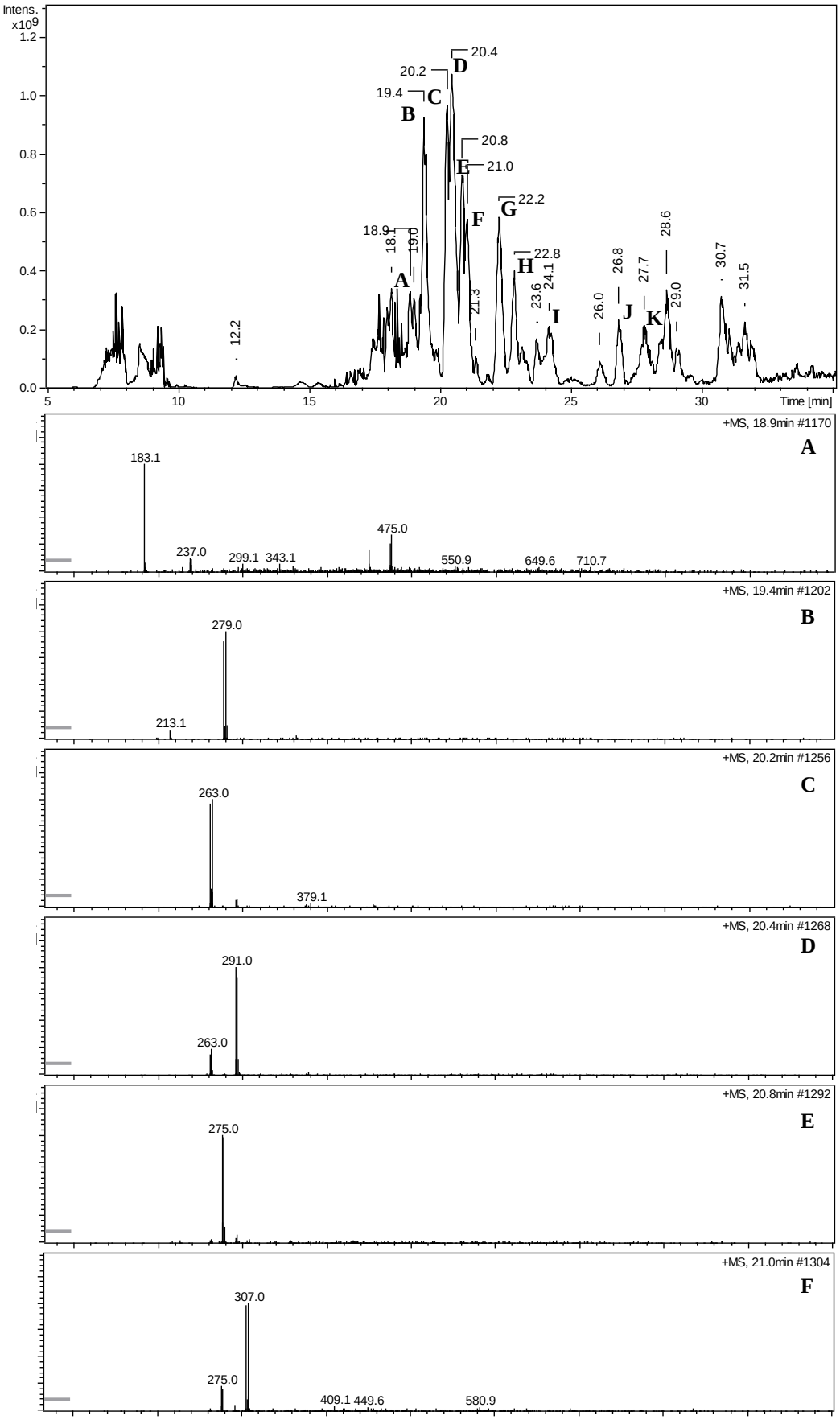

Appendix 2.6 (cont.): BPC of fraction AW1.115.7 and mass spectra of significant metabolites

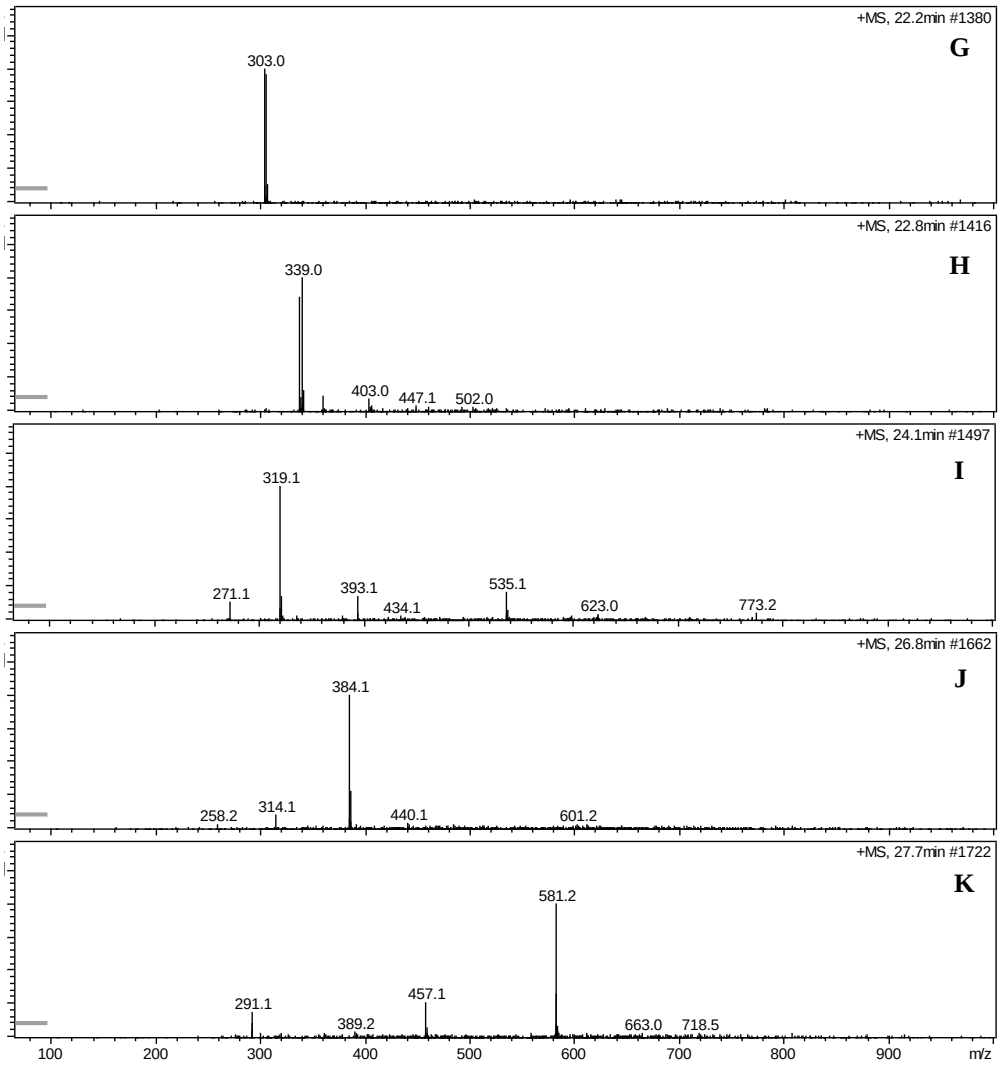

Appendix 2.7: TLC analysis of the size-exclusion column fractions AW1.140.1 – 19.

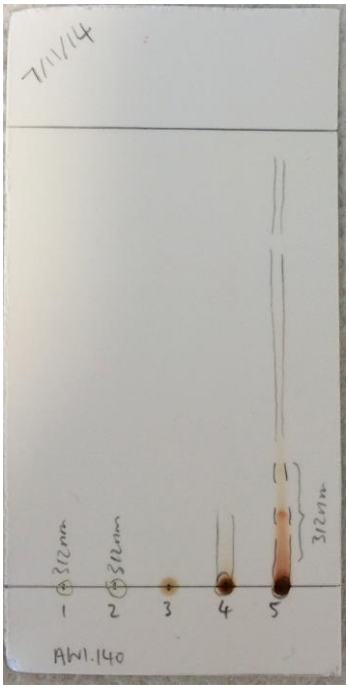

AW1.140.1 – 5

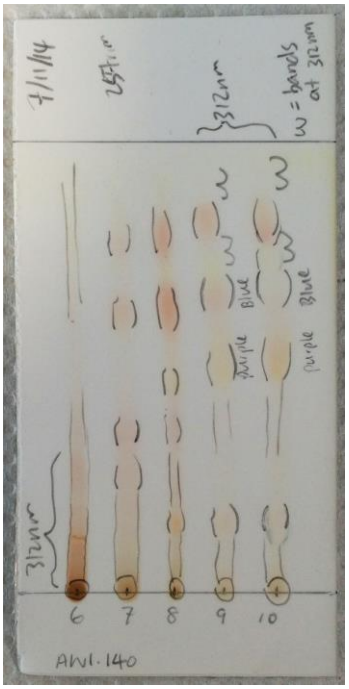

AW1.140.6 – 10

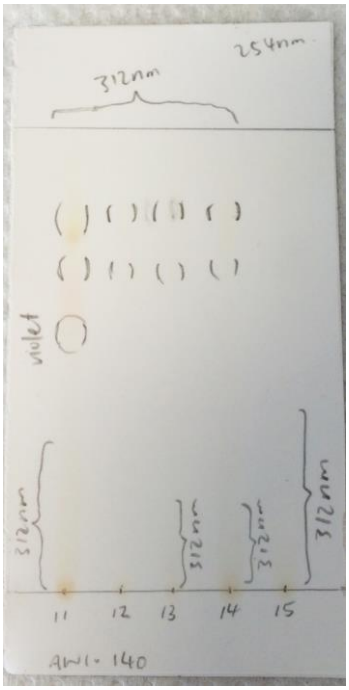

AW1.140.11 – 15

AW1.140.16 – 19

Appendix 2.8: BPC of fraction AW1.140.7 and mass spectra of significant metabolites

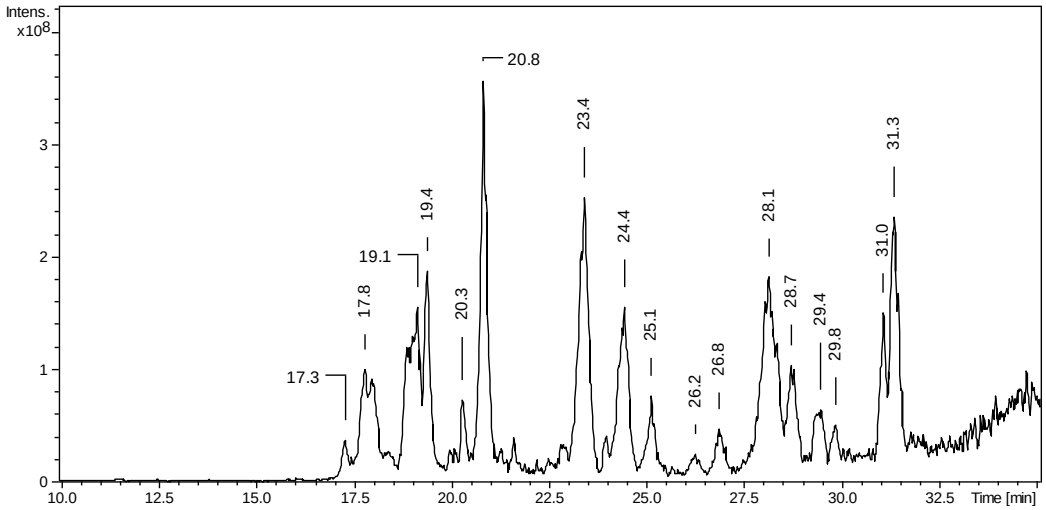

Appendix 2.9: BPC of fraction AW1.140.8 and mass spectra of significant metabolites

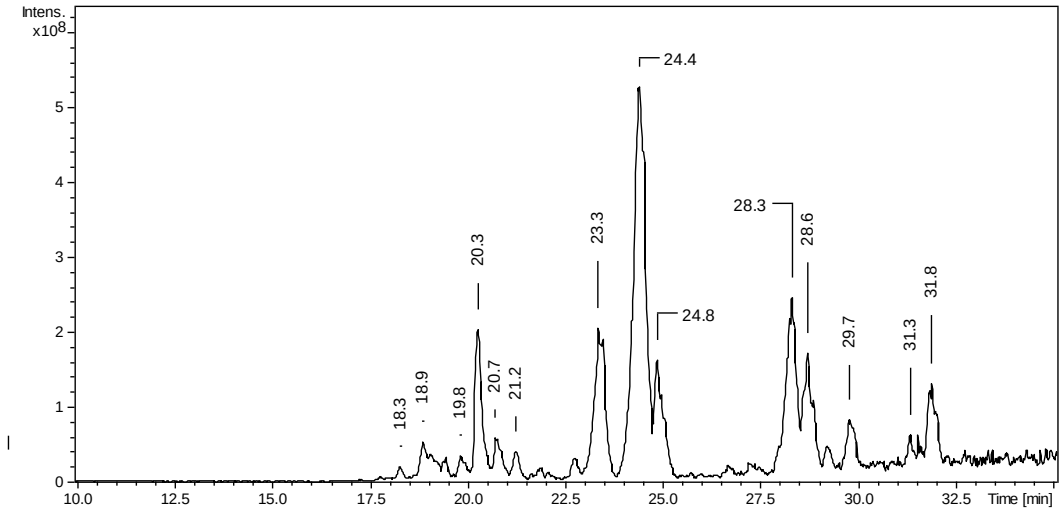

Appendix 2.10: BPC of fraction AW1.140.9 and mass spectra of significant metabolites

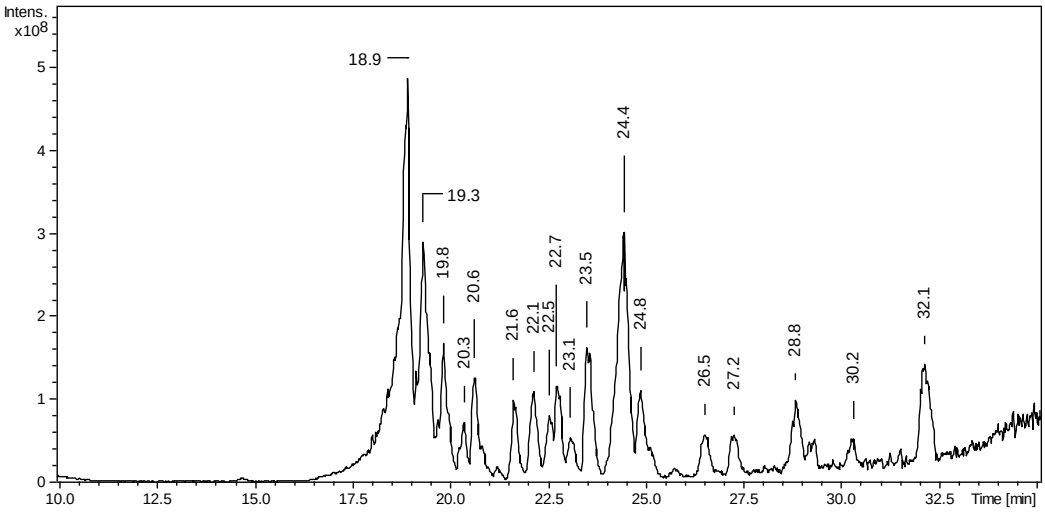

Appendix 2.11: BPC of fraction AW1.140.10 and mass spectra of significant metabolites

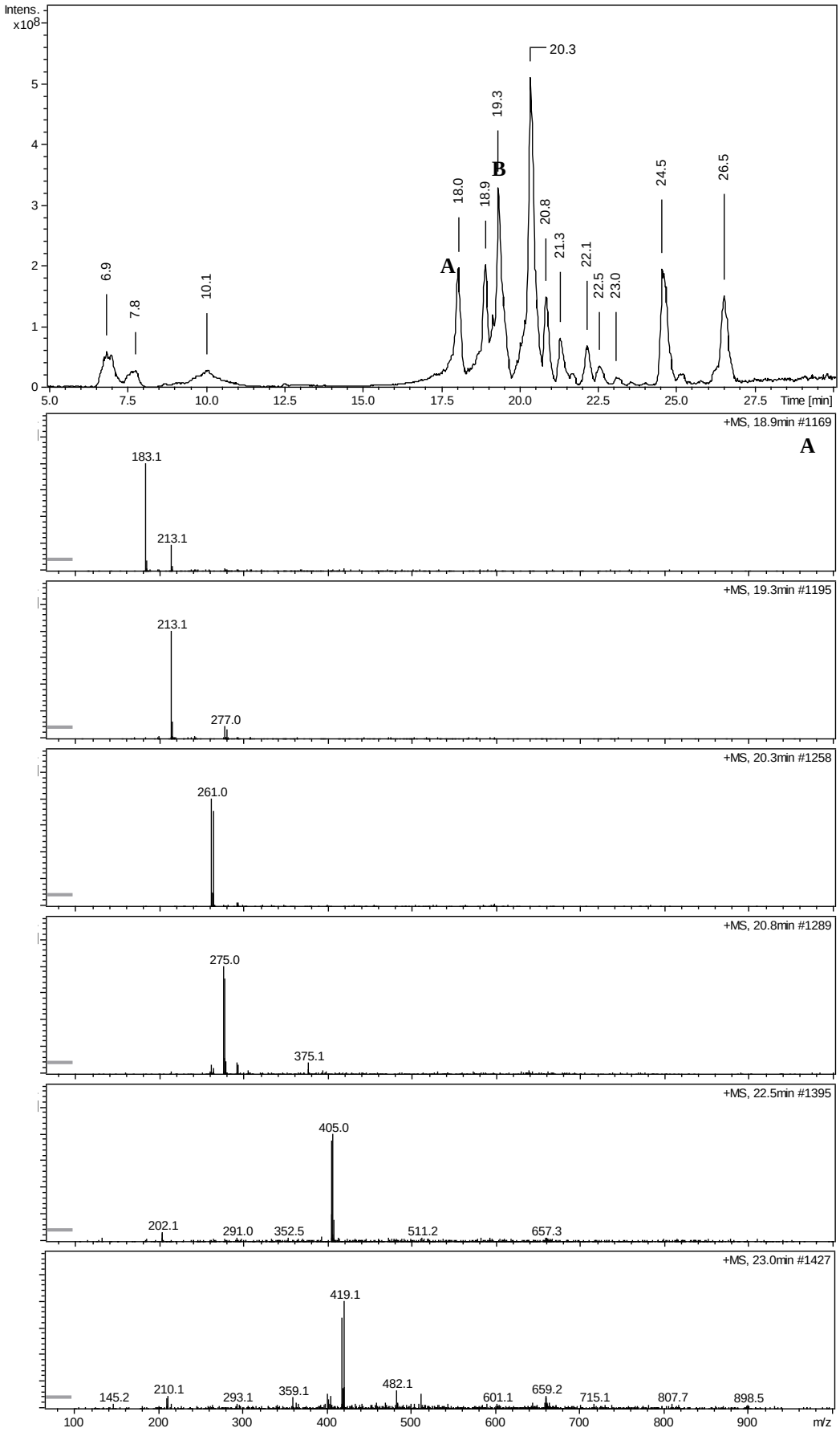

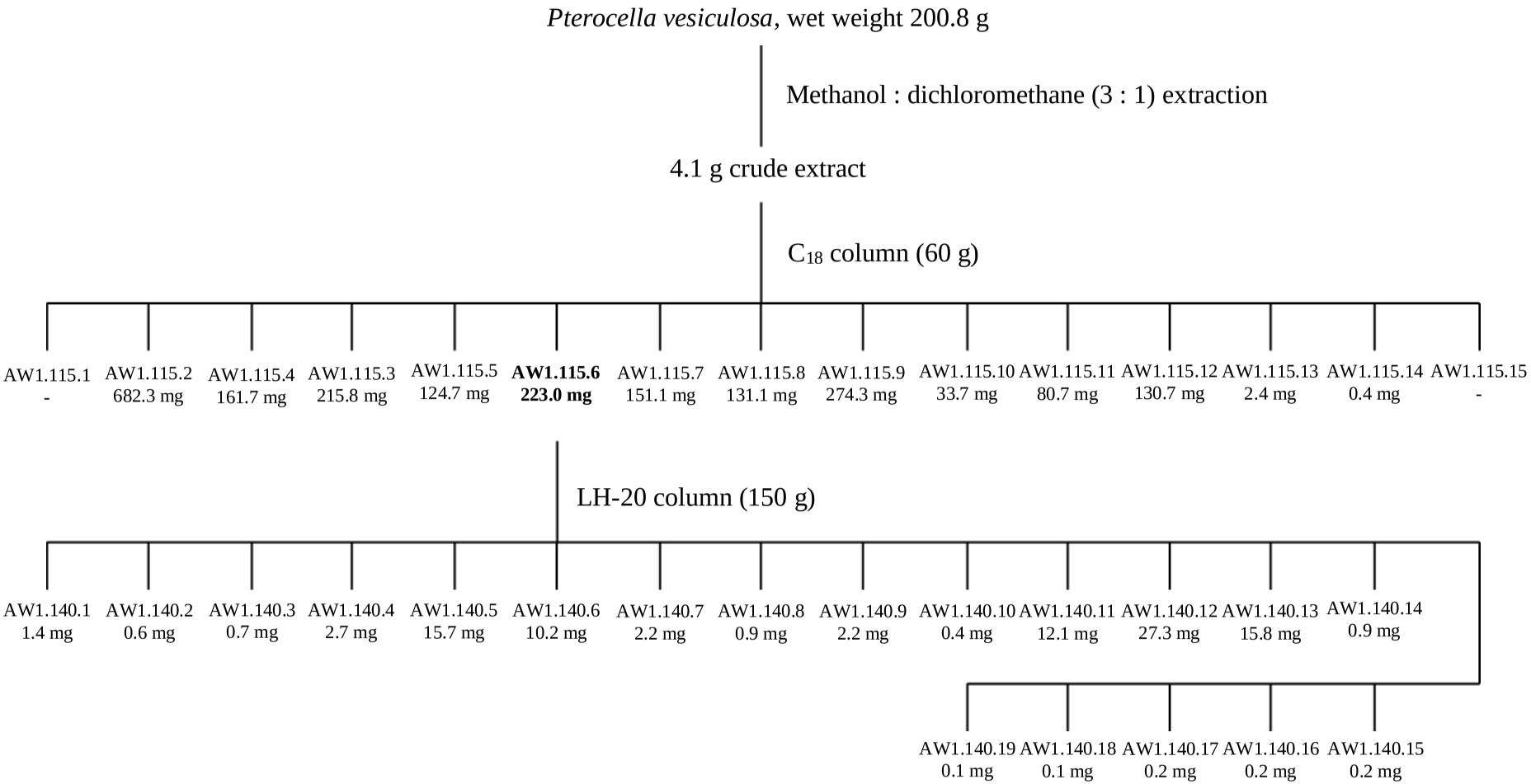

Appendix 2.12: Separation tree for the *Pterocella vesiculosa* extract

References

1. Williams, D. H.; Stone, M. J.; Hauck, P. R.; Rahman, S. K., Why are secondary metabolites (natural products) biosynthesized? *Journal of Natural Products* **1989**, *52*, 1189-208.

2. Verpoorte, R., Exploration of nature's chemodiversity: the role of secondary metabolites as leads in drug development. *Drug Discovery Today* **1998**, *3*, 232-238.

3. Koehn, F. E.; Carter, G. T., The evolving role of natural products in drug discovery. *Nature Reviews. Drug Discovery* **2005**, *4*, 206-20.

4. Dias, D. A.; Urban, S.; Roessner, U., A historical overview of natural products in drug discovery. *Metabolites* **2012**, *2*, 303-36.

5. Sharp, J. H.; Winson, M. K.; Porter, J. S., Bryozoan metabolites: an ecological perspective. *Natural Product Reports* **2007**, *24*, 659-73.

6. Rishton, G. M., Natural products as a robust source of new drugs and drug leads: past successes and present day issues. *The American Journal of Cardiology* **2008**, *101*, 43D-49D.

7. Donia, M.; Hamann, M. T., Marine natural products and their potential applications as anti-infective agents. *The Lancet. Infectious Diseases* **2003**, *3*, 338-48.

8. Colegate, S. M., *Bioactive Natural Products : Detection, Isolation, and Structural Determination (2nd Edition)*. CRC Press: Boca Raton, FL, USA, 2007.

9. Hay, M. E.; Fenical, W., Chemical ecology and marine biodiversity: insights and products from the sea. *Oceanography* **1996**, *9*, 10-20.

10. Van Minh, C.; Van Kiem, P.; Dang, N. H., Marine natural products and their potential application in the future. *ASEAN Journal on Science and Technology for Development* **2005**, *22*, 297.

11. Beesoo, R.; Neergheen-Bhujun, V.; Bhagooli, R.; Bahorun, T., Apoptosis inducing lead compounds isolated from marine organisms of potential relevance in cancer treatment. *Mutation Research/Fundamental and Molecular Mechanisms of Mutagenesis* **2014**, *768*, 84-97.

12. Pechenik, J., *Biology of the Invertebrates*. McGraw-Hill Education: 2014.

13. Ryland, J. S., *Bryozoans*. Hutchinson: London,, 1970; p 175 p.

14. Gordon, D. P., New bryozoan taxa from a new marine conservation area in New Zealand, with a checklist of Bryozoa from Greater Cook Strait. *Zootaxa* **2009**, *1987*, 39-60.

15. Faulkner, D. J., Marine natural products. *Natural Product Reports* **1986**, *3*, 1-33.

16. Faulkner, D. J., Marine natural products. *Natural Product Reports* **1987**, *4*, 539-76.

17. Faulkner, D. J., Marine natural products. *Natural Product Reports* **1988**, *5*, 613-63.

18. Faulkner, D. J., Marine natural products. *Natural Product Reports* **1990**, *7*, 269-309.

19. Faulkner, D. J., Marine natural products. *Natural Product Reports* **1991**, *8*, 97-147.

20. Faulkner, D. J., Marine natural products. *Natural Product Reports* **1992**, *9*, 323-364.

21. Faulkner, D. J., Marine natural products. *Natural Product Reports* **1993**, *10*, 497-539.

22. Faulkner, D. J., Marine natural products. *Natural Product Reports* **1994**, *11*, 355-94.

23. Faulkner, D. J., Marine natural products. *Natural Product Reports* **1995**, *12*, 223-269.

24. Faulkner, D. J., Marine natural products. *Natural Product Reports* **1996**, *13*, 75-125.

25. Faulkner, D. J., Marine natural products. *Natural Product Reports* **1997**, *14*, 259-302.

26. Faulkner, D. J., Marine natural products. *Natural Product Reports* **1998**, *15*, 113-58.

27. Faulkner, D. J., Marine natural products. *Natural Product Reports* **1999**, *16*, 155-198.

28. Faulkner, D. J., Marine natural products. *Natural Product Reports* **2000**, *17*, 7-55.

29. Faulkner, D. J., Marine natural products. *Natural Product Reports* **2001**, *18*, 1-49.

30. Faulkner, D. J., Marine natural products. *Natural Product Reports* **2002**, *19*, 1-48.

31. Blunt, J. W.; Copp, B. R.; Munro, M. H.; Northcote, P. T.; Prinsep, M. R., Marine natural products. *Natural Product Reports* **2003**, *20*, 1-48.

32. Blunt, J. W.; Copp, B. R.; Munro, M. H.; Northcote, P. T.; Prinsep, M. R., Marine natural products. *Natural Product Reports* **2004**, *21*, 1-49.

33. Blunt, J. W.; Copp, B. R.; Munro, M. H.; Northcote, P. T.; Prinsep, M. R., Marine natural products. *Natural Product Reports* **2005**, *22*, 15-61.

34. Blunt, J. W.; Copp, B. R.; Munro, M. H.; Northcote, P. T.; Prinsep, M. R., Marine natural products. *Natural Product Reports* **2006**, *23*, 26-78.

35. Blunt, J. W.; Copp, B. R.; Hu, W. P.; Munro, M. H.; Northcote, P. T.; Prinsep, M. R., Marine natural products. *Natural Product Reports* **2007**, *24*, 31-86.

36. Blunt, J. W.; Copp, B. R.; Hu, W. P.; Munro, M. H.; Northcote, P. T.; Prinsep, M. R., Marine natural products. *Natural Product Reports* **2008**, *25*, 35-94.

37. Blunt, J. W.; Copp, B. R.; Hu, W. P.; Munro, M. H.; Northcote, P. T.; Prinsep, M. R., Marine natural products. *Natural Product Reports* **2009**, *26*, 170-244.

38. Blunt, J. W.; Copp, B. R.; Munro, M. H.; Northcote, P. T.; Prinsep, M. R., Marine natural products. *Natural Product Reports* **2010**, *27*, 165-237.

39. Blunt, J. W.; Copp, B. R.; Munro, M. H.; Northcote, P. T.; Prinsep, M. R., Marine natural products. *Natural Product Reports* **2011**, *28*, 196-268.

40. Blunt, J. W.; Copp, B. R.; Keyzers, R. A.; Munro, M. H.; Prinsep, M. R., Marine natural products. *Natural Product Reports* **2012**, *29*, 144-222.

41. Blunt, J. W.; Copp, B. R.; Keyzers, R. A.; Munro, M. H.; Prinsep, M. R., Marine natural products. *Natural Product Reports* **2013**, *30*, 237-323.

42. Blunt, J. W.; Copp, B. R.; Keyzers, R. A.; Munro, M. H.; Prinsep, M. R., Marine natural products. *Natural Product Reports* **2014**, *31*, 160-258.

43. Blunt, J. W.; Copp, B. R.; Keyzers, R. A.; Munro, M. H.; Prinsep, M. R., Marine natural products. *Natural Product Reports* **2015**, *32*, 116-211.

44. Pettit, G. R.; Herald, C. L.; Doubek, D. L.; Herald, D. L.; Arnold, E.; Clardy, J., Isolation and structure of bryostatin 1. *Journal of the American Chemical Society* **1982**, *104*, 6846-6848.

45. Pettit, G. R.; Herald, C. L.; Kamano, Y., Structure of the Bugula neritina (marine bryozoa) antineoplastic component bryostatin 3. *The Journal of Organic Chemistry* **1983**, *48*, 5354-5356.

46. Pettit, G. R.; Herald, C. L.; Kamano, Y.; Gust, D.; Aoyagi, R., The structure of bryostatin 2 from the marine bryozoan *Bugula neritina*. *Journal of Natural Products* **1983**, *46*, 528-531.

47. Pettit, G. R.; Kamano, Y.; Herald, C. L.; Tozawa, M., Structure of bryostatin. 4. An important antineoplastic constituent of geographically diverse *Bugula neritin*a (Bryozoa). *Journal of the American Chemical Society* **1984**, *106*, 6768-6771.

48. Pettit, G.; Kamano, Y.; Aoyagi, R.; Herald, C.; Doubek, D.; Schmidt, J.; Rudloe, J., Antineoplastic agents, 100. The marine bryozoan *Amathia convoluta*. *Tetrahedron* **1985**, *41*, 985-994.

49. Pettit, G. R.; Kamano, Y.; Herald, C. L.; Tozawa, M., Isolation and structure of bryostatins 5-7. *Canadian Journal of Chemistry* **1985**, *63*, 1204-1208.

50. Pettit, G. R.; Kamano, Y.; Herald, C. L., Antineoplastic agents, 118. Isolation and structure of bryostatin 9. *Journal of Natural Products* **1986**, *49*, 661-4.

51. Pettit, G. R.; Kamano, Y.; Herald, C. L., Isolation and structure of bryostatins 10 and 11. *The Journal of Organic Chemistry* **1987**, *52*, 2848-2854.

52. Pettit, G. R.; Leet, J. E.; Herald, C. L.; Kamano, Y.; Boettner, F. E.; Baczynskyj, L.; Nieman, R. A., Isolation and structure of bryostatins 12 and 13. *The Journal of Organic Chemistry* **1987**, *52*, 2854-2860.

53. Pettit, G.; Gao, F.; Sengupta, D.; Coll, J.; Herald, C.; Doubek, D.; Schmidt, J.; Van Camp, J.; Rudloe, J.; Nieman, R., Isolation and structure of bryostatins 14 and 15. *Tetrahedron* **1991**, *47*, 3601-3610.

54. Pettit, G. R.; Gao, F.; Blumberg, P. M.; Herald, C. L.; Coll, J. C.; Kamano, Y.; Lewin, N. E.; Schmidt, J. M.; Chapuis, J.-C., Antineoplastic Agents, 340. Isolation and Structural Elucidation of Bryostatins 16-18. *Journal of Natural Products* **1996**, *59*, 286-289.

55. Lin, H.; Yi, Y.; Li, W.; Yao, X.; Wu, H., Bryostatin 19: A new antineoplastic component from *Bugula neritina* in the South China Sea. *Chinese Journal of Marine Drugs* **1997**, *1*, 1-3.

56. Lopanik, N.; Gustafson, K. R.; Lindquist, N., Structure of bryostatin 20: a symbiont produced chemical defense for larvae of the host bryozoan, *Bugula neritina*. *Journal of Natural Products* **2004**, *67*, 1412-1414.

57. Davidson, S. K.; Allen, S. W.; Lim, G. E.; Anderson, C. M.; Haygood, M. G., Evidence for the biosynthesis of bryostatins by the bacterial symbiont "*Candidatus Endobugula sertula*" of the bryozoan *Bugula neritina*. *Applied and Environmental Microbiology* **2001**, *67*, 4531-7.

58. Lopanik, N.; Lindquist, N.; Targett, N., Potent cytotoxins produced by a microbial symbiont protect host larvae from predation. *Oecologia* **2004**, *139*, 131-9.

59. Sun, M. K.; Alkon, D. L., Bryostatin‐1: Pharmacology and Therapeutic Potential as a CNS Drug. *CNS Drug Reviews* **2006**, *12*, 1-8.

60. Mutter, R.; Wills, M., Chemistry and clinical biology of the bryostatins. *Bioorganic & Medicinal Chemistry* **2000**, *8*, 1841-60.

61. Trindade-Silva, A. E.; Lim-Fong, G. E.; Sharp, K. H.; Haygood, M. G., Bryostatins: biological context and biotechnological prospects. *Current Opinion in Biotechnology* **2010**, *21*, 834-42.

62. Wang, Y.; Zhang, J.; Wang, Q.; Zhang, T.; Yang, Y.; Yi, Y.; Gao, G.; Dong, H.; Zhu, H.; Li, Y.; Lin, H.; Tang, H.; Chen, X., Bryostatin 5 induces apoptosis in acute monocytic leukemia cells by activating PUMA and caspases. *European Journal of Pharmacology* **2013**, *718*, 340-9.

63. Milanowski, D. J.; Gustafson, K. R.; Kelley, J. A.; McMahon, J. B., Caulibugulones A-F, novel cytotoxic isoquinoline quinones and iminoquinones from the marine bryozoan *Caulibugula intermis*. *Journal of Natural Products* **2004**, *67*, 70-3.

64. Brisson, M.; Foster, C.; Wipf, P.; Joo, B.; Tomko, R. J., Jr.; Nguyen, T.; Lazo, J. S., Independent mechanistic inhibition of cdc25 phosphatases by a natural product caulibugulone. *Molecular Pharmacology* **2007**, *71*, 184-92.

65. Cheng, J. F.; Lee, J. S.; Sakai, R.; Jares-Erijman, E. A.; Silva, M. V.; Rinehart, K. L., Myriaporones 1-4, cytotoxic metabolites from the Mediterranean bryozoan *Myriapora truncata*. *Journal of Natural Products* **2007**, *70*, 332-6.

66. Tapiolas, D. M.; Bowden, B. F.; Abou-Mansour, E.; Willis, R. H.; Doyle, J. R.; Muirhead, A. N.; Liptrot, C.; Llewellyn, L. E.; Wolff, C. W.; Wright, A. D.; Motti, C. A., Eusynstyelamides A, B, and C, nNOS inhibitors, from the ascidian *Eusynstyela latericius*. *Journal of Natural Products* **2009**, *72*, 1115-20.

67. Tadesse, M.; Tabudravu, J. N.; Jaspars, M.; Strom, M. B.; Hansen, E.; Andersen, J. H.; Kristiansen, P. E.; Haug, T., The antibacterial ent-eusynstyelamide B and eusynstyelamides D, E, and F from the Arctic bryozoan *Tegella cf. spitzbergensis*. *Journal of Natural Products* **2011**, *74*, 837-41.

68. Yao, B.; Prinsep, M. R.; Nicholson, B. K.; Gordon, D. P., The pterocellins, novel bioactive alkaloids from the marine bryozoan *Pterocella vesiculosa*. *Journal of Natural Products* **2003**, *66*, 1074-7.

69. Prinsep, M. R., Further pterocellins from the New Zealand marine bryozoan *Pterocella vesiculosa*. *Journal of Natural Products* **2008**, *71*, 134-6.

70. Rae, J. M.; Creighton, C. J.; Meck, J. M.; Haddad, B. R.; Johnson, M. D., MDA-MB-435 cells are derived from M14 Melanoma cells—a loss for breast cancer, but a boon for melanoma research. *Breast cancer research and treatment* **2007**, *104*, 13-19.

71. Chambers, A. F., MDA-MB-435 and M14 cell lines: identical but not M14 melanoma? *Cancer research* **2009**, *69*, 5292-5293.

72. Prinsep, M. R., Private Communcations. University of Waikato, Hamilton, 2014.

73. Anderson, A. Investigations of Natural Products from Bryozoa Inhabiting Aotearoa New Zealand. MSc Thesis. The University of Waikato, Hamilton, New Zealand, 2012.

74. Till, M. Studies of New Zealand Marine Organisms. MSc Thesis. The University of Waikato, Hamilton, New Zealand, 2007.

75. Prinsep, M. R.; Blunt, J. W.; Munro, M. H., New cytotoxic β-carboline alkaloids from the marine bryozoan, *Cribricellina cribraria*. *Journal of Natural Products* **1991**, *54*, 1068-76.

76. Till, M.; Prinsep, M. R., 5-Bromo-8-methoxy-1-methyl-beta-carboline, an alkaloid from the New Zealand marine bryozoan *Pterocella vesiculosa*. *Journal of Natural Products* **2009**, *72*, 796-8.

77. Blackman, A. J.; Matthews, D. J.; Narkowicz, C. K., β-Carboline alkaloids from the marine bryozoan *Costaticella hastata*. *Journal of Natural Products* **1987**, *50*, 494-496.

78. Beutler, J. A.; Cardellina, J. H., 2nd; Prather, T.; Shoemaker, R. H.; Boyd, M. R.; Snader, K. M., A cytotoxic β-carboline from the bryozoan *Catenicella cribraria*. *Journal of Natural Products* **1993**, *56*, 1825-6.

79. Jacobson, M. D.; Weil, M.; Raff, M. C., Programmed cell death in animal development. *Cell* **1997**, *88*, 347-54.

80. Kerr, J. F.; Wyllie, A. H.; Currie, A. R., Apoptosis: a basic biological phenomenon with wide-ranging implications in tissue kinetics. *British Journal of Cancer* **1972**, *26*, 239-57.

81. de Bruin, E. C.; Medema, J. P., Apoptosis and non-apoptotic deaths in cancer development and treatment response. *Cancer Treatment Reviews* **2008**, *34*, 737-749.

82. Mattson, M. P., Apoptosis in neurodegenerative disorders. *Nature Reviews. Molecular Cell Biology* **2000**, *1*, 120-9.

83. Evan, G. I.; Vousden, K. H., Proliferation, cell cycle and apoptosis in cancer. *Nature* **2001**, *411*, 342-8.

84. Gill, C.; Mestril, R.; Samali, A., Losing heart: the role of apoptosis in heart disease--a novel therapeutic target? *FASEB journal : official publication of the Federation of American Societies for Experimental Biology* **2002**, *16*, 135-46.

85. Nagata, S., Apoptosis and autoimmune diseases. *Annals of the New York Academy of Sciences* **2010**, *1209*, 10-6.

86. Hengartner, M. O., The biochemistry of apoptosis. *Nature* **2000**, *407*, 770-6.

87. Elmore, S., Apoptosis: a review of programmed cell death. *Toxicologic Pathology* **2007**, *35*, 495-516.

88. Reed, J. C., Mechanisms of apoptosis. *The American Journal of Pathology* **2000**, *157*, 1415-30.

89. Indran, I. R.; Tufo, G.; Pervaiz, S.; Brenner, C., Recent advances in apoptosis, mitochondria and drug resistance in cancer cells. *Biochimica et Biophysica Acta* **2011**, *1807*, 735-45.

90. Fadok, V. A.; Bratton, D. L.; Rose, D. M.; Pearson, A.; Ezekewitz, R. A.; Henson, P. M., A receptor for phosphatidylserine-specific clearance of apoptotic cells. *Nature* **2000**, *405*, 85-90.

91. Garrido, C.; Galluzzi, L.; Brunet, M.; Puig, P. E.; Didelot, C.; Kroemer, G., Mechanisms of cytochrome c release from mitochondria. *Cell Death and Differentiation* **2006**, *13*, 1423-33.

92. Krysko, D. V.; Vanden Berghe, T.; D'Herde, K.; Vandenabeele, P., Apoptosis and necrosis: detection, discrimination and phagocytosis. *Methods* **2008**, *44*, 205-21.

93. Sawai, H.; Domae, N., Discrimination between primary necrosis and apoptosis by necrostatin-1 in Annexin V-positive/propidium iodide-negative cells. *Biochemical and Biophysical Research Communications* **2011**, *411*, 569-573.

94. Chaabane, W.; User, S. D.; El-Gazzah, M.; Jaksik, R.; Sajjadi, E.; Rzeszowska-Wolny, J.; Los, M. J., Autophagy, apoptosis, mitoptosis and necrosis: interdependence between those pathways and effects on cancer. *Arch Immunol Ther Exp (Warsz)* **2013**, *61*, 43-58.

95. Kroemer, G.; Galluzzi, L.; Vandenabeele, P.; Abrams, J.; Alnemri, E. S.; Baehrecke, E. H.; Blagosklonny, M. V.; El-Deiry, W. S.; Golstein, P.; Green, D. R.; Hengartner, M.; Knight, R. A.; Kumar, S.; Lipton, S. A.; Malorni, W.; Nunez, G.; Peter, M. E.; Tschopp, J.; Yuan, J.; Piacentini, M.; Zhivotovsky, B.; Melino, G.; Nomenclature Committee on Cell, D., Classification of cell death: recommendations of the Nomenclature Committee on Cell Death 2009. *Cell Death and Differentiation* **2009**, *16*, 3-11.

96. Majno, G.; Joris, I., Apoptosis, oncosis, and necrosis. An overview of cell death. *The American Journal of Pathology* **1995**, *146*, 3-15.

97. Golstein, P.; Kroemer, G., Cell death by necrosis: towards a molecular definition. *Trends in Biochemical Sciences* **2007**, *32*, 37-43.

98. Galluzzi, L.; Kroemer, G., Necroptosis: a specialized pathway of programmed necrosis. *Cell* **2008**, *135*, 1161-3.

99. Degterev, A.; Huang, Z.; Boyce, M.; Li, Y.; Jagtap, P.; Mizushima, N.; Cuny, G. D.; Mitchison, T. J.; Moskowitz, M. A.; Yuan, J., Chemical inhibitor of nonapoptotic cell death with therapeutic potential for ischemic brain injury. *Nature Chemical Biology* **2005**, *1*, 112-9.

100. Feoktistova, M.; Leverkus, M., Programmed necrosis and necroptosis signalling. *The FEBS journal* **2015**, *282*, 19-31.

101. Hood, K. A.; West, L. M.; Northcote, P. T.; Berridge, M. V.; Miller, J. H., Induction of apoptosis by the marine sponge (*Mycale*) metabolites, mycalamide A and pateamine. *Apoptosis* **2001**, *6*, 207-19.

102. Nguyen, V. T.; Lee, J. S.; Qian, Z. J.; Li, Y. X.; Kim, K. N.; Heo, S. J.; Jeon, Y. J.; Park, W. S.; Choi, I. W.; Je, J. Y.; Jung, W. K., Gliotoxin isolated from marine fungus *Aspergillus* sp. induces apoptosis of human cervical cancer and chondrosarcoma cells. *Marine Drugs* **2014**, *12*, 69-87.

103. Wijesekara, I.; Zhang, C.; Van Ta, Q.; Vo, T. S.; Li, Y. X.; Kim, S. K., Physcion from marine-derived fungus *Microsporum* sp. induces apoptosis in human cervical carcinoma HeLa cells. *Microbiological Research* **2014**, *169*, 255-61.

104. Poot, M.; Zhang, Y. Z.; Kramer, J. A.; Wells, K. S.; Jones, L. J.; Hanzel, D. K.; Lugade, A. G.; Singer, V. L.; Haugland, R. P., Analysis of mitochondrial morphology and function with novel fixable fluorescent stains. *The Journal of Histochemistry and Cytochemistry* **1996**, *44*, 1363-72.

105. Srivastava, P.; Panda, D., Rotenone inhibits mammalian cell proliferation by inhibiting microtubule assembly through tubulin binding. *The FEBS Journal* **2007**, *274*, 4788-801.

106. Berridge, M. V.; Herst, P. M.; Tan, A. S., Tetrazolium dyes as tools in cell biology: new insights into their cellular reduction. *Biotechnology Annual Review* **2005**, *11*, 127-152.

107. Modok, S.; Mellor, H. R.; Callaghan, R., Modulation of multidrug resistance efflux pump activity to overcome chemoresistance in cancer. *Current Opinion in Pharmacology* **2006**, *6*, 350-4.

108. Silva, M. T., Secondary necrosis: the natural outcome of the complete apoptotic program. *FEBS Letters* **2010**, *584*, 4491-9.

109. Skulachev, V. P.; Bakeeva, L. E.; Chernyak, B. V.; Domnina, L. V.; Minin, A. A.; Pletjushkina, O. Y.; Saprunova, V. B.; Skulachev, I. V.; Tsyplenkova, V. G.; Vasiliev, J. M.; Yaguzhinsky, L. S.; Zorov, D. B., Thread-grain transition of mitochondrial reticulum as a step of mitoptosis and apoptosis. *Molecular and Cellular Biochemistry* **2004**, *256-257*, 341-58.

110. Gao, W.; Pu, Y.; Luo, K. Q.; Chang, D. C., Temporal relationship between cytochrome c release and mitochondrial swelling during UV-induced apoptosis in living HeLa cells. *Journal of Cell Science* **2001**, *114*, 2855-2862.

111. Skulachev, V. P., Mitochondrial filaments and clusters as intracellular power-transmitting cables. *Trends in Biochemical Sciences* **2001**, *26*, 23-29.

112. Youle, R. J.; Karbowski, M., Mitochondrial fission in apoptosis. *Nature Reviews. Molecular Cell Biology* **2005**, *6*, 657-63.

113. Skulachev, V. P., Bioenergetic aspects of apoptosis, necrosis and mitoptosis. *Apoptosis* **2006**, *11*, 473-85.

114. Brown, W. M.; George, M., Jr.; Wilson, A. C., Rapid evolution of animal mitochondrial DNA. *Proceedings of the National Academy of Sciences of the United States of America* **1979**, *76*, 1967-71.

115. Schulze-Osthoff, K.; Walczak, H.; Droge, W.; Krammer, P. H., Cell nucleus and DNA fragmentation are not required for apoptosis. *Journal of Cell Biology* **1994**, *127*, 15-20.

116. Sundquist, T.; Moravec, R.; Niles, A.; O'Brien, M.; Riss, T., Timing your apoptosis assays. *Cell Notes* **2006**, *16*, 18-21.